Physiological properties of mature adult-born neurons in the olfactory bulb of awake mice

Dissertation

zur Erlangung des Grades eines
Doktors der Naturwissenschaften

der Mathematisch-Naturwissenschaftlichen Fakultät
und
der Medizinischen Fakultät
der Eberhard-Karls-Universität Tübingen

vorgelegt
von

Natalie Fomin-Thunemann
aus Omsk, Russland

Januar 2018

Tag der mündlichen Prüfung: 16. April 2018

Dekan der Math.-Nat. Fakultät: Prof. Dr. W. Rosenstiel
Dekan der Medizinischen Fakultät: Prof. Dr. I. B. Autenrieth

1. Berichterstatter: Prof. Dr. Olga Garaschuk
2. Berichterstatter: Prof. Dr. Bernd Antkowiak

Prüfungskommission: Prof. Dr. Thomas Euler
                                                     Prof. Dr. Konrad Kohler

Erklärung / Declaration:

Ich erkläre, dass ich die zur Promotion eingereichte Arbeit mit dem Titel: *"Physiological properties of mature adult-born neurons in the olfactory bulb of awake mice"* selbständig verfasst, nur die angegebenen Quellen und Hilfsmittel benutzt und wörtlich oder inhaltlich übernommene Stellen als solche gekennzeichnet habe. Ich versichere an Eides statt, dass diese Angaben wahr sind und dass ich nichts verschwiegen habe. Mir ist bekannt, dass die falsche Abgabe einer Versicherung an Eides statt mit Freiheitsstrafe bis zu drei Jahren oder mit Geldstrafe bestraft wird.

I hereby declare that I have produced the work entitled "Physiological properties of mature adult-born neurons in the olfactory bulb of awake mice", submitted for the award of a doctorate, on my own (without external help), have used only the sources and aids indicated and have marked passages included from other works, whether verbatim or in content, as such. I swear upon oath that these statements are true and that I have not concealed anything. I am aware that making a false declaration under oath is punishable by a term of imprisonment of up to three years or by a fine.

Tübingen, den ....
                    Datum / Date   Unterschrift /Signature

Abstract

The adult brain undergoes various forms of plasticity. Besides synaptic plasticity where connections between neurons are strengthened or weakened, another form of plasticity is the addition of new neurons into the pre-existing neuronal network throughout life. It is believed that this form of neuronal plasticity adjusts the behavior to the ever-changing environment. In the mammalian brain, continuous addition of 'adult-born cells' (ABCs) has been observed in the olfactory bulb (OB) and the hippocampus. ABCs migrate into the OB, mature to GABAergic cells – juxtaglomerular cells and granule cells – and integrate into the existent neuronal network. These ABCs are believed to be involved in many olfactory functions, as for instance odor detection, odor discrimination, and olfactory learning. *In vivo* measurements in anesthetized mice suggest that adult-born juxtaglomerular cells mature at 8-9 weeks of age and acquire physiological properties that are similar to that of pre-existing, resident cells. Yet, a few studies reported that even after maturation, some physiological properties remain different. However, all these comparisons have been performed in anesthetized animals and since several years it is clear that brain activity changes under anesthesia. Therefore, the major goal of this work was to test whether mature ABCs (mABCs) in awake animals retain unique features that distinguish them from resident GABAergic (Res$_{GABA}$) cells.

For this, we labeled mABCs and Res$_{GABA}$ cells via viral transduction with the genetically encoded calcium (Ca^{2+}) indicator Twitch-2B and performed two-photon-based Ca^{2+} measurements in awake head-restrained mice. We measured basal Ca^{2+} levels (i.e., Ca^{2+} levels recorded in the absence of any experimental manipulation) and found that they are similar between mABCs and Res$_{GABA}$ cells. In order to measure odor-evoked Ca^{2+} signals, we applied the odorant ethyl tiglate in front of the mouse snout and observed that, compared to Res$_{GABA}$ cells, fewer mABCs responded to odor application. Furthermore, the odor-evoked responses showed lower reliability upon repeated odor application, but reached higher levels than in Res$_{GABA}$ cells. In addition, we tested if anesthesia-induced alterations in brain state modulate mABCs differently than Res$_{GABA}$ cells. Under anesthesia, basal Ca^{2+} levels of both, mABCs and Res$_{GABA}$ cells, were reduced. One specific anesthetic mixture, ketamine/xylazine anesthesia, reduced basal Ca^{2+} levels significantly stronger in mABCs than in Res$_{GA}$-

BA cells, indicating that mABCs might have a higher sensitivity to NMDA receptor blockers compared to Res$_{GABA}$ cells. Furthermore, under anesthesia, mABCs responded to odorant application more reliably but still less often compared to Res$_{GABA}$ cells. The odor-evoked responses reached again higher levels. Anesthetic agents are known to modulate the brain state by affecting the ascending reticular activating system (ARAS). ARAS centers give rise to various centrifugal fibers that project to the OB and target GABAergic cells. These centrifugal fibers arising from the locus coeruleus, dorsal raphe nucleus, and basal forebrain, release noradrenaline, serotonin, and acetylcholine, respectively. In addition, these projections were reported to target ABCs and to promote their survival. We tested if the centrifugal projections target mABCs differently compared to Res$_{GABA}$ cells. In response to application of cholinergic receptor blockers, both mABCs and Res$_{GABA}$ cells showed a drop in basal Ca^{2+} levels. Surprisingly, however, only mABCs showed a drop in basal Ca^{2+} levels in the presence of the serotonergic receptor blocker methysergide.

Thus, our results demonstrate that mABCs differ from Res$_{GABA}$ cells in (1) odor-response properties, (2) modulation by K/X anesthesia, and (3) innervation by serotonergic fibers or responsiveness to activation of serotonin receptors. Larger Ca^{2+} signals in mABCs in response to odor application might be relevant in the context of activity-dependent plasticity as a basis of olfactory learning, the function suggested for mABCs. The observation that serotonergic inputs might innervate specifically mABCs indicates that mABCs could exert a specific function via serotonin, such as sensory gain control in dependence of the brain state of the animal.

Zusammenfassung

Im adulten Gehirn existieren verschiedene Formen neuronaler Plastizität. Neben der Plastizität synaptischer Verbindungen werden während des gesamten Lebens neugeborene Nervenzellen in bestehende neuronale Netzwerke hinzugefügt (adulte Neurogenese). Es wird angenommen, dass adulte Neurogenese die Anpassung des Verhaltens an eine sich ständig verändernde Umwelt erlaubt. In Säugetieren wurde die kontinuierliche Einwanderung von adult-geborenen Nervenzellen in Riechkolben und Hippocampus nachgewiesen. Adult-geborene Zellen wandern in den Riechkolben ein, reifen zu GABAergen Nervenzellen (juxtaglomeruläre Zellen und Körnerzellen) heran und integrieren sich in das bestehende neuronale Netzwerk. Von diesen adult-geborenen Zellen wird angenommen, dass sie an vielen Funktionen des Riechsystems beteiligt sind, unter anderem Geruchsdetektion, Geruchs-diskriminierung und olfaktorisches Lernen. *In-vivo*-Untersuchungen in anästhesierten Mäusen legen nahe, dass juxtaglomeruläre Zellen im Alter von 8-9 Wochen ausreifen und physiologische Eigenschaften bekommen, die denen bereits existierender (residenter) Zellen ähnlich sind. Einige Studien berichten jedoch, dass auch nach der Reifung einige physiologische Eigenschaften unterschiedlich bleiben. All diese Vergleiche wurden jedoch in anästhesierten Tieren durchgeführt, was neuronale Aktivitätsmuster im Vergleich zum Wachzustand stark verändern kann. Daher war das Hauptziel dieser Arbeit in wachen Tieren zu testen, ob reife adult-geborene Zellen im Riechkolben physiologische Merkmale behalten, die sie von residenten GABAergen Zellen unterscheiden.

Dazu wurden adult-geborene und residente GABAerge Zellen über eine virale Transduktion mit dem Calcium-Sensorprotein Twitch-2B genetisch markiert und in wachen, fixierten Mäusen Zweiphotonen-Messungen durchgeführt. Basale Ca^{2+}-Spiegel (in Abwesenheit jeglicher experimenteller Manipulation aufgezeichnet) sind zwischen adult-geborenen und residenten GABAergen Zellen ähnlich. Um Ca^{2+}-Signale in Antwort auf Duftstoffstimulation zu messen, applizierten wir Ethyltiglat und beobachteten, dass weniger adult-geborene Zellen auf Duftstoffapplikation reagieren. Darüber hinaus zeigten die Duftstoff-evozierten Ca^{2+}-Signale eine geringere Zuverlässigkeit bei wiederholter Duftstoffapplikation, erreichten jedoch höhere Ca^{2+}-Spiegel als residente GABAerge Zellen. Zusätzlich wurde getestet, ob durch Anästhesie hervorgeru-

fene Veränderungen des Hirnzustands adult-geborene Zellen anders modulieren als residente GABAerge Zellen. Anästhesie reduzierte die basalen Ca^{2+}-Spiegel von adult-geborenen und residenten GABAergen Zellen. Hier reduzierten Ketamin/Xylazin basale Ca^{2+}-Spiegel signifikant stärker in adult-geborenen als in residenten GABAergen Zellen, was darauf hindeuten könnte, dass adult-geborene Zellen eine höhere Empfindlichkeit gegenüber NMDA-Rezeptorblockern aufweisen. Unter Anästhesie reagierten adult-geborene Zellen zuverlässiger, aber immer noch seltener als residente GABAerge Zellen. Die Duftstoff-evozierten Ca^{2+}-Signale erreichten auch hier höhere Werte. Anästhetika modulieren den Gehirnzustand durch Beeinflussung des aufsteigenden retikulären Aktivierungssystems (ARAS). ARAS-Zentren senden verschiedene Nervenfasern aus, von denen einige den Riechkolben erreichen und dort GABAerge Zellen innervieren. Diese Nervenfasern kommen aus Locus Coeruleus, dorsalem Raphe-Kern und basalem Vorderhirn und setzen Noradrenalin, Serotonin, bzw. Acetylcholin frei. Es wurde berichtet, dass diese Nervenfasern auch adult-geborene Zellen innervieren und deren Überleben fördern. Hier haben wir getestet, ob die Modulation dieser Nervenfasern sich unterscheidlich auf adult-geborene und residente GABAerge Zellen auswirkt. Cholinerge Rezeptorblocker führten bei adult-geborenen und residenten GABAergen Zellen zu einer Reduktion des basalen Ca^{2+}-Spiegels. Überraschenderweise führte der serotonerge Rezeptorblocker Methysergide nur bei adult-geborenen Zellen zu einer Reduktion des basalen Ca^{2+}-Spiegels.

Diese Ergebnisse zeigen, dass sich reife adult-geborene Zellen von residenten GABAergen Zellen in (1) Duftstoff-evozierter Aktivität, (2) Modulation durch Ketamin/Xylazin-Anästhesie und in (3) serotonerger Innervierung oder ihrer Empfindlichkeit auf die Aktivierung von Serotoninrezeptoren unterscheiden. Größere Ca^{2+}-Signale bei Duftstoffapplikation in adult-geborenen Zellen könnten mit aktivitätsabhängiger Plastizität als Grundlage für olfaktorisches Lernen im Zusammenhang stehen. Die Beobachtung, dass serotonerge Nervenfasern eventuell ausschliesslich reife adult-geborene Zellen innervieren, zeigt, dass diese eine über Serotonin vermittelte Funktion ausüben könnten, wie z. B. die Filterung von sensorischen Reizen in Abhängigkeit vom Gehirnzustand.

Acknowledgements

Table of Contents

List of Figures

List of Tables

Abbreviations

3CN ....3-Component narcosis
5-HT........................Serotonin
AAV ....Adeno-associated virus
ABC ....Adult-born cell
ACh ....Acetylcholine
AMPAR...................α-Amino-3-hydroxy-5-methyl-4-isoxazole-propionic acid receptor
ANOVA ....Analysis of variance
AP ....Action potential
ARAS.......................Ascending reticular activating system
BW..........................Body weight
DCX ....Doublecortin
DPI ....Days post injection
dSAC ....Deep short axon cell
EEG ....Electroencephalography
ETC ....External tufted cell
ETI..........................Ethyl tiglate
FRET ....Förster resonance energy transfer
GABA.......................Gamma-aminobutyric acid
GC ....Granule cell
HDB ....Horizontal limb of the diagonal band
i.p...........................Intraperitoneal
K/M ....Ketamine/medetomidine
K/X..........................Ketamine/xylazine
Kwik-Cast/Sil ....Kwik-Cast and Kwik-Sil
LH...........................Lateral hypothalamic
M/T ....Mitral/tufted cell
mABC ....Mature adult-born cell
mAChR ....Muscarinic acetylcholine receptor
MC ....Mitral cell
NA ....Noradrenaline
nAChR ....Nicotinergic acetylcholine receptor
NMDARs..................N-methyl-D-aspartate receptors
NREM ....Non-rapid eye movement
OB ....Olfactory bulb
OSN.........................Olfactory sensory neuron
P ....Postnatal day
PBS ....Phosphate-buffered saline
PGC.........................Periglomerular cell
PSD95 ....Postsynaptic density 95
Res$_{GABA}$ ....Resident GABAergic
REM……………….Rapid eye movement
RMS.........................Rostral migratory stream
ROI ....Region of interest
s.c...........................Subcutaneous
SAC ....Short axon cell
SVZ..........................Subventricular zone
TC............................Tufted cell
TM ....Tuberomammillary

1 Introduction

1.1 The olfactory sensory system

The olfactory sensory system is an evolutionarily old sensory system conserved throughout species (Ache and Young 2005). It mediates a vast variety of odor-guided behaviors important for survival in mammals (Ache and Young 2005; Pinto 2011), like searching for food, finding a sexual partner, mother-child interactions, predator avoidance, and avoidance of dangerous odorants arising from spoiled food or fire. In addition, olfactory stimuli have an influence on emotions and moods in humans (Kadohisa 2013). Loss of smell (anosmia) in humans increases health risks arising from spoiled food and dangerous vapors such as gas and fire (Doty 2005). The ability to smell declines naturally with age (Doty and Kamath 2014), but can as well be diminished through mechanical or chemical damage to the nose epithelium (Doty 2005; Doty 2017). A mild-to-severe loss of smell has been considered as an early marker of neurodegenerative diseases such as Alzheimer's or Parkinson's disease (Godoy *et al.* 2015), which is detectable decades before other disease-related symptoms like memory or motor impairments become apparent (Ross *et al.* 2008; Devanand *et al.* 2015).

In the environment, various odorants from different sources are intermixed. The olfactory system is able (1) to detect the odor signal of interest within this noisy environment, (2) to extract the signal from a changing and complex odor background, and (3) to associate it with previously experienced odors. Unlike other sensory systems, the olfactory system does not relay sensory information via the thalamus to the olfactory cortex but sends signals from the sensory neurons via the olfactory bulb (OB), which is the first processing stage of olfactory signals, to the olfactory cortex. Odorants activate olfactory sensory neurons (OSNs), which reside in the olfactory epithelium of the nasal cavity. OSNs transmit the signal to the OB where their axons congregate into spherical structures called glomeruli (Mombaerts *et al.* 1996)(Figure 1). In rodents, each OSN expresses only one out of ~1000 odorant receptors, but these receptors can bind a variety of related odorants. OSNs expressing the same odorant receptor converge onto one or two glomeruli per hemibulb (Vassar *et al.* 1994). Within glomeruli, OSN inputs can either activate the principal neurons directly, which are called mitral cells (MCs) and tufted cells (TCs), summarized as 'M/Ts', or OSN inputs are

first processed by a group of interneurons, collectively referred to as 'juxtaglomerular cells' (Nagayama *et al.* 2014).
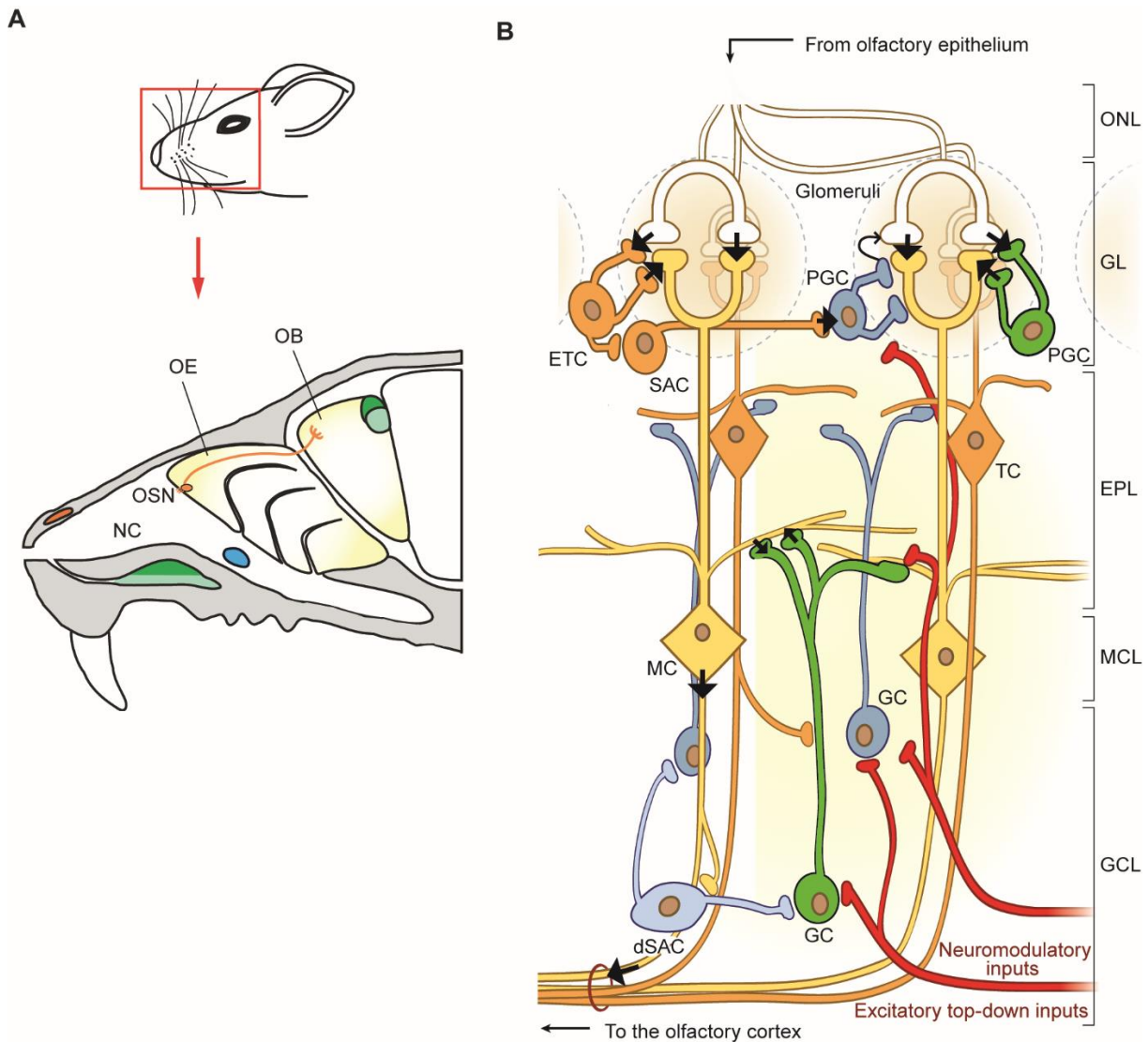
Figure 1. Schematic representation of the mouse olfactory bulb.
(A) In the nose, odorants can enter through the nasal cavity (NC) and access the olfactory epithelium (OE), where they bind to the receptors of olfactory sensory neurons (OSNs). Upon activation, OSNs send the signal via their axons to the olfactory bulb (OB). Figure modified from Ferrero and Liberles (2010). **(B)** In the OB, axons from OSNs terminate in spherical structures called glomeruli. In glomeruli, the signal can be processed by excitatory external tufted cells (ETCs) and inhibitory short axon cells (SACs) and periglomerular cells (PGCs), before it is forwarded to the output neurons, mitral cells (MCs) and tufted cells (TCs), summarized as 'M/Ts'. M/Ts form synapses with inhibitory granule cells (GCs) in deeper layers. Another type of inhibitory cell, the deep SAC (dSAC), inhibits GCs. In the end, the computed signal leaves the OB via axons of MCs and TCs to the olfactory cortex. Inhibitory cells receive neuromodulatory inputs (as described in section 1.4.1). Illustration modified from Lepousez *et al.* (2013). ONL, olfactory nerve layer; GL, glomerular layer; EPL, external plexiform layer; MCL, mitral cell layer; GCL, granule cell layer.

2

Compared to most other central nervous system regions, an unique feature of the olfactory system is the relation of inhibitory cells (which release the neurotransmitter gamma-aminobutyric acid, GABA) to excitatory cells (which release the neurotransmitter glutamate): inhibitory interneurons outnumber excitatory principal cells by approximately 100:1 (Imai 2014). The juxtaglomerular cells are composed of inhibitory periglomerular cells (PGCs) and short-axon cells (SACs), as well as excitatory external tufted cells (ETCs). In deeper layers of the OB, M/Ts can be inhibited by granule cells (GCs) before they transfer the output signal to the olfactory cortex (anterior olfactory nucleus, olfactory tubercle, and piriform cortex), the cortical nucleus of the amygdala and the entorhinal area (Kevetter and Winans 1981; Shepherd 2004; Wilson and Mainen 2006). GCs in the deeper layer account for about 90% of all bulbar interneurons (Shepherd *et al.* 2007), and PGCs together with SACs make up the remaining 10% in the superficial glomerular layer. In the glomerular layer, half of the juxtaglomerular cells are GABAergic PGCs and SACs, and half are glutamatergic ETCs (Parrish-Aungst *et al.* 2007). The initial information about odorant identity and intensity is thought to be extracted by bulbar interneurons in the glomerular layer as well as in the deeper external plexiform and granule cell layer. One conceivable way to achieve this extraction might be via decorrelation of signals arriving from OSNs. There are several hypotheses how OSN signals could be decorrelated (Cleland and Linster 2005) by each cell in different OB layers, which is discussed in the following section.

1.1.1 Sensory processing in the olfactory bulb

Each cell in different OB layers is assumed to play a different role in the processing of olfactory signals arriving from OSNs. The inhibitory PGC is the most abundant GABAergic cell type in the glomerular layer (Parrish-Aungst *et al.* 2007). It has the smallest cell body among all juxtaglomerular cell types and thus a very high input resistance (~1 GΩ). Typically, it extends its dendrites to a single glomerulus, only occasionally to multiple glomeruli. In this one particular glomerulus, the PGC is thought to mediate 'intra-glomerular' inhibition of M/Ts and juxtaglomerular cells in addition to presynaptic feedback-inhibition of OSNs (McGann *et al.* 2005; Murphy *et al.* 2005; Gire and Schoppa 2009). Intra-glomerular inhibition within one glomerulus is a potential mechanism to decorrelate OSN signals and to enhance contrast between similar odorants. 'Contrast enhancement is a common property of sensory systems

that serves to narrow, or sharpen, sensory representations by specifically inhibiting neurons on the periphery of the representation' (Cleland and Sethupathy 2006). However, in the OB, an approximately 1000-dimensional sensory space, provided by the around 1000 odorant receptors expressed by OSNs, is projected onto a two-dimensional glomerular layer. Therefore, center and periphery of a receptive field are not necessarily located in spatially close glomeruli. Thus, a contrast enhancement independent of the topography of glomeruli is a more likely property of this sensory system. This 'nontopographical contrast enhancement hypothesis' proposes that an inhibitory PGC within a glomerulus, which receives a weak input, will be excited before excitatory cells (ETCs or M/Ts) because the PGC has a higher input resistance (Cleland and Sethupathy 2006; Gire and Schoppa 2009). Then, the PGC would inhibit excitatory cells in this glomerulus. In comparison, a strong input in another glomerulus could excite excitatory cells directly, and M/Ts could forward the signal to the olfactory cortex. Thus, only the strong and not the weak input would be transmitted, resulting in less noisy signals arriving in the olfactory cortex. Furthermore, PGCs are thought to inhibit OSNs via $GABA_B$ receptors. Several studies investigated the underlying mechanism of this feedback inhibition (Aroniadou-Anderjaska *et al.* 2000; McGann *et al.* 2005; Murphy *et al.* 2005; Wachowiak *et al.* 2005; Vucinic *et al.* 2006). Research suggests that feedback inhibition on OSNs is dependent on sensory activity (strength of odorant stimulus, sampling frequency of the nose) or spatial distribution of glomeruli. Pirez and Wachowiak challenged this idea in 2008 by *in vivo* experiments demonstrating that inhibition is not necessarily dependent on sensory activity, but rather tonically present even before an odorant is presented (Pirez and Wachowiak 2008). Presynaptic inhibition is thought to be necessary for several reasons (reviewed in McGann (2013)): first, the OSN synapse has an unusually high release probability, and without controlled inhibition, the vesicle pool would be rapidly depleted at high firing rates. Second, the dynamic range of response amplitudes to various odorant concentrations can be extended by shifting the level at which OSNs would saturate to a higher value. Third, tonic inhibition could serve as a gain control limiting sensory input as a function of the animal's brain state and behavior. Indeed, Petzold and colleagues showed that the presynaptic inhibition of OSNs is regulated by serotonergic inputs from the dorsal raphe nucleus in the brain stem (Petzold *et al.* 2009) and serotonergic neurons are known to change their activity depending on brain state (Jacobs and Azmitia 1992; Jones 2005). In conclusion, the suggested function of

PGCs is to decorrelate signals via intra-glomerular inhibition and to control the release of glutamate from OSNs via presynaptic inhibition.

Inter-glomerular inhibition, i.e., inhibition between glomeruli, is thought to be mediated by the inhibitory SACs and might serve lateral contrast enhancement (Cleland and Linster 2005). The cell bodies of SACs are slightly larger than the cell bodies of PGCs, and their dendrites course in the inter-glomerular space. SACs can extent their dendrites and contact 5-12 glomeruli (oligo-glomerular) or more than 30 glomeruli (poly-glomerular) (Kiyokage *et al.* 2010). As a result, SACs, in contrast to PGCs, can inhibit glomerular cells in far-distanced locations within the OB and not only in the glomerulus where they received synaptic input. The current model is that those SACs that receive a strong excitatory input from OSNs would inhibit weakly activated M/Ts in neighboring or distant glomeruli.

Lateral contrast enhancement was also suggested for GCs in the external plexiform layer. Here, a GC activated by a strongly activated M/T cell can inhibit weakly activated neighboring M/T cells via reciprocal dendro-dendritic synapses laying in the external plexiform layer. Besides contrast enhancement, another suggested function of GCs in the OB is facilitation of MC synchronizations and network oscillations (Bathellier *et al.* 2006; Lagier *et al.* 2007).

In summary, bulbar interneurons seem to be essential for the extraction of odorant identity and intensity from OSN inputs via intra- and inter-glomerular inhibition before the signal is forwarded by M/Ts to higher cortical areas. Another suggested function of PGCs is to adjust the sensory inputs of OSNs; while an additional suggested function of GCs is to facilitate MC synchronization.

1.2 Adult neurogenesis in the olfactory bulb

Contrary to the previous acknowledged dogma that the adult brain loses its potential to regenerate and refine synaptic connections after development, it has been shown that an established mature neuronal network can undergo various forms of plasticity (Holtmaat and Svoboda 2009; Yang and Zhou 2009; Piochon *et al.* 2016). One form is structural plasticity, where new synaptic connections are formed or existing connections are eliminated; another form is molecular plasticity, where synaptic connections are strengthened or weakened (Holtmaat and Svoboda 2009; Yang and Zhou

2009; Piochon *et al.* 2016). These refinements are thought to enable some flexibility in the response to new signals arising from complex and ever-changing environments. In addition to these refinements, a new form of neuronal plasticity was discovered in the last few decades: the addition of entirely new neurons into a pre-existing functional network, called 'neurogenesis' (Gage 2004). Here, new connections can be formed with neurons that have not been present before. Neither is it understood why entirely new neurons need to arise and structural/molecular plasticity is not sufficient, nor how connectivity and function of the network are preserved when new neurons integrate. Interestingly, in more complex nervous systems, neurogenesis seems to be less prominent (Kaslin *et al.* 2008), which could imply that integrity of complex neuronal circuits is incompatible with neurogenesis. In contrast to other vertebrates like birds and fishes, which show widespread neurogenesis in many brain regions (Kaslin *et al.* 2008), in mammalians, neurogenesis has only been observed in two brain regions: hippocampus and OB (Ming and Song 2011).

Thousands of these new 'adult-born cells' (ABCs) arrive every day in the OB after migrating from the subventricular zone (SVZ), which is a layer of tissue covering the walls of the lateral ventricles. In turn, elimination of neurons in the OB was also shown to take place (Sawada *et al.* 2011). In the rodent SVZ, neural stem cells give rise to neuroblasts (Doetsch *et al.* 1999), which migrate several days via the rostral migratory stream (RMS) into the OB (Lois and Alvarez-Buylla 1994)(Figure 2). More than 95% of these cells terminate their migration in deeper layers of the OB and become inhibitory GCs, while the remaining 5% migrate further radially to the glomerular layer and become mainly PGCs and, to a lesser extent, SACs (Alvarez-Buylla and Garcia-Verdugo 2002; Lledo and Saghatelyan 2005).
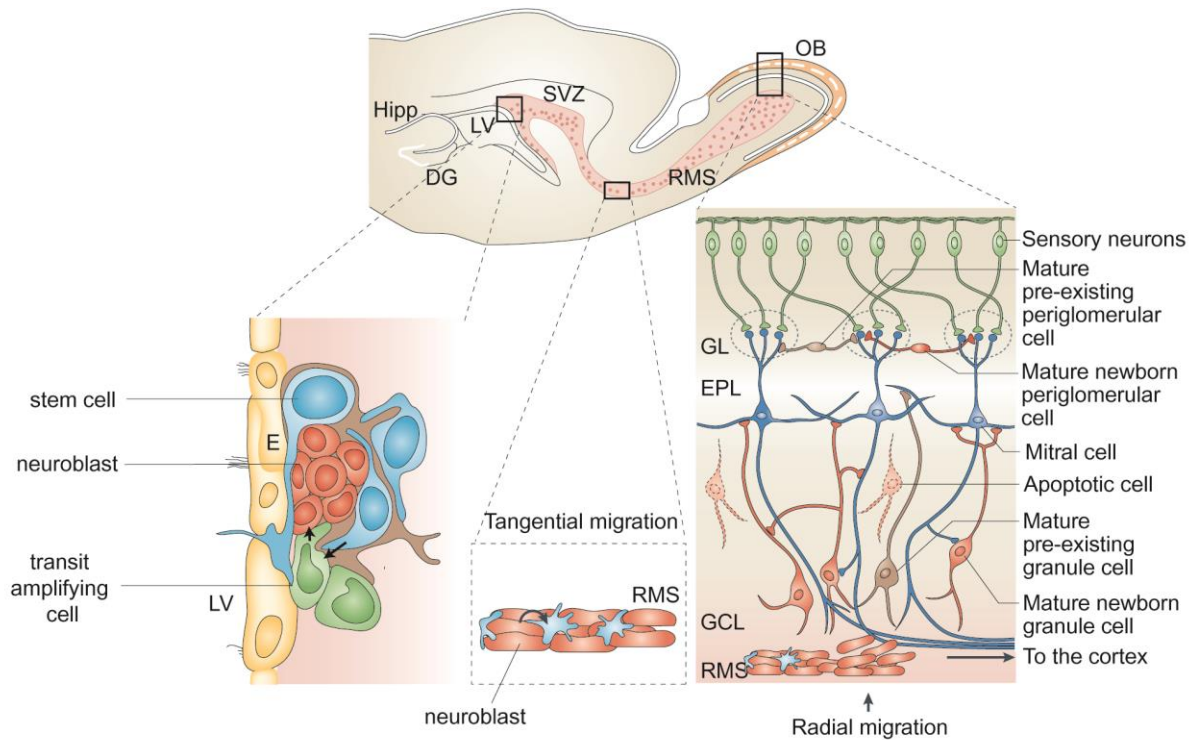
Figure 2. Production, migration, and integration of adult-born cells (ABCs).
ABCs arise from stem cells in the subventricular zone (SVZ) and migrate along the rostral migratory stream (RMS) to the olfactory bulb (OB). There, they migrate radially into the granule cell layer to become GCs and into the glomerular layer to become PGCs and SACs. One part of the ABCs dies, and the other part differentiates into mature cells and integrates into the pre-existing circuitry (modified after Lledo *et al.* (2006)). LV, lateral ventricle; E, epithelial cell; DG, dentate gyrus; Hipp, hippocampus.

It has been postulated that these ABCs enable a new form of plasticity for the neuronal system to adapt to the ever-changing environment. Thus, ABCs are suggested to detect new signals compared to pre-existing, resident cells. This hypothesis was tested by presentation of novel signals and subsequent measurement of ABCs' activity. In the OB, Magavi and colleagues showed that presentation of novel odorants increased the expression of the immediate-early gene Arc, a marker for neuronal activity, in adult-born but not resident olfactory GCs (Magavi *et al.* 2005). In the hippocampus, a different study by Danielson *et al.* showed in awake mice that adult-born GCs are crucial for the discrimination between novel and familiar contexts: by optogenetic silencing of adult-born GCs in the hippocampus, contextual discrimination was impaired (Danielson *et al.* 2016). Since ABCs were shown to detect new signals, it raised the question what would happen if signals from the environment are blocked. When sensory signals to the OB were blocked by closure of one nostril (naris occlusion), survival of ABCs was reduced in the respective hemibulb (Mandairon *et al.* 2006). On the other hand, an increase in sensory inputs via enrichment with odorants

has been shown to increase survival of ABCs in the OB (Rochefort *et al.* 2002; Bovetti *et al.* 2009; Bonzano *et al.* 2014). Thus, ABCs seem to be important for detection of new signals, and their survival depends on olfactory signals from the environment. Furthermore, it was observed that their survival is potentiated in animals undergoing specific behavioral tasks, like the odor discrimination task (Alonso *et al.* 2006), and that successful discrimination of odorants in this task depends on the activation of these neurons (Alonso *et al.* 2012). Reduction of adult neurogenesis impaired the animal's performance in odor discrimination tasks (Gheusi *et al.* 2000; Enwere *et al.* 2004). Besides detection and discrimination of odorants, it is believed that ABCs contribute to plasticity within the system, which is potentially required to learn new odor-driven behaviors, e.g. remembering to act in response to one specific odorant but not to another. Several studies confirmed their contribution to learning processes: ABCs have been shown to influence short-term olfactory memory (Rochefort *et al.* 2002; Breton-Provencher *et al.* 2009; Pan *et al.* 2012; Wang *et al.* 2015), long-term olfactory memory (Lazarini *et al.* 2009; Sultan *et al.* 2010), perceptual learning (Moreno *et al.* 2009), associative olfactory learning (Pan *et al.* 2012; Sakamoto *et al.* 2014; Wang *et al.* 2015), and fear learning (Valley *et al.* 2009; Pan *et al.* 2012). Furthermore, it has been described that ABCs may play a role in innate olfactory responses like pregnancy, mating behavior, male offspring recognition and male-male aggressive behavior (Shingo *et al.* 2003; Mak *et al.* 2007; Larsen *et al.* 2008; Feierstein *et al.* 2010; Mak and Weiss 2010; Sakamoto *et al.* 2011).

In several of these studies, adult neurogenesis was inhibited, and learning performance was measured. For example, after cytosine arabinoside infusion into the lateral ventricles (where the SVZ is located) or after irradiation of the SVZ with ultraviolet (UV) light, changes in short-term but not long-term memory were observed, while other authors described effects on long-term, but not short-term memory. These contradictory findings are a matter of discussion (Lledo *et al.* 2006; Lazarini and Lledo 2011; Breton-Provencher and Saghatelyan 2012; Gheusi and Lledo 2014) and might be probably due to the different ways how adult neurogenesis was inhibited. As it was the case for sensory inputs and odor discrimination tasks, also olfactory learning increases ABC survival (Moreno *et al.* 2009; Kermen *et al.* 2010; Sultan *et al.* 2010). The effect on odor discrimination and olfactory learning depends on the task and on the age of the ABCs (Mandairon *et al.* 2011; Alonso *et al.* 2012). Alonso *et al.*

showed that a direct activation of ABCs *in vivo* facilitated the discrimination between two odorants, but only when the task was difficult and involved perceptually similar odorants (Alonso *et al.* 2012). The observed effects on learning and memory were dependent on neuronal age (Mouret *et al.* 2008; Belnoue *et al.* 2011). Belnoue and colleagues showed that odorant stimulation preferentially activated immature neurons (around 2 weeks old) whereas associative learning based on odor discrimination activated mature neurons (5-9 weeks old) (Belnoue *et al.* 2011). Another function of ABCs has been proposed to be circuit maintenance (Cummings *et al.* 2014): maintenance of neuronal connections is of particular interest since it is in contrast to the idea that newly arriving cells might distort already present connections in the neuronal circuit as they form new connections. Cummings *et al.* described that the principal neurons of the OB, TCs, usually send their axons to the 'partner' glomerulus of the contralateral OB. There, the axons ramify in a specific constellation between the MC and GC layer. After blocking sensory input by naris occlusion, these ramifications broadened, but became refined again when the nostril was reopened. In a transgenic mouse where neurogenesis in the SVZ was inhibited, this refinement after nostril reopening was not possible anymore.

In summary, olfactory ABCs are believed to play a role in odor detection, odor discrimination, olfactory learning, innate olfactory behavior, and circuit maintenance.

1.2.1 *Comparison of adult-born and resident cells in the olfactory bulb*

As it is believed that ABCs are important for specific olfactory functions, it raised the question if they possess specific morphological and physiological properties. Indeed, it was shown that ABCs express more N-methyl-D-aspartate receptors (NMDARs) compared to α-amino-3-hydroxy-5-methyl-4-isoxazole-propionic acid receptors (AMPARs) in their plasma membrane (Grubb *et al.* 2008). ABCs also show different spontaneous activities (Belluzzi *et al.* 2003; Grubb *et al.* 2008; Livneh *et al.* 2014; Kovalchuk *et al.* 2015). For instance, Livneh *et al.* demonstrated in ketamine/medetomidine (K/M) anesthetized mice *in vivo* that 2-week-old adult-born PGCs had a lower spontaneous action potential (AP) firing rate than resident cells (Livneh *et al.* 2014), while Kovalchuk *et al.* showed in ketamine/xylazine (K/X) anesthetized mice, that 9-day-old adult-born PGCs had a lower spontaneous AP firing rate (Kovalchuk *et al.* 2015). Furthermore, Kovalchuk *et al.* described that ABCs show

different odor-evoked responses: odorant stimulation induced lower AP firing rates in 9-day-old PGCs at a specific stimulus concentration (9% saturated vapor) compared to resident cells, while Livneh *et al.* showed that adult-born PGCs at 4 weeks of age show higher odor-evoked AP firing rates (Livneh *et al.* 2014). Besides spontaneous and odor-evoked activity, response selectivity was also reported to be different (Livneh *et al.* 2014). Livneh *et al.* demonstrated that 2- and 4-week-old PGCs are less selective, i.e. they respond to more odorants than resident cells in K/M anesthetized mice. ABCs also show different morphological properties when they are young compared to when they mature (Mizrahi 2007; Livneh *et al.* 2009; Livneh and Mizrahi 2011). It was observed that the dendritic trees of immature adult-born PGCs were less densely branched with a lower total dendritic branch length, lower number of branching points and fewer intersections compared to mature adult-born PGCs (Mizrahi 2007; Livneh *et al.* 2009; Livneh and Mizrahi 2011). In addition, Livneh *et al.* described a lower number of postsynaptic density 95 (PSD95) puncta in immature adult-born PGCs (Livneh *et al.* 2009), an indication for fewer synaptic contacts. These puncta were more dynamic in immature adult-born PGCs, with a higher percentage of newly created PSD95 puncta and a lower percentage of stable PSD95 puncta described. Furthermore, the connectivity between adult-born GCs and MCs has been described to be more dynamic than the connectivity between resident GCs and MCs (Huang *et al.* 2016; Quast *et al.* 2017). For instance, Quast *et al.* analyzed connectivity in the context of receptive fields: when a GC has more connections with MCs, its receptive field is larger. The authors observed that receptive fields broadened during maturation, implying that GCs receive more inputs from MCs when they mature. This phenomenon was shown to be activity-dependent: upon sensory deprivation, the connections of MCs onto adult-born GCs reduced leading to shrinkage of their receptive fields. The authors suggested that these plastic receptive fields could act as a substrate for olfactory learning.

When ABCs mature, the ratio of AMPARs/NMDARs increases: these 'typical mature' glutamatergic synapses were observed in adult-born PGCs/SACs at 45 days of age (Grubb *et al.* 2008). Also spontaneous activity of ABCs becomes similar to resident cells as they mature: Livneh *et al.* showed for 8-to-9-week-old and Kovalchuk *et al.* for 7-to-13-week-old adult-born PGCs that their AP firing rates matched the firing rates of resident cells (Livneh *et al.* 2014; Kovalchuk *et al.* 2015). In both studies,

odor-evoked AP firing rates of mature adult-born PGCs and resident cells were similar (Livneh *et al.* 2014; Kovalchuk *et al.* 2015). Apart from that, odor-evoked activity was demonstrated to become more selective during maturation and thus similar to that of resident cells (Livneh *et al.* 2014; Wallace *et al.* 2017). Furthermore, the dynamics of dendrites and spines were shown to become more stable and thus similar to the dynamics found in resident cells (Mizrahi 2007; Livneh *et al.* 2009; Livneh and Mizrahi 2011). According to these findings, ABCs from an age of ~7/8 weeks on are assumed to be 'mature'.

On the other hand, mature ABCs (mABCs) still showed some properties that differed from those of resident cells. For instance, Livneh *et al.* showed that mature PGCs become more selective to odorants than resident cells if the environment was enriched with odorants when PGCs were 2-5 weeks old (Livneh *et al.* 2014). Wallace *et al.* showed in awake mice that adult-born GC dendrites become less selective after odorant enrichment (Wallace *et al.* 2017), in contrast to Livneh's finding for PGCs. However, in both cases, their selectivity was variable and dependent on sensory inputs from the environment. Interestingly, Wallace *et al.* showed that adult-born GCs consist of two subpopulations, one becoming more selective with maturation, and the other becoming less selective and instead broadening their responsiveness with maturation. Thus, even when the sensory inputs from the environment were not changed, one subpopulation of adult-born GCs will develop differently and become distinct to resident cells. In the hippocampus, the second region where significant adult neurogenesis has been observed in mammals, Ramirez-Amaya and colleagues showed that adult-born GCs stay more responsive towards new environmental contexts even when they mature, as indicated by an increased expression of the immediate-early gene Arc (Ramirez-Amaya *et al.* 2006).

Moreover, the dendritic morphology of mABCs remains plastic for a long time. *In vivo* time-lapse imaging studies in the OB have shown that new dendrites and spines were constantly formed or retracted on mature adult-born PGCs (Mizrahi 2007; Livneh *et al.* 2009; Livneh and Mizrahi 2011). Also in adult-born GCs, spines remained plastic after they matured (Sailor *et al.* 2016). Using a linear rate model let Sailor *et al.* to suggest that this spine plasticity might serve odor discrimination during learning processes (Sailor *et al.* 2016). Besides the so far described spine remodeling (addition and deletion of spines), which takes hours to days, also spine relocation

(extension of spine filopodia towards active dendrites) has been reported. Spine relocation has been observed on adult-born GCs in the OB and was described to take only minutes (Breton-Provencher *et al.* 2016). Since this relocation happens within minutes and not hours, it might serve other learning processes on a faster timescale. This behavior was found only in adult-born GCs, but not resident GCs. Breton-Provencher *et al.* performed sensory deprivation experiments and observed that filopodia-harboring spines were preserved after the deprivation while other spines were deleted. The authors speculated that this selection might help spines on GC dendrites to find and connect to an active MC dendrite faster. A modeling approach in the same study suggested that filopodia extension might provide a rapid way to change the set of synchronized MCs and as such, odorant information processing (Breton-Provencher *et al.* 2016).

In summary, the adult brain is capable of plasticity by adding ABCs into pre-existing neuronal networks. In the OB, ABCs are believed to detect new signals, discriminate between odorants, facilitate olfactory learning, contribute to innate olfactory responses, and maintain circuit specificity. Although the properties of ABCs became more similar to those of the pre-existing resident cells upon maturation, it has been observed that they retain some morphological and physiological differences. Studies about the physiological properties of ABCs and resident cells have been conducted so far predominantly in anesthetized mice. However, it is well known that anesthesia has a profound effect on brain activity (see next section) and might therefore affect the investigation and comparison of ABCs and resident cells in the OB.

1.3 Modulation of brain states by anesthesia

1.3.1 Effect of anesthesia on bulbar interneurons

Spontaneous and odor-evoked activity of olfactory GCs was shown to decrease under K/X anesthesia, as well as under urethane anesthesia (Kato *et al.* 2012). Moreover, GCs responded less selective to odorants in the awake state but became more selective under anesthesia (Kato *et al.* 2012; Cazakoff *et al.* 2014). Furthermore, it was reported that immature adult-born GCs respond less selective to odorants compared to mature adult-born GCs, and that this difference was stronger in awake state than under anesthesia (Wallace *et al.* 2017). Spontaneous and odor-evoked activities

of PGCs and SACs in the glomerular layer were shown to be lower under isoflurane anesthesia compared to the awake state (Wachowiak *et al.* 2013). However, in the study by Wachowiak *et al.*, measurements of PGCs and SACs were performed immediately after removal of isoflurane, so that the mouse has perhaps not completely recovered from anesthesia (see, e.g. Eger (1981)) Hence, it might be difficult to draw a clear conclusion from this data on how activities of PGCs and SACs change between awake and anesthetized state. As activity of OB interneurons was indicated to decline under anesthesia, it implies that some excitatory inputs to interneurons are active in the awake state, but not under anesthesia. Indeed, the OB receives centrifugal projections from various brain areas that modulate the activity of interneurons (see section 1.4.1 and Figure 4). Boyd and coworkers observed that optogenetic activation of pyramidal neurons in the olfactory cortex increases activity in inhibitory neurons in the OB (PGCs, SACs, and GCs) (Boyd *et al.* 2012), indicating a direct excitatory drive onto these interneurons. In a study by Boyd *et al.*, the activity of centrifugal projections from the olfactory cortex was compared between anesthesia and awake state. Since the OB forwards signals to the olfactory cortex, projections from the olfactory cortex back to the OB are also called 'feedback projections'. Boyd *et al.* labeled these feedback projections with a calcium (Ca^{2+}) indicator and measured activity of their terminals in the OB; they observed that spontaneous and odor-evoked activity in those terminals decreased when K/X or urethane anesthesia was induced (Boyd *et al.* 2015). The decrease in spontaneous activity of feedback projections under anesthesia was also observed in another study (Otazu *et al.* 2015).

1.3.2 The ascending reticular activating system (ARAS)

Anesthesia is known to suppress parts of the ascending reticular activating system (ARAS) leading to a state comparable to non-rapid eye movement (NREM) sleep (see 1.3.3). The ARAS consists of the ventral and the dorsal pathway and activates the cortex (including the OB) in the awake state (Dringenberg and Vanderwolf 1998; Detari *et al.* 1999; Semba 2000; Jones 2003). In the following, I will focus on the ventral pathway (Figure 3) which also targets the OB (see 1.4; Figure 4).
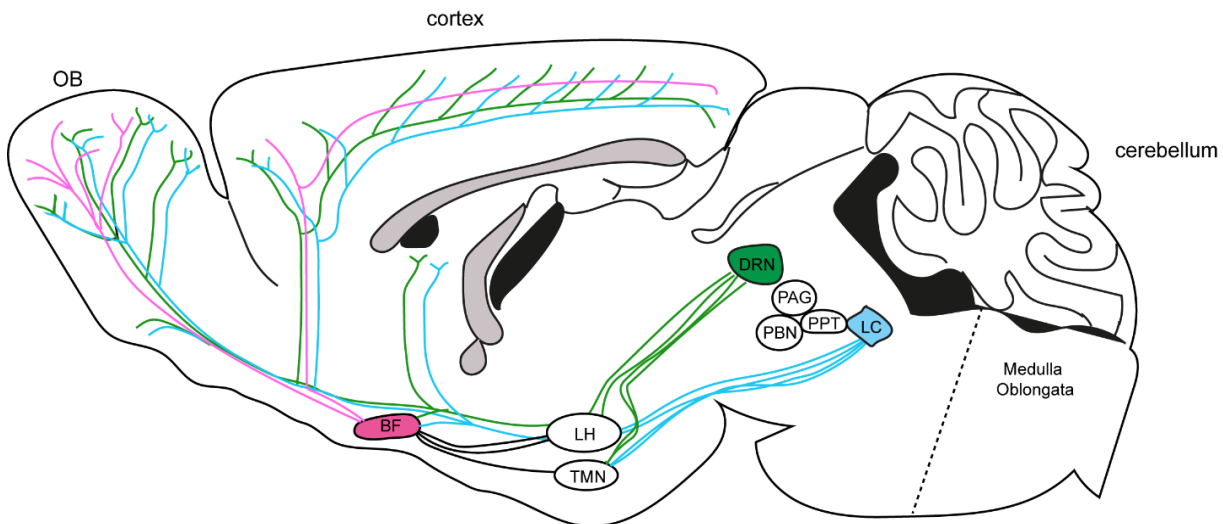
Figure 3. Ventral ARAS pathway excites cortex in the transition from sleep to arousal.
The dorsal raphe nucleus (DRN), the locus coeruleus (LC), the periaqueductal gray (PAG) and the parabrachial nucleus (PBN) send their axons to the lateral hypothalamic (LH) and tuberomammillary (TM) nuclei of the hypothalamus, as well as the basal forebrain. The LH and TM nuclei also ascend to the basal forebrain. The basal forebrain projects to the cortex and increases cortical activity. PPT, pedunculopontine tegmental nuclei. Illustration modified from Lorincz and Adamantidis (2017).

The ventral pathway of the ARAS consists of noradrenergic projections from the locus coeruleus, serotonergic projections from the dorsal raphe nucleus, dopaminergic projections from the periaqueductal gray and glutamatergic projections from the parabrachial nucleus. These projections target the lateral hypothalamic (LH) and tuberomammillary (TM) nuclei of the hypothalamus, as well as the basal forebrain. Projections from the LH and TM nuclei also ascend to the basal forebrain (Jones and Yang 1985). The basal forebrain projects to the cortex (Brown *et al.* 2010), leading to a higher state of cortical excitability. As reviewed in Brown *et al.*, firing rates of cholinergic neurons from the basal forebrain correlate with cortical activation, which is highest during wakefulness. Like acetylcholine, noradrenaline and serotonin promote wakefulness in the cortex. The average firing rates of cholinergic, noradrenergic, and serotonergic neurons decline during NREM sleep (Brown *et al.* 2012). In rapid eye movement (REM) sleep, noradrenergic and serotonergic neurons remain silent, while cholinergic neurons fire at higher rates (Lee *et al.* 2005; Brown *et al.* 2012; Lee and Dan 2012).

1.3.3 Action of anesthetic agents

'General anesthesia is a drug-induced, reversible condition that includes specific behavioral and physiological traits - unconsciousness, amnesia, analgesia, and akinesia - with concomitant stability of the autonomic, cardiovascular, respiratory, and ther-

moregulatory systems' (Brown *et al.* 2010). A critical issue in medicine and neuroscience is to understand how anesthetic agents mediate the suppression of arousal and cause other effects seen under anesthesia, of which many can be related to modulation of ARAS nuclei. Anesthetic drugs that are commonly used in mice, and which were used in this study are: (1) K/X, (2) 3-component narcosis (3CN), which is a combination of midazolam, medetomidine, and fentanyl, and (3) the volatile anesthetic isoflurane. Studies tested, for instance, the effect of GABA$_A$ potentiators (such as midazolam), α2 adrenergic receptor agonists (such as xylazine and medetomidine) and opioids (such as fentanyl) onto the brain nuclei that are part of the ARAS (reviewed in Brown *et al.* (2010)). These studies reported that GABA$_A$ potentiators increase the inhibition of the TMN, and thereby stop promotion of wakefulness (Nelson *et al.* 2002). The α2 adrenergic receptor agonists have been shown to inhibit release of noradrenaline from neurons in the locus coeruleus (Correa-Sales *et al.* 1992; Nelson *et al.* 2003). The electroencephalographic (EEG) patterns under α2 adrenergic receptor agonists closely resembled those of NREM sleep (Huupponen *et al.* 2008). Furthermore, it was described that opioids hyperpolarize cells in the periaqueductal gray via binding to μ, δ and κ opioid receptors. In addition, presynaptically activated opioid receptors can inhibit the release of acetylcholine, noradrenaline, serotonin, glutamate, and the neuropeptide substance P (Brown *et al.* 2010). Different anesthetic agents act on preferred target receptors, but the number of target receptors can change dependent on anesthesia depth (see Table 1). Xylazine and medetomidine are α2 adrenergic receptor agonists and lead to a block of noradrenaline release via activation of α2 receptors on presynapses of noradrenergic fibers whereby medetomidine is ten times more specific to α2 receptors than xylazine. Isoflurane potentiates GABA$_A$ receptors but was also shown to inhibit glutamatergic NMDARs, block AMPARs, and stimulate Kainate receptors. Furthermore, it can inhibit nicotinergic acetylcholine receptors (nAChRs), stimulate serotonin receptors, and interact with Na$^+$ channels, L-type Ca^{2+} channels, and K$^+$ channels. Moreover, midazolam and isoflurane potentiate the effect of the main inhibitory neurotransmitter in the spinal cord, glycine, inducing immobility during anesthesia. Ketamine is known to be a NMDAR antagonist, but it was also shown to inhibit nAChRs, to bind μ, δ and κ receptors of the opioid system and to interact with Na$^+$ channels, L-type Ca^{2+} channels and K$^+$ channels (Mion and Villevieille 2013). Furthermore, ketamine affects the serotonergic system, stimulates the release of noradrenaline, and inhibits the reuptake of

catecholamines (noradrenaline, adrenaline, dopamine), provoking a hyperadrenergic state. This hyperadrenergic state can be decreased when ketamine is applied to-gether with xylazine or medetomidine.

Table 1. Actions of different anesthetic agents used in this study on neurotransmitter receptors (Rec.). **+** denotes agonism, **-** denotes antagonism of the receptor, *dep.* means depolarization and **hyp.** means hyperpolarization of the cell after binding of the agent to the receptor. 5-HT, serotonin; NA, noradrenaline.

	GABA$_A$ Rec	nACh Rec	5-HT system	NA system	AMPA Rec	Kainate Rec	NMDA Rec	opioid Rec	Na$^+$-, Ca^{2+}-, K$^+$- channels
Ketamine		- → hyp	+/- → hyp/dep	+ → dep			- → hyp	+ → hyp	+/- → hyp/dep
Xylazine				+ (α2) → hyp					
Medetomidine				+ (α2) → hyp					
Midazolam	+ → hyp								
Isoflurane	+ → hyp	- → hyp	+ → dep		- → hyp	+ → dep	- → hyp		+/- → hyp/dep
Fentanyl								+ → hyp	

Anesthesia-induced reduction of interneuron activity in the OB, which was described in section 1.3.1, can have several common reasons, including potentiation of GABA$_A$ receptors on interneurons leading to increased inhibition, or blockade of glutama-tergic receptors (AMPARs, NMDARs) and nAChRs on interneurons leading to de-creased excitation. Finally, yet importantly, it was observed that centrifugal projec-tions from the olfactory cortex (see section 1.3.1) decrease their activity under anes-thesia and thus the excitatory drive onto interneurons could be missing. Further cen-trifugal inputs targeting the OB are described in the following section and arise from the ARAS nuclei, which are suppressed by anesthesia (see section 1.3.3).

1.4 Centrifugal inputs to the olfactory bulb

1.4.1 Neuromodulation of the olfactory bulb neurons

The OB receives a variety of neuromodulatory centrifugal projections from the olfac-tory cortex, and some ARAS nuclei, namely locus coeruleus, dorsal raphe nucleus and basal forebrain (Shepherd 2004; Willhite *et al.* 2006; Mouret *et al.* 2009).
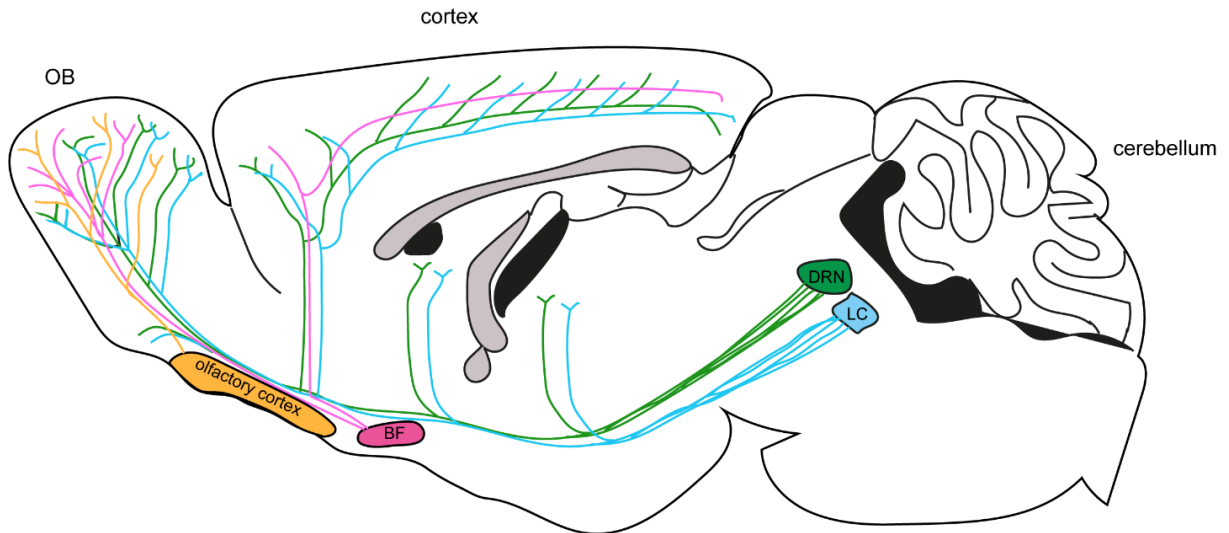
Figure 4. Centrifugal projections to the olfactory bulb.
The OB receives glutamatergic projections from the olfactory cortex (orange), noradrenergic projections from the locus coeruleus (LC, blue), serotonergic projections from the dorsal raphe nucleus (green) and cholinergic projections from the basal forebrain (BF, pink). Illustration modified from Lorincz and Adamantidis (2017).

The olfactory cortex provides glutamatergic inputs to the OB. These feedback projections target predominantly the GC and external plexiform layer and excite inhibitory neurons: PGCs, SACs, GCs and dSACs (Boyd *et al.* 2012; Otazu *et al.* 2015).

The locus coeruleus provides noradrenergic inputs to the external plexiform-, GC- and MC-layer (McLean *et al.* 1989; McLean and Shipley 1991). Noradrenaline binds to α1 adrenergic receptors on MCs resulting in depolarization (Hayar *et al.* 2001). Furthermore, noradrenaline was shown to excite or inhibit GCs via α1 or α2 adrenergic receptors, respectively (Nai *et al.* 2010). The strength of adrenergic innervation was reported to be sensory activity-dependent: naris occlusion increased fiber density in the external plexiform layer (Brinon *et al.* 2001). The noradrenergic transmission in the OB was suggested to be important for odor discrimination (Doucette *et al.* 2007; Mandairon *et al.* 2008) and olfactory learning processes (Rosser and Keverne 1985; Brennan *et al.* 1990; Sara *et al.* 1994; Shea *et al.* 2008; Shakhawat *et al.* 2012). Pandipati and colleagues suggested that noradrenaline might exert its effect on learning processes via inhibiting GCs, which would lead to MC disinhibition, so that MCs can fire synchronously to enable learning (Pandipati *et al.* 2010).

The dorsal raphe nucleus provides serotonergic inputs predominantly to the glomerular layer in the OB; and this in a heterogeneous fashion (McLean and Shipley 1987; Gomez *et al.* 2005). Larger glomeruli receive few serotonergic fibers, in con-

trast to relatively smaller glomeruli, which are highly innervated by serotonergic fibers. The serotonergic innervation is as well sensory activity-dependent, showing increased serotonergic fiber innervation after unilateral naris occlusion (Gomez *et al.* 2007). Application of serotonin has been shown to depolarize tonically active juxtaglomerular cells (Hardy *et al.* 2005) and stimulation of the dorsal raphe nucleus increased activity of PGCs and SACs (Brunert *et al.* 2016). PGCs express metabotropic 5-HT$_{2C}$ receptors. Upon activation by serotonin, PGCs release GABA and inhibit OSNs presynaptically (Petzold *et al.* 2009), enabling brain state-dependent control of odor sensitivity. On a faster timescale, serotonergic activation was also shown to modulate activity of the output neurons in the OB, TCs and MCs (Kapoor *et al.* 2016). McLean *et al.* found an impairment in olfactory learning after depleting serotonergic fibers in neonatal rat pups (McLean *et al.* 1993). Moriizumi *et al.* reported that olfactory learned avoidance of a repellent failed after serotonergic fiber depletion in rats. Furthermore, Moriizumi observed glomerular dystrophy, implying that serotonin is involved in cell survival and circuit maintenance (Moriizumi *et al.* 1994). Overall, the suggested function of serotonin in the OB is sensory gain control and facilitation of learning and memory.

The basal forebrain provides cholinergic inputs from a nucleus called 'horizontal limb of the diagonal band' (HDB). In contrast to the other centers, cholinergic projections target all bulbar layers (Macrides *et al.* 1981; Shipley and Adamek 1984; Zaborszky *et al.* 1986; Durand *et al.* 1998), although there are also studies indicating a preference for the glomerular layer (Kasa 1986; Porteros *et al.* 2007). The cholinergic innervation in the glomerular layer is also heterogeneous (Gomez *et al.* 2005; Salcedo *et al.* 2011). In addition, the extent of innervation is age-dependent: cholinergic innervation is sparse 2 days after birth (postnatal day 2, 'P2'), becomes greatest at P12 and then declines in the adulthood (Le Jeune *et al.* 1996; Durand *et al.* 1998; Salcedo *et al.* 2011), which implies a role of cholinergic projections in postnatal development. In the adult mouse, innervation has been shown to be sensory activity-dependent, showing diminished cholinergic innervation after naris occlusion (Salcedo *et al.* 2011). The action of acetylcholine in the OB is controversially discussed. It has various effects, depending on cell type and receptor type targeted in experiments. An application of cholinergic receptor agonists *in situ* in tissue slices (Castillo *et al.* 1999; D'Souza and Vijayaraghavan 2012; D'Souza *et al.* 2013) or *in vivo* in anesthetized

mice (Ravel *et al.* 1990) induced an increase in excitability of ETCs, MCS, and PGCs, whereby the bipolar PGCs described in Castillo's study rather resemble the nowadays classified SACs. The increase was mediated by nAChRs. Furthermore, Rothermel *et al.* showed that M/T cell firing is enhanced after optogenetic activation of cholinergic terminals in the OB of anesthetized mice (Rothermel *et al.* 2014). However, activation of cholinergic cells in the HDB itself led to reduced spontaneous activity of PGCs and M/Ts (Ma and Luo 2012). This discrepancy could arise from the different areas used to stimulate cholinergic transmission: stimulating the HDB may lead to indirect inhibition of M/Ts and other bulbar neurons through different pathways than direct activation of cholinergic terminals in the bulb as a more immediate method to alter cholinergic tone in the OB. The action of acetylcholine on GCs has been reported to be mediated via muscarinic acetylcholine receptors (mAChRs); GCs express various mAChR subtypes, which can result in either excitation via the M1 receptor (Castillo *et al.* 1999; Pressler *et al.* 2007), or inhibition via the M2 receptor (Kunze *et al.* 1992; Ma and Luo 2012). Activation of OB neurons by acetylcholine is believed to serve mainly three OB computations as reviewed in Devore and Linster (2012) and Li and Cleland (2013): (1) filtering of strong versus weak OSN inputs; (2) decorrelation of similar odorants to enhance contrast and (3) generation of gamma oscillations to facilitate learning and memory. These computations might underlie the so far described function of acetylcholine, which is the improvement of performance in learning and memory. Acetylcholine release from HDB fibers was shown to be involved in the enhancement of sensory perception during wakefulness, particularly during periods of sustained attention (Sarter and Bruno 1997; Himmelheber *et al.* 2000; Jones 2005; Hasselmo and Giocomo 2006), opposite to serotonergic action, which is highest during non-attentive states (Jacobs and Azmitia 1992; Jones 2005). Enhanced attention to sensory stimuli might be needed to facilitate sensory processing and improve memory encoding. Indeed, blockade of cholinergic transmission in the OB resulted in deficits in odor discrimination (Linster *et al.* 2001; Fletcher and Wilson 2002; Mandairon *et al.* 2006) as well as various forms of learning and memory such as habituation (Hunter and Murray 1989), odor-reward association (Roman *et al.* 1993) and short-term olfactory memory (Ravel *et al.* 1994). Furthermore, acetylcholine was reported to switch the dynamics of the piriform cortex network between the modes of olfactory learning (acetylcholine 'on') and memory recall (acetylcholine 'off') (de Almeida *et al.* 2013). From a clinical perspective, it is noteworthy that cholinergic neu-

rons degenerate early during neurodegenerative diseases (Coyle *et al.* 1983; Pepeu and Grazia Giovannini 2017) at the same time as olfaction declines (Coyle *et al.* 1983; Christen-Zaech *et al.* 2003).

In summary, centrifugal projections innervate different layers of the OB, whereby serotonergic and cholinergic projections predominantly target the glomerular layer and the noradrenergic projections target the external plexiform-, GC- and MC-layer. The innervation of those centrifugal projections is dependent on sensory inputs, and their activity is dependent on brain state (awake versus sleep; low versus high attention). Centrifugal projections to the OB mainly excite inhibitory neurons and mediate odor discrimination, learning and memory, and sensory gain control.

1.4.2 Neuromodulation of adult-born cells

Centrifugal inputs have been shown to target ABCs (Mouret *et al.* 2009; Lazarini and Lledo 2011). For example, projections from the olfactory cortex target immature (18-day-old) adult-born GCs (Deshpande *et al.* 2013). The strength of this innervation was increased after learning as shown in 32-day-old GCs (Lepousez *et al.* 2014). Noradrenergic projections were described to target immature adult-born GCs and control their survival (Bauer *et al.* 2003; Moreno *et al.* 2012). Moreover, serotonin was reported to influence ABCs by regulating neurogenesis: depletion of serotonin decreased neurogenesis in the SVZ (Brezun and Daszuta 1999) whereas injection of serotonin receptor antagonists increased neurogenesis (Soumier *et al.* 2010). In addition, in a mouse model of anxiety and depression, application of a selective serotonin reuptake inhibitor restored survival of ABCs and attenuated olfactory deficits (Siopi *et al.* 2016). Also cholinergic projections target immature ABCs. It was described that 14-day-old GCs receive cholinergic projections as their first neuromodulatory input during development and maturation (Whitman and Greer 2007). Furthermore, cholinergic projections have been shown to modulate survival of ABCs (Cooper-Kuhn *et al.* 2004; Kaneko *et al.* 2006). Mechawar *et al.* found that this modulation is dependent on the cholinergic receptor and cell type activated (Mechawar *et al.* 2004): activation of β2-nAChRs decreased the survival of adult-born GCs but not PGCs. In summary, so far, it has been reported that centrifugal projections promote the survival of adult-born immature GCs and PGCs. Anatomical projections have been investigated, to the best of my knowledge, only onto immature GCs, but not onto adult-born PGCs. Fur-

thermore, no studies comparing centrifugal projections between ABCs and resident cells have been published.

1.5 Aim of this project

The precise function of ABCs in the OB is not fully understood. Specifically, whether they become and remain a discrete cell population, or if they 'simply' replace pre-existing resident cells. Studies suggest that ABCs become like resident cells when they mature, but may retain some unique properties. The aim of this work was to understand if ABCs (specifically adult-born juxtaglomerular cells) retain unique features after their maturation regarding (1) spontaneous activity, (2) odor-evoked activity, (3) modulation by brain state via anesthesia, and (4) innervation by centrifugal projections.

Previously, the physiology of ABCs was measured predominantly in anesthetized animals. However, for several years it is well known that the activity of bulbar interneurons differs between awake and anesthetized state (see 1.3.1). Thus, to understand the genuine physiological properties of mABCs, we measured their spontaneous and odor-evoked activity in awake mice via measuring basal Ca^{2+} levels and odor-evoked Ca^{2+} signals, respectively, and compared these properties to those of resident cells.

Furthermore, it was tested if the brain state modulates mABCs differently than resident cells. As brain state is changed under anesthesia (see 1.3.3), anesthetic agents were used to modulate the brain state, and basal and odor-evoked Ca^{2+} signals of mABCs and resident cells were measured. Various anesthetic agents share some target receptors but also act specifically on other receptors. To avoid modulation of only specific receptors by one anesthetic agent, basal Ca^{2+} levels in mABCs and resident cells were compared under three commonly used anesthetic mixtures (K/X, 3CN, and isoflurane) that target a wide range of receptors (see Table 1).

Finally, brain state is regulated by the ARAS. OB neurons are known to receive centrifugal projections from ARAS nuclei (1.4) and these projections target ABCs and promote their survival. However, if these centrifugal projections target mABCs differently compared to resident cells is unknown. Therefore, we measured basal Ca^{2+} levels of both cell types in awake mice before and after topical application of pharmacological agents that block centrifugal target receptors in the OB.

2 Materials and Methods

2.1 Animals and viral vectors

To label ABCs, we used predominantly lentiviral vectors as they label more cells and result in higher transgene expression. The HIV-based lentiviral vector (FUGW as the backbone, Addgene 14883) was produced by Dr. Yajie Liang and Kaizhen Li in the Institute for Physiology II through transfection of HEK293T cells (Thermo-Fisher Scientific Inc.). To a lesser extent we used retroviruses, which were transfected in GPG-1F8 cells. Both vectors deliver a transgene to the cells for expression of the fluorescent Ca^{2+} indicator protein Twitch-2B. Expression was under control of ubiquitin or cytomegalovirus immediate early enhancer/chicken β-actin/ß-globin (CAG) promotor in lentiviruses or retroviruses, respectively. Lentiviral or retroviral vectors were injected into the RMS of 2-to-6-month-old C57BL/6 wildtype mice (Charles River).

Previous studies compared ABCs to neighboring resident cells, whose transmitter type (GABAergic/glutamatergic) or age was unknown. However, the ABCs in the OB mature into GABAergic interneurons and 3% new neurons arrive every month in the OB and integrate into the network (Mizrahi *et al.* 2006; Ninkovic *et al.* 2007; Brill *et al.* 2009). Thus, approximately 50% of neighboring cells is glutamatergic and one part is newborn. Therefore, in our study, we planned to compare mABCs to mature resident GABAergic cells (Res$_{GABA}$ cells). To label GABAergic cells in the OB, we used the transgenic mouse strain Viaat-Cre (B6.FVB-Tg(Slc32a1-cre)2.1Hzo/FrkJ; The Jackson Laboratories). 'Viaat' is the abbreviation for 'vesicular inhibitory amino acid transporter' and so expression is directed to inhibitory cells. Chao and colleagues reported specific Cre expression in GABAergic neurons in this mouse strain (Chao *et al.* 2010). The Viaat-Cre transgenic mice were injected at young age (3-to-4-week-old) with an adeno-associated virus (AAV) carrying a Cre-inducible transgene for Twitch-2B expression under control of the synapsin promotor (AAV1.CAG.Flex.Twitch2B.WPRE.SV40, Addgene 49531M; Penn Vector Core, University of Pennsylvania). Around 6 months after AAV injection, two-photon imaging was started, so that labeled GABAergic cells had time to mature.

C57BL/6 wildtype mice and Viaat-Cre transgenic mice of both sexes were kept under a 12-hour-light-12-hour-dark cycle with free access to food and water in the facilities of the Pharmacology and Toxicology Institute, University of Tübingen. All experimental procedures were performed in accordance with institutional animal welfare guidelines and were approved by the government of Baden-Württemberg, Germany.

2.2 Viral transfection to express a Ca^{2+} indicator in target cells

2.2.1 The genetically encoded Ca^{2+} indicator Twitch-2B

The Ca^{2+} indicator used in this project was the genetically encoded ratiometric Ca^{2+} indicator Twitch-2B (Thestrup *et al.* 2014), which consists of two fluorescent proteins, or 'fluorophores', (mCerulean3 and cpVenus^{CD}) and a troponin C-derived Ca^{2+} binding linker. Each of the fluorophores can be excited with a specific wavelength and emit at longer wavelengths. Upon binding of Ca^{2+} ions, the indicator changes its conformation, and the fluorophores move closer and change their orientation to each other (Figure 5A). In a distance (and orientation)-dependent manner, Förster resonance energy transfer (FRET) (Förster 1948) occurs from the donor fluorophore mCerulean3 to the acceptor fluorophore cpVenus^{CD}. With an increase in FRET efficiency, mCerulean3 fluorescence decreases while cpVenus^{CD} fluorescence increases. Thus, an increase of the cpVenus^{CD}/mCerulean3 ratio indicates an increased level of Ca^{2+} ions. When expressed in a cell, the rise in cpVenus^{CD}/mCerulean3 ratio indicates an increased level of Ca^{2+} ions in the cell's cytosol. Since the indicator is a ratiometric Ca^{2+} indicator based on FRET between the two fluorophores, it can detect basal Ca^{2+} levels, recorded in the absence of any experimental manipulation, as well as sensory-evoked Ca^{2+} signals. Upon rise in Ca^{2+} concentration after sensory stimulation, the increase in the cpVenus^{CD}/mCerulean3 ratio (from now on 'cpVenus/mCerulean ratio' or simply 'ratio') can be displayed as $\Delta R/R$; whereby ΔR is the difference between the ratio during stimulation minus the baseline ratio before stimulation. This difference is divided by the baseline ratio, R. When multiplied by 100, it results in $\Delta R/R$ in percent, which can range from ~26 % in hippocampal slices up to ~800% in the cuvette (Thestrup *et al.* 2014). Furthermore, Thestrup and colleagues showed that Twitch-2B binds Ca^{2+} with a sensitivity of ~200 nM (K_d) and that $\Delta R/R$ of Twitch-2B correlates linearly with the increase in the intracellular Ca^{2+} concentration at low (log Ca^{2+} [M] of -7.25 to -6.5) Ca^{2+} concentrations (Figure 5B). Note

that this correlation becomes logarithmic at higher Ca^{2+} concentrations. Besides indicating intracellular Ca^{2+} levels, when Twitch-2B is expressed in neurons, it can also indicate spiking activity (AP firing). In the same study by Thestrup *et al.*, it was shown that $\Delta R/R$ is correlated linearly with the number of APs that the cell fired (Figure 5C).
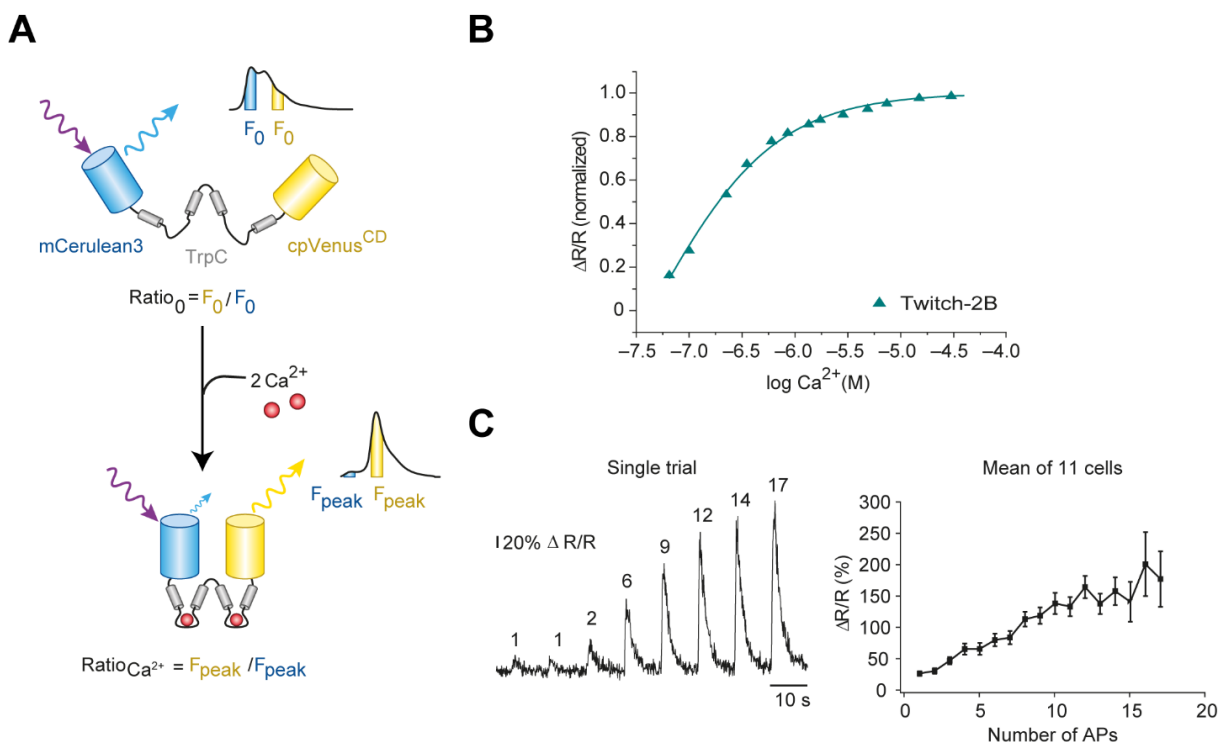
Figure 5. Working principle of the Ca^{2+} indicator Twitch-2B.
(A) Schematic drawing illustrating the conformational change of Twitch-2B upon binding of Ca^{2+} ions. The donor fluorophore mCerulean3 (blue) and the acceptor fluorophore cpVenus^{CD} (yellow) are connected with a troponin C-derived Ca^{2+} binding linker (TrpC). Modified after (Wilms and Hausser 2014). **(B)** Relationship between $\Delta R/R$ and the Ca^{2+} concentration in a cuvette. **(C)** Left panel: cortical pyramidal neuron in a brain slice was patched and Ca^{2+} transients were measured concomitantly with the number of underlying APs fired (number of APs is indicated above each Ca^{2+} transient). Right panel: relationship between $\Delta R/R$ and APs of cells. Displayed is the mean ± s.e.m. for 11 cells from 4 animals. Panels B and C are from Thestrup *et al.* 2014.

2.2.2 Preparation of mice for surgery

First, mice were anesthetized by intraperitoneal (i.p.) injection of either K/X (Sigma-Aldrich, 80/4 mg/kg of body weight (BW)), or 3CN (0.5 mg/kg BW medetomidine, Alfavet Tierarzneimittel GmbH; 5 mg/kg BW midazolam, Hameln Pharma plus GmbH; 0.05 mg/kg BW fentanyl, Albrecht GmbH). After 5-10 minutes, the animal's head was shaved using a veterinarian trim and povidone-iodine solution (B. Braun) was used to sterilize the shaved skin. Before an incision with a razor blade was made, local anes-

thesia was induced by subcutaneous (s.c.) injection of 0.2 ml xylocaine (2% w/v). An eye ointment (Bepanthen, Bayer) was used to prevent corneal drying during surgery. Next, the animal was positioned on a custom-made heating pad and its body temperature was monitored continuously using a rectal temperature probe. The body temperature was maintained between 35-37°C. Ear bars were used to fix the mouse head in a stereotactic device. Subsequent anesthesia maintenance was accomplished by injecting either half of the initial dose of K/X or one third of the initial dose of 3CN. Deep anesthesia was confirmed by the absence of a toe pinch reflex throughout surgery.

2.2.3 Stereotactic viral injection

After the mouse was prepared for surgery as described above (2.2.2), an incision into the skin was made with a razor blade, and the skin was pulled back to each side of the ear to reveal periosteum and bone. The periosteum was scraped off and the bone was cleaned with sterile ringer solution (in mM: 147 Na^+, 4 K^+, 2.2 Ca^{2+}, 156 Cl^-; B. Braun). The bone was dried using absorbent swabs (Kettenbach GmbH). To label ABCs, the coordinates for RMS injection were 3.0 mm anterior and 0.84 mm lateral to bregma. A high-speed dental drill (ultimate 500, NSK) was used to make a 0.5x0.5 mm hole in the skull above the injection site. A glass pipette (~10-40 μm internal diameter) was navigated to the coordinates.

For labeling of ABCs in the RMS, the lentivirus was sonicated in an ultrasonic bath and around 1.5-2.0 μl of pure virus was applied onto parafilm and drawn into the pipette. Then, the pipette was lowered into the brain to a depth of 3.0 mm, and 0.5 μl of the virus suspension were injected at three different depths (3.0, 2.9, 2.8 mm) over 3 minutes per depth.

For labeling of resident cells in the OB, virus suspension was not sonicated. The rostral rhinal vein between the prefrontal cortex and the OB was used as landmark. From there, the coordinates were 0.84 mm anterior and 0.93 mm lateral from the midline between the two hemispheres. The penetration angle for OB injections was set 45-50° from the horizontal plane to minimize tissue damage overlying the imaging field. Around 1.0-1.5 μl of virus suspension (1:7 diluted in ringer solution) was injected at three different depths: 0.35, 0.25, 0.15 mm with 0.33-0.50 μl over 3 minutes per depth.

At the end of the injection procedure, the skin incision was closed with sutures and droplets of xylocaine were administered on the wound. The non-steroidal anti-inflammatory drug carprofen (5 mg/kg BW, Pfizer GmbH) was injected s.c. to suppress inflammation and pain. When 3CN was used, the effect of its components (medetomidine, midazolam and fentanyl) was antagonized with a mixture of atipamezole (2.5 mg/kg BW, Alfavet Tier-arzneimittel GmbH), flumazenil (0.5 mg/kg BW, Fresenius Kabi Deutschland GmbH), and naloxone (1.2 mg/kg BW, Hameln Pharma plus GmbH) at the end of the surgery.

The mouse was brought back to its home cage for either one month (when ABC imaging was planned) or five months (when Res$_{GABA}$ cell imaging was planned), before a cranial window was implanted (see below). Mice were housed individually for several days after surgery.

2.3   Chronic cranial window implantation

2.3.1   Window implantation to measure basal and odor-evoked Ca^{2+} signals

After the preparation of the animal for surgery (as described in 2.2.2), dexamethasone (0.2 mg/kg BW, Sigma-Aldrich) was injected s.c. before the start of the surgery (to prevent swelling of the brain upon removal of the bone above the OB). A flap of skin above the OB was removed using razor blade and scissors. The periosteum was scraped off; the bone was cleaned with sterile ringer solution, and afterwards dried using absorbent swabs. Two craniotomies were made for each olfactory hemibulb: the region around both OB hemispheres and the midline bone covering the olfactory sinus between both hemispheres was thinned until two loosely attached islands formed. During drilling, sterile ringer solution was applied to prevent excessive heating that could damage the underlying tissue. When two loosely attached islands formed, first ringer solution was applied to prevent drying of the brain surface and then islands were gently removed with forceps while the midline bone was kept intact above the olfactory sinus.

As soon as bleeding occurred, ringer solution was applied again and subsequently removed with absorbent swabs. This procedure was repeated until bleeding stopped. After removal of the bone islands, a glass coverslip with 3 mm diameter (Warner Instruments) was positioned over both OB hemispheres. The coverslip was held with

forceps in place to allow application of cyanoacrylate glue around the border. After the glue dried, the rest of the skull surface was thoroughly dried with absorbent swabs and gentle airflow. In addition, the bone at the posterior part between the ears, near lambda, was scratched with a razor blade to facilitate adherence of the cement applied in further steps to the bone surface. This procedure was necessary to enable stable head fixation of awake mice during subsequent imaging experiments. After scratching the bone, a holder (see Figure 7, butterfly-shaped holder in right panel) was attached with dental cement (Tetric EvoFlow, Ivoclar Vivadent AG), which was solidified with UV light. Areas of the skull that remained exposed, as well as the border around the coverslip were covered with dental cement and solidified. The mouse was allowed to recover on the heating pad before it was returned to its home cage. To improve recovery, wet food was supplied in a petri dish for several days. To prevent bacterial infection, 0.2% (w/v) of the antibiotic enrofloxacin (Baytril, Bayer) was administered for 10 days with the drinking water. Furthermore, at the end of the surgery and for three days after surgery once a day, pain was prevented by s.c. carprofen injections. Mice were housed individually for several days after surgery. Typically, mice were imaged 21-28 days after surgery.

2.3.2 Implantation of window with slit for local application of antagonists

The coverslip used here (produced by Karlsruhe Nano Micro Facility, Wilhelm Pfleging) contained a slit with a size of 1.0x0.1 mm (Figure 6). Surgery and implantation of the coverslip were performed as described in 2.3.1. The OB is convex having its highest point in the center of the hemispheres, so that the slit was positioned rostral above the cavity between the OB hemispheres (see Figure 6). This ensured that no pressure was applied by the edges of the slit onto the brain surface, preventing swelling of the brain, as it would be the case by positioning the slit above the center of one hemisphere. In addition, a larger part in the center of the OB hemisphere would stay free for imaging. The slit was covered with Kwik-Cast and sealed on top with Kwik-Sil (both are silicon elastomers from World Precision Instruments). After surgery, mice were injected with carprofen and received wet food in the cage. Around 1 day later, animals underwent imaging experiments where the silicon elastomers Kwik-Cast and Kwik-Sil (Kwik-Cast/Sil) were removed before application of receptor antagonists (see 2.5.5).

rostral (towards nose)

open slit

drug

olfactory bulb

glass coverslip

caudal (towards ears)
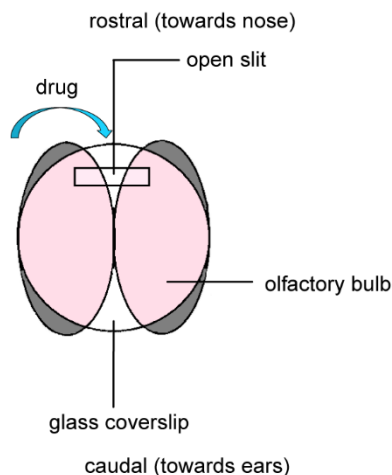
Figure 6. Glass coverslip implanted on the olfactory bulbs for chronic imaging.
The indicated open slit, positioned rostral, was only present in those mice that received antagonists to block neurotransmitter receptors (see 2.5.5).

2.4 Establishment of awake imaging

2.4.1 Fixation system

In order to perform two-photon imaging in awake mice, the holder and fixation system in the imaging setup had to be changed. A measurement of mice with the previous available holder and aluminum ring (see Figure 7, left panel) in the awake state was not possible as the mouse applied enough force while fixed in the system so that the holder broke off. To guarantee stable fixation, a different holder in the form of a but-terfly (see Figure 7), made of stainless steel or titanium, was created. The holder was modified according to a previous published version in Wienisch *et al.* (2012). The concave opening is pointing towards the OB. This holder had holes in the middle that could be filled with cement to allow attachment to the bone. Furthermore, the holder was fixed with screws on two sides into an aluminum ring to enable more stable fixa-tion by two spots instead of one spot, limiting the shaking of the imaging field.

Figure 7. Holder and aluminum ring for mouse fixation in the imaging setup.
Left panel displays the old version available in the lab. Right panel displays the new butterfly holder and the modified ring. Scale shows centimeters.

Additionally, the dental cement that we used was harder than the previous bone cement from Palacos R (Heraeus Medical). Furthermore, we scraped the bone with a razorblade to achieve a larger surface area for attachment of the cement. UV light, used to solidify the cement, was applied four times, from the rostral, the caudal, and from lateral sides. When the mouse was fixed for awake imaging, the respiration rate was monitored using a thermistor positioned in front of one nostril since the pressure sensor, which was usually attached to the back of anesthetized mice, was shaking on the awake moving mouse.

2.4.2 Training for awake imaging

Around two weeks before imaging, mice with implanted window and holder were habituated to the imaging setup. First, the mouse was lifted from the cage and brought back so it could adapt to sit on the hand. Afterwards, the mouse was placed on a table below the objective in the imaging setup to explore the unfamiliar environment. It was left there for around 10 minutes for 2-3 times a day. On the next day, the head of the mouse was secured with the butterfly holder in the aluminum ring, which was itself embedded in an x-y stage, thus enabling adjustments of the imaging field during imaging. The first fixation was ~2-5 minutes and was repeated ~2-3 times a day. After fixation, mice received sugar pellets as reward. The following day, fixation time was increased to Ten minutes. On every subsequent day, the duration was increased until the fixation time reached around one hour (in approx. 12 days). After this, two-photon imaging experiments were started. If mice were used in experiments where pharmacological agents were applied, they were trained before implantation of the cranial

window. In this case only, the head holder was fixed to the skull with dental cement, leaving the skin above the OB intact.

2.5 *In vivo* two-photon calcium imaging

2.5.1 *Imaging setup*

An Olympus Fluoview 1000 laser scanning microscope (BX61WI, Olympus Europa GmbH) was used, coupled to a mode-locked Ti:Sapphire laser (Mai Tai Deep See, Spectra Physics GmbH) which operates at 690-1040 nm with a pulse width of <100 fs and a repetition rate of 80 MHz. Images were acquired using a 20x UMPlan FI 1.0 NA water-immersion objective (Olympus Europa GmbH).

2.5.2 *Monitoring of mouse physiological parameters and anesthesia induction*

In awake mice, the respiration rate was monitored using a custom-built thermistor positioned in front of one nostril. When shifting from awake to anesthesia measurements, the mouse was kept fixed in the setup and injected i.p. with K/X or 3CN. To reduce movement, the mouse was briefly (for 1-2 minutes) sedated with isoflurane (2.5% in O_2) to prevent potential damage to the internal organs by the injection needle. When isoflurane was chosen as anesthetic, the isoflurane concentration was reduced to 0.9-1.5% in O_2 and kept constant after induction. Deep anesthesia was determined by loss of the toe pinch reflex and breathing rates were kept between 110 and 160 beats per minute. Ten minutes after anesthesia induction, two-photon imaging experiments were continued. In anesthetized mice, the respiration rate was monitored with a pressure sensor attached to the back. The respiration signals were sent to the computer and displayed with AD-Instruments software (AD Instruments GmbH).

2.5.3 *Measurement of basal Ca^{2+} levels*

Twitch-2B-expressing cells were imaged with a 20x objective and a zoom factor of 2 using an excitation wavelength of 890 nm. Fluorescence from mCerulean and cpVenus was separated using a 515 nm dichroic mirror; a 475/64 nm band pass filter was used to detect mCerulean fluorescence, while a 500 nm long pass filter was used to detect cpVenus fluorescence. Signals were collected by photomultiplier tube photodetectors. Time-series were recorded with an image size of 512x256 pixels, 100-250

frames at a rate of 4-7 Hz. The cells were measured 3-5 times to make an average of trials afterwards. In some experiments, mCerulean and cpVenus signals were derived from single frames of a 3-dimensional (3D) Z-series through the glomerular layer of the olfactory bulb. These 3D Z-series were acquired from the dura mater to a depth of around 120 µm with an image size of 640x640 pixels, using a Kalman-filter of 2 and a step size of 2 µm.

2.5.4 Measurement of odor-evoked Ca^{2+} signals

Ethyl tiglate (ETI, Sigma-Aldrich), an odorant known to activate the dorsal OB (Soucy *et al.* 2009) was filled into a tube, and a custom-built flow-dilution olfactometer (similar design as in Vucinic *et al.* (2006)) was used to mix saturated odorant vapor with clean air for a final concentration of 1.7% saturated vapor. The olfactometer tube was positioned approximately one centimeter in front of the mouse's snout. Six seconds were measured as a baseline before the odorant was applied. The odorant was delivered at a flow rate of 300 ml/min for four seconds per trial with an inter-trial interval of 1-2 minutes. Up to 8 trials were recorded.

2.5.5 Local application of antagonists in awake mice

Four weeks after surgery, we aimed to apply blocker solutions. However, this was not successful, as the dura mater in the slit became impermeable. This required us to perform functional imaging experiments as soon as possible after window implantation. Experiments immediately after or 1-2 days after surgery have been described before (Komiyama *et al.* 2010; Wachowiak *et al.* 2013; Roome and Kuhn 2014). In our study, we performed experiments around 1 day after cranial window implantation. This allowed the animal to recover from surgery before imaging, and anesthetics as well as the anti-inflammatory drug carprofen should have largely been removed from the body. Previous studies showed that 2 days after window implantation, astrocytes and microglia are in an activated state (Xu *et al.* 2007; Holtmaat *et al.* 2009), indicative of inflammatory processes. Furthermore, Park *et al.* described that the microvasculature changed, it showed stronger bleeding, vasodilation, and impaired blood flow 3 days after surgery compared to the day of surgery (Park *et al.* 2015). Therefore, experiments were performed around 12-24 hours after surgery, essentially to avoid states of strong inflammation occurring between 2 and ca. 30 days after window implantation (Xu *et al.* 2007; Holtmaat *et al.* 2009).

As no perfusion was performed, drugs were diluted in HEPES-buffered ringer solution (in mM: 150 NaCl, 4.5 KCl, 10 HEPES, 1 MgCl$_2$, 1.6 CaCl$_2$) to keep the pH constant.

To block noradrenergic receptors, the nonselective α1- and α2- adrenergic receptor antagonist prazosin (Sigma-Aldrich, used in Pan *et al.* (2004)) was used. First, prazosin was dissolved in dimethyl sulfoxide to a concentration of 25 mM before the solution was diluted to a final concentration of 100 µM in HEPES-buffered ringer solution. To block serotonergic receptors, the nonselective 5-HT$_1$-, 5-HT$_2$-, 5-HT$_7$- serotonin receptor antagonist methysergide (Sigma-Aldrich, used in Petzold *et al.* (2009)) was dissolved to a final concentration of 4 mM in HEPES-buffered ringer solution. To block cholinergic receptors, the mAChR-antagonist scopolamine and the nAChR-antagonist mecamylamine (both purchased from Sigma-Aldrich, used in Rothermel *et al.* (2014)) were prepared in HEPES-buffered ringer solution and mixed together to a final concentration of 50 mM and 115 mM, respectively.

To block AP firing (see 3.1.1, Figure 9), the voltage-gated sodium channel blocker tetrodotoxin (TTX) was dissolved to a concentration of 5 µM in HEPES-buffered ringer solution.

The coverslip had only a small (0.1x1.0 mm) opening, and this opening was located rostral above the cavity between the OB hemispheres (see Figure 6). To ensure that sufficient drug concentrations reached the target cells via diffusion, we used higher concentrations than the ones described previously in anesthetized mice where a wide area of the OB surface was perfused (Petzold *et al.* 2009; Rothermel *et al.* 2014).

On the imaging day, the mouse was head-fixed and control imaging sessions were performed with the Kwik-Cast/Sil still covering the slit. Then, Kwik-Cast/Sil was removed and the vehicle (HEPES-buffered ringer solution) was placed as a drop of around 40 µl on top of the coverslip with slit. Afterwards, antagonists were applied. Measurements of cpVenus and mCerulean fluorescence intensities were performed as time-series or 3D Z-series in the glomerular layer. Every cell was measured 3-5 times. To observe the effect of each antagonist on the same cell and to reduce the number of experimental animals, all blockers were applied sequentially on the same day. Two imaging series were performed with a gap of around 5 hours in-between sessions.

2.6 Data analysis

2.6.1 Time-series of basal and odor-evoked Ca^{2+} signals

The regions of interest (ROIs) were drawn manually in ImageJ (https://imagej.nih.gov/ij) and Fiji (http://imagej.net/Fiji) from an average image of all frames in a trial. Within the selected ROI, the intensity was averaged for the mCerulean and the cpVenus channel. The background ROI (comparable size as cell soma) was drawn in the darkest spot of the image. Further analyses were performed using custom-written scripts in MATLAB (The MathWorks, Inc.). In MATLAB, background intensity was subtracted from mCerulean and cpVenus signals. Then, the cpVenus signal was divided by the mCerulean signal to calculate the ratio trace. When no odorants were applied, these ratio values were averaged over all time points to receive a readout of the basal ratio. When odorants were applied, 1-5 seconds of the baseline period (before odorant application) were averaged to obtain the basal ratio. Since measurements were repeated 3-5 or 8 times in case of odorant application, respective individual ratio values were averaged to receive the mean basal ratio.

Odor-evoked Ca^{2+} transients were automatically detected when their ΔR/R signal was six times larger than the standard deviation of noise, and when a minimum as well as mean of 15% was reached. Those transients were defined as 'clear' responses. To acquire maximal ratios (R$_{max}$) of the Ca^{2+} transients, the ratio trace was smoothed two times with a binomial filter (time window: 0.3 seconds) and the maximum was determined between the 6th and 12th second after beginning of the recording.

Cells were considered as 'responding' when producing at least one Ca^{2+} transient in 8 trials, and as 'reliably responding' when producing a minimum of 5 Ca^{2+} transients in 8 trials. To investigate the variability between responses of 8 trials, the coefficient of variation (CV) was determined with the following formula:

$$cv = \frac{SD}{\bar{x}} * \left(1 + \frac{1}{4*n}\right)$$

Where SD is the standard deviation, $\bar{x}$ is the average maximal ratio of the 8 Ca^{2+} transients, and n is the number of trials. The part in brackets is the correction for small sample sizes.

2.6.2 Three-dimensional Z series of basal Ca^{2+} signals

A MATLAB script, written by a student (Marie Schmidt) in the lab during her internship, was used to load 3D-stacks, draw ROIs, and extract fluorescence intensity values of mCerulean and cpVenus out of one frame for each cell. Fluorescence intensity values were processed further as described for time-series: the background fluorescence was subtracted and a ratio of cpVenus/mCerulean was calculated. This ratio value was averaged over several trials (3-5) to receive the mean basal ratio.

2.6.3 Calculation of the effect size

In experiments where anesthesia or neurotransmitter receptor antagonists were applied, a reduction of basal ratios, indicative of basal Ca^{2+} levels, was calculated as percentage of block that was reached, termed 'effect size'. This allowed a comparison of the effects of different anesthetic agents or receptor antagonists, and a quantification of the reduction for each cell independently of its starting ratio (in control condition). For instance, cells with low basal ratios or high basal ratios (see Figure 9B for distribution of ratio levels) may all be reduced to a lower ratio, but the absolute reduction for each cell is different; cells at lower ratios will show a smaller reduction than cells with higher ratios. Thus, we calculated an effect size. First, the minimum ratio level that was ever measured throughout all conditions in both the mABC and Res$_{GABA}$ cell population was determined: 1.25. Next, the maximum theoretically possible block was defined as the reduction towards this lowest ratio level. Thus, the difference between the basal ratio measured in the control condition and 1.25 was calculated, (R_{ctr} - 1.25). On the other hand, the observed difference in ratio between control and test condition was calculated, (R_{ctr} - R_{test}). Effect size was calculated by dividing the actual difference by the maximal theoretically possible difference.

$$\text{effect size } (\%) = \frac{R_{ctr} - R_{test}}{R_{ctr} - 1.25} \text{ x } 100$$

2.7 Immunohistochemistry

To test how many immature cells we have in our mABC population, we stained OB slices from C57BL/6 mice injected with lentiviruses encoding Twitch-2B. We used the immature cell marker doublecortin (DCX). After perfusion with phosphate-buffered saline (PBS, Sigma-Aldrich) followed by 4% formaldehyde (in PBS), both OBs were removed and post-fixed with 4% formaldehyde overnight at 4°C. Next, the OBs were cryoprotected overnight at 4°C in PBS containing 25% sucrose, followed by embedding in TissueTek (Sakura, Inc.) and freezing at -80°C. Antibody staining was performed with free-floating sagittal cryoslices (50 μm thick) at room temperature. To prevent nonspecific binding, sections were treated with a blocking solution (5% normal donkey serum and 1% Triton X-100 in PBS) for one hour. After blockage, slices were exposed to primary antibodies diluted in blocking solution at room temperature overnight. On the next day, the sections were washed in PBS three times for 10 minutes and incubated with secondary antibodies diluted 1:1000 in PBS containing 2% bovine serum albumin for two hours in the dark at room temperature. Finally, the sections were washed three times in PBS, transferred to Superfrost Plus charged glass slides (R. Langenbrink GmbH) and mounted with Vectashield Mounting Medium (Vector Laboratories) or ProLong Gold Mounting Medium (Thermo-Fisher Scientific Inc). Stained slices were imaged with a 40x water-immersion objective (Nikon 40x, 0.8 NA) using the Olympus Fluoview 300 laser scanning microscope system coupled to a Mai Tai mode-locked Ti:Sapphire laser operating at 690-1040 nm wavelength (Spectra Physics GmbH). Alexa Fluor 488 and 594 were excited simultaneously at 800 nm and their fluorescence emission was split with a 570 nm dichroic mirror.

Table 2. Antibodies used to label Twitch-2B-expressing immature cells in the ABC population.

Species	Antibody	Company	Dilution
goat	primary polyclonal antibody against GFP	Rockland 600-101-215	1:2500
rabbit	primary polyclonal antibody against DCX	Abcam ab18723	1:2000
donkey	secondary anti-goat IgG-conjugated Alexa Fluor 488	Thermo-Fisher Scientific Inc. A11055	1:1000
donkey	secondary anti-rabbit IgG-conjugated Alexa Fluor 594	Thermo-Fisher Scientific Inc. A21207	1:1000

2.8 Statistical analysis

Statistical tests were performed with MATLAB, GraphPad Prism (GraphPad Software, www.graphpad.com), or Vassar Stats (website for statistical computation, http://vassarstats.net/, Richard Lowry 1998-2017). The one-sample Kolmogorov-Smirnov test was used to check for normality of the data. All statistical tests were two-sided, unless otherwise noted. The p values smaller than 0.05 were considered significant.

3 Results

3.1 Ca^{2+} signaling in mABCs and Res$_{GABA}$ cells of awake mice

ABCs in the OB are thought to serve specific functions in the processing of olfactory information and so the question arose if they also possess specific physiological properties to enable these functions. Previous studies suggested that ABCs become similar to resident cells when they mature, but might retain some unique physiological properties. Here, it was investigated if the basal and odor-evoked Ca^{2+} signals of mABCs are different to those of Res$_{GABA}$ cells. For this, cells were first labeled with the Ca^{2+} indicator Twitch-2B. After labeling ABCs by viral transfection into the RMS, we waited for at least 8 weeks (56 days/DPI, 'days post injection') to ensure maturity of cells. However, because lentiviruses, commonly used in this kind of experiments (see Grubb *et al.* 2008; Livneh *et al.* 2014; Kovalchuk *et al.* 2015; Wallace *et al.* 2017), infect not only dividing cells, it is possible that a fraction of the labeled population might be generated during later divisions of the labeled precursor cells and thus be younger than DPI 56. To estimate the fraction of young cells in the mABC population, we labeled mABCs with DCX, known to be expressed in ABCs up to an age of 21 days (Brown *et al.* 2003; Grubb *et al.* 2008). Figure 8A shows an example field-of-view that contains 14 Twitch-2B-expressing cells (green), of which one is DCX-positive (red). On average, the proportion of cells expressing both DCX and Twitch-2B was 18% (Figure 8B); estimated from 511 cells in 5 mice. This indicates that 18% in the mABC population were younger than 21 days.
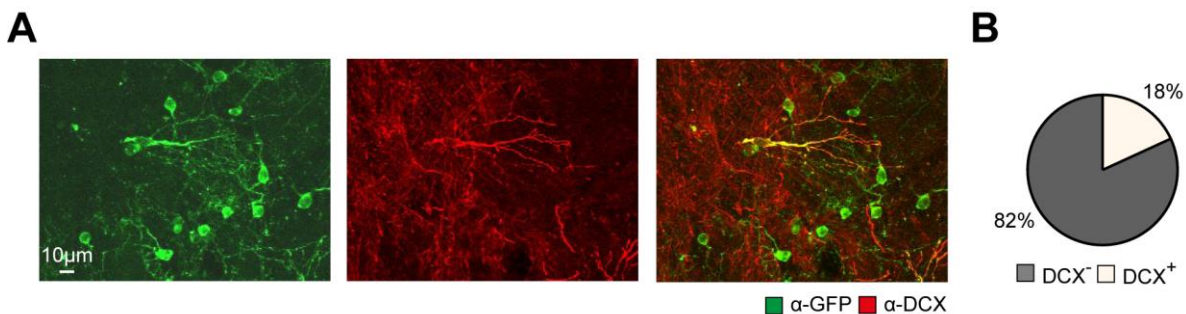

Figure 8. Percentage of immature cells in the mABC population.
(A) Maximal intensity projections of a Z series (40 frames at 1-µm step size) show mABCs expressing Twitch-2B (green, identified with anti-GFP antibody) and DCX (red); merged channel on the right shows co-labeling (yellow). **(B)** Percentage of DCX$^+$ and DCX$^-$ cells (511 cells from 5 mice).

3.1.1 Mature ABCs have high basal Ca^{2+} levels in awake state

Figure 9A shows a representative *in vivo* image of mABCs expressing Twitch-2B. As explained in the methods chapter 2.2.1, when Ca^{2+} binds to Twitch-2B, the cpVenus/mCerulean ratio increases. Thus, a higher ratio indicates a higher level of Ca^{2+} in the cell. In awake mice, the basal ratios (without external stimulation) for mABCs ranged from 1.55 to 8.41 (Figure 9B; 154 cells, 13 mice). While higher ratios correspond to higher intracellular Ca^{2+} levels and ΔR/R was shown to correlate linearly with AP firing of a cell, we wanted to know which basal ratio levels correspond to which activity states (in terms of AP firing). To identify ratios corresponding to spiking and non-spiking states respectively, we blocked AP firing via a topical application of the voltage-gated sodium channel blocker TTX (see 2.3.2 and 2.5.5 methods section). Upon application of TTX, ratios of mABCs shifted below 2 (Figure 9C; 35 cells, 2 mice). The inset in Figure 9C shows a representative cell where the mCerulean (green) and the cpVenus (red) channel were merged. This predominantly resulted in red color in the control condition, indicating a higher ratio and thus a higher Ca^{2+} level. The cell changed its color from red in the control condition to yellow (low Ca^{2+} level) under TTX. Since TTX reduced ratio levels below 2, in further analyses cells with ratio levels <2 were classified as 'non-spiking'. Figure 9D displays a cumulative probability histogram of the data shown in Figure 9B, indicating that only around 18% of mABCs were non-spiking (ratio <2) in the awake state. To account for cells that change from spiking to non-spiking states and vice versa (observed over prolonged imaging repetitions, data not shown), or for a possible variability in estimating the exact ratio due to background subtraction, we introduced a safety margin between ratios of 2 and 2.4. Only cells with high average basal ratios >2.4 were considered 'spiking', while cells with ratios between 2 and 2.4 were considered 'uncertain'. Using this categorization, 59% of mABCs were classified as spiking in the awake state, while 23% had ratios above 2 but below 2.4 and thus were classified as uncertain. The remaining 18% were non-spiking (Figure 9D).
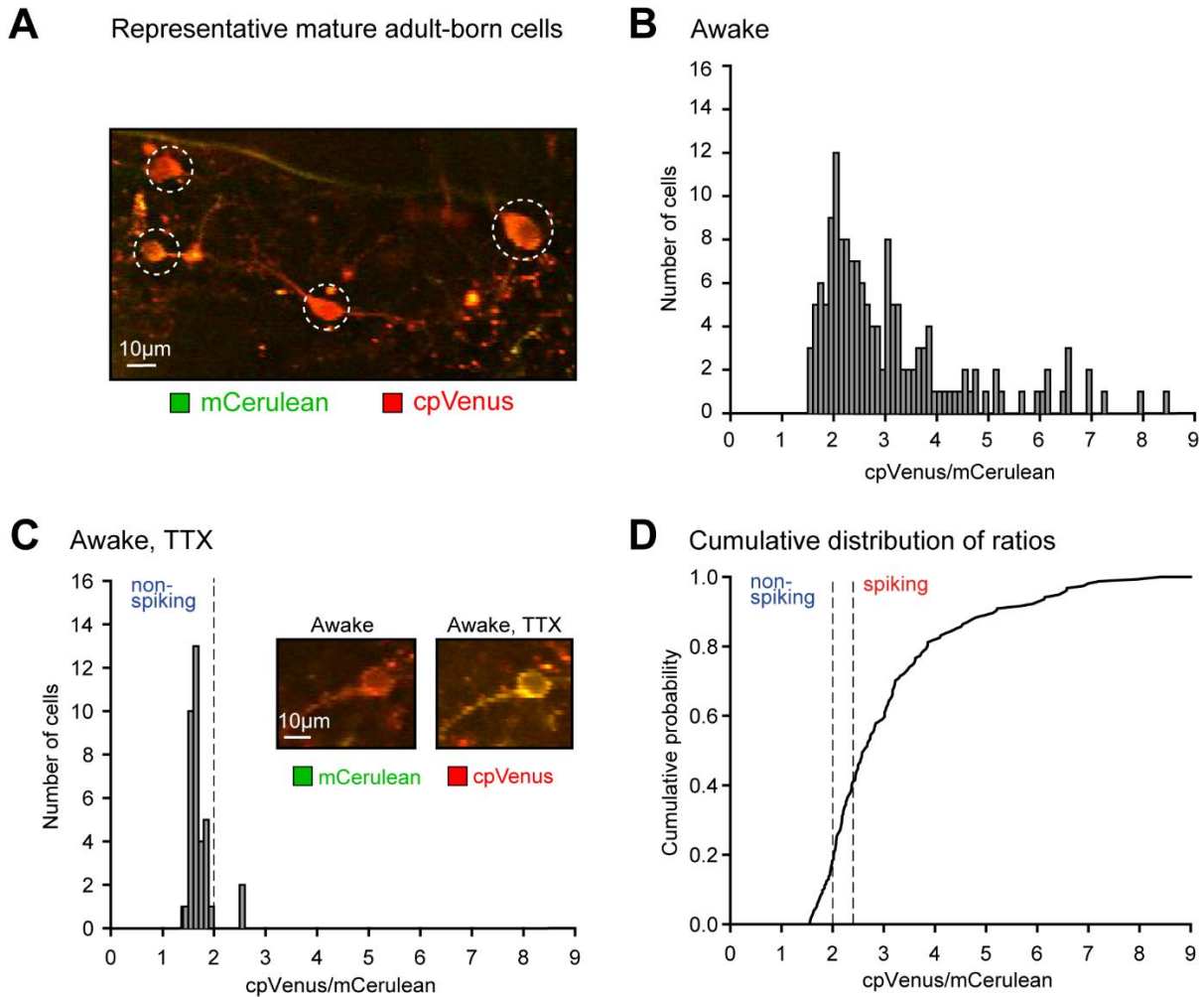
Figure 9. Basal ratios of mABCs in the awake state.
(A) Average intensity projection of a time-series (100 frames, ~4 frames/second) showing mABCs at 56 DPI. The cells express the FRET-based Ca^{2+} indicator Twitch-2B, which increases its cpVenus/mCerulean ratio upon Ca^{2+} binding. Merging mCerulean (green) and cpVenus (red) channel results in predominantly red color of cells, indicating a higher intracellular Ca^{2+} level. **(B)** A histogram illustrating the ratio distribution in 154 mABCs from 13 mice. **(C)** A histogram illustrating the ratio distribution of mABCs in the presence of TTX (35 cells from 2 mice). Inset displays a cell before (left, ratio 4.0) and during (right, ratio 1.6) TTX application. Vertical broken line indicates the border below which cells were non-spiking. **(D)** Cumulative probability histogram of the data shown in B with broken lines indicating borders between non-spiking and spiking populations. Cells with ratios between 2.0 and 2.4 were considered uncertain.

Next, we tested whether basal ratios of individual cells were stable over time. Ratios of the same cells were measured on one day and re-examined 3 and 6 days later. The scatter plot in Figure 10A shows basal ratios measured on day 0 plotted against basal ratios of the same cells on day 3 or 6 (35 cells, 5 mice). Some cells showed higher or lower ratios at later time points indicating that their basal Ca^{2+} levels were increased or decreased, respectively. Nevertheless, on a population level, the ratios at later time points were similar to the ratios measured on day 0, as shown by a box

plot displaying the medians of normalized ratios per mouse (Figure 10B; p=0.312 day3/day0 and p=0.187 day6/day0; 5 mice; Wilcoxon Signed-Rank test).
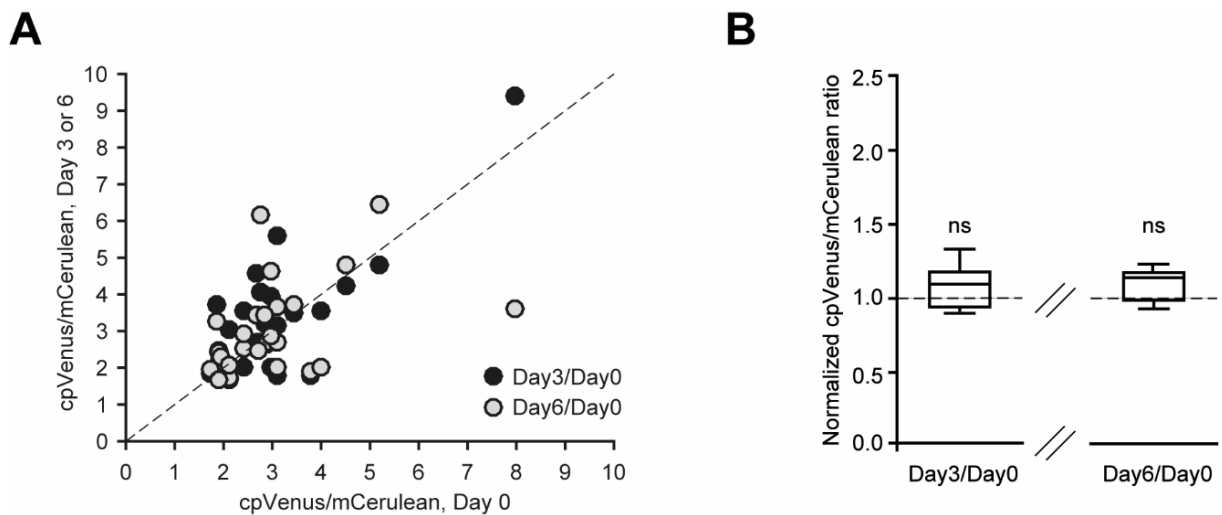

Figure 10. Stability of basal ratios in mABCs.
(A) Scatter plot showing the ratios of a cell on one day plotted against the ratio 3 or 6 days later (35 cells from 5 mice). Diagonal broken line indicates the unity line. **(B)** Box plots represent the medians of normalized ratios per mouse for ratios measured on day 0 and 3 or 6 days later. There was no significant change in ratios on day 3 or on day 6 (p=0.313 and p=0.187 respectively; n=5 mice; Wilcoxon Signed-Rank test).

3.1.2 Basal Ca^{2+} levels are similar between mABCs and Res_{GABA} cells

As ABCs mature to become GABAergic interneurons, we compared mABCs to mature Res_{GABA} cells. An example field-of-view in Figure 11A shows Twitch-2B-expressing Res_{GABA} cells. In the Res_{GABA} cell population, the distribution of basal ratios ranged from 1.27 to 6.05 in awake mice (Figure 11B; 382 cells, 5 mice). The cumulative probability histogram of basal ratios was not significantly different between mABCs and Res_{GABA} cells (Figure 11C; p=0.215; 154 mABCs from 13 mice, 382 Res_{GABA} cells from 5 mice; Kolmogorov-Smirnov test). As indicated by the broken line at a ratio of 2.0 in Figure 11C, most cells in both groups showed ratios higher than 2.0. The fraction of non-spiking cells as well as the fraction of spiking and uncertain cells was not significantly different between the mABCs and Res_{GABA} cells (Figure 11D; p=0.074; Chi-Square Test). Median ratios per mouse were also not significantly different between the mABCs and Res_{GABA} cells (Figure 11E; p=0.503; 5 mice versus 13 mice; Mann-Whitney test).
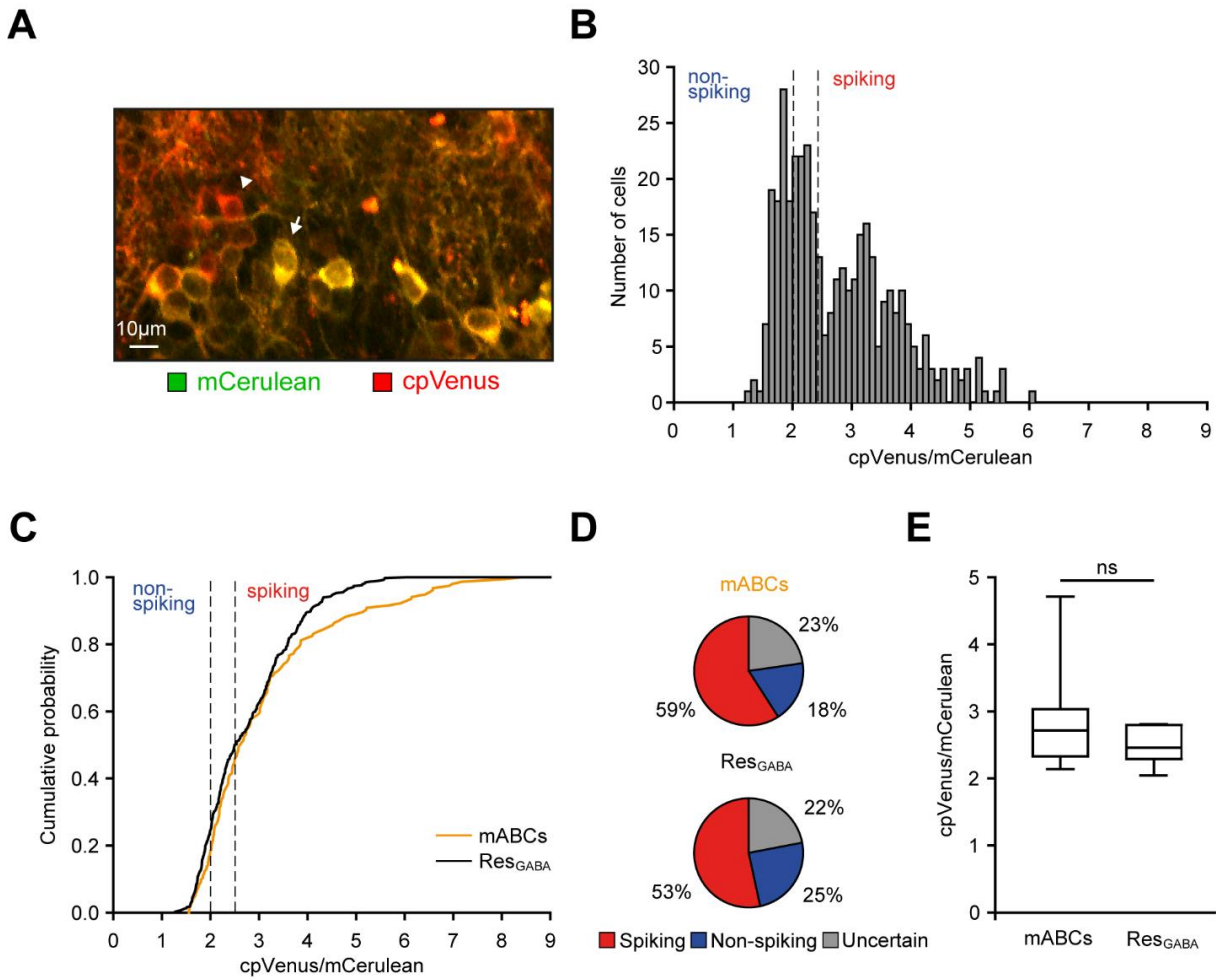
Figure 11. Basal ratios of Res$_{GABA}$ cells and comparison to mABCs in awake mice.
(A) Average intensity projection of a time-series (250 frames, ~7.7 frames/second) showing Twitch-2B-expressing Res$_{GABA}$ cells around 6 months post injection. The arrowhead points to a cell with a high basal ratio (>2.4), whereas the arrow points to a cell with a low basal ratio (<2). **(B)** A histogram illustrating the ratio distribution in 382 Res$_{GABA}$ cells from 5 mice. Broken vertical lines mark the borders for spiking and non-spiking cells. **(C)** Cumulative probability histograms illustrating the distribution of ratios of mABCs and Res$_{GABA}$ cells, which were not significantly different from each other (p=0.215; 154 versus 382 cells; Kolmogorov-Smirnov test). Broken vertical lines mark the borders for spiking and non-spiking cells. **(D)** Pie charts showing the fractions of spiking, non-spiking and uncertain cells, which were not significantly different between mABCs and Res$_{GABA}$ cells (p=0.074; Chi-Square Test). **(E)** Box plots showing the medians of ratios per mouse, which did not differ significantly between mABCs and Res$_{GABA}$ cells (p=0.503; 13 mice versus 5 mice; Mann-Whitney test).

In summary, the basal ratios, indicative of basal Ca^{2+} levels, were similar between mABCs and Res$_{GABA}$ cells. Furthermore, the basal ratios of cells were stable over days. In the awake state, around 60% of mABCs and 50% of Res$_{GABA}$ cells had high basal ratio levels above 2.4 and were therefore considered 'active', or spiking.

3.1.3 Odor-response properties are different between mABCs and Res$_{GABA}$ cells in the awake state

Next, we analyzed odor-evoked Ca^{2+} signals induced by application of the odorant ETI at a concentration of 1.7% saturated vapor in front of the mouse's snout. The odorant was applied 8 times with an interval of 1-2 minutes between the trials and induced clear Ca^{2+} transients in mABCs (Figure 12A) and Res$_{GABA}$ cells (Figure 12B). Cells that responded at least once in 8 trials were classified as 'responding'. From these responding cells, those that responded to minimum 5 out of 8 trials were termed 'reliably responding'. Compared to Res$_{GABA}$ cells, mABCs had a significantly lower percentage of responding cells (Figure 12C; $p<0.0001$; 83 mABCs from 7 mice, 222 Res$_{GABA}$ cells from 5 mice; Chi-Square test). Furthermore, mABCs responded less reliably (Figure 12D; $p<0.001$; 57 mABCs from 7 mice, 203 Res$_{GABA}$ cells from 5 mice; Chi-Square test). At the same time, reliably responding mABCs responded with a higher maximal ratio during the odorant application phase (Figure 12E; $p=0.038$; 36 mABCs from 7 mice, 174 Res$_{GABA}$ cells from 5 mice; Kolmogorov-Smirnov test). The variability between maximal ratios of 8 trials was estimated using the coefficient of variation (CV, see methods chapter 2.6.1). The distribution of CVs was not significantly different between mABCs and Res$_{GABA}$ cells (Figure 12F; $p=0.930$; $n=36$ mABCs from 7 mice, 174 Res$_{GABA}$ cells from 5 mice; Kolmogorov-Smirnov test). As shown in Figure 11, basal ratios of mABCs did not differ from those of Res$_{GABA}$ cells, but the maximal ratios in response to odorant application were higher in mABCs compared to Res$_{GABA}$ cells (Figure 12E). Thus, we tested if there is any correlation between basal and odor-evoked maximal ratios. Figure 12G shows that the basal ratios significantly correlated with the odor-evoked maximal ratios in both cell groups (mABCs: $r=0.54$, $p<0.0001$; Res$_{GABA}$ cells: $r=0.58$, $p<0.0001$; Spearman's rank correlation).
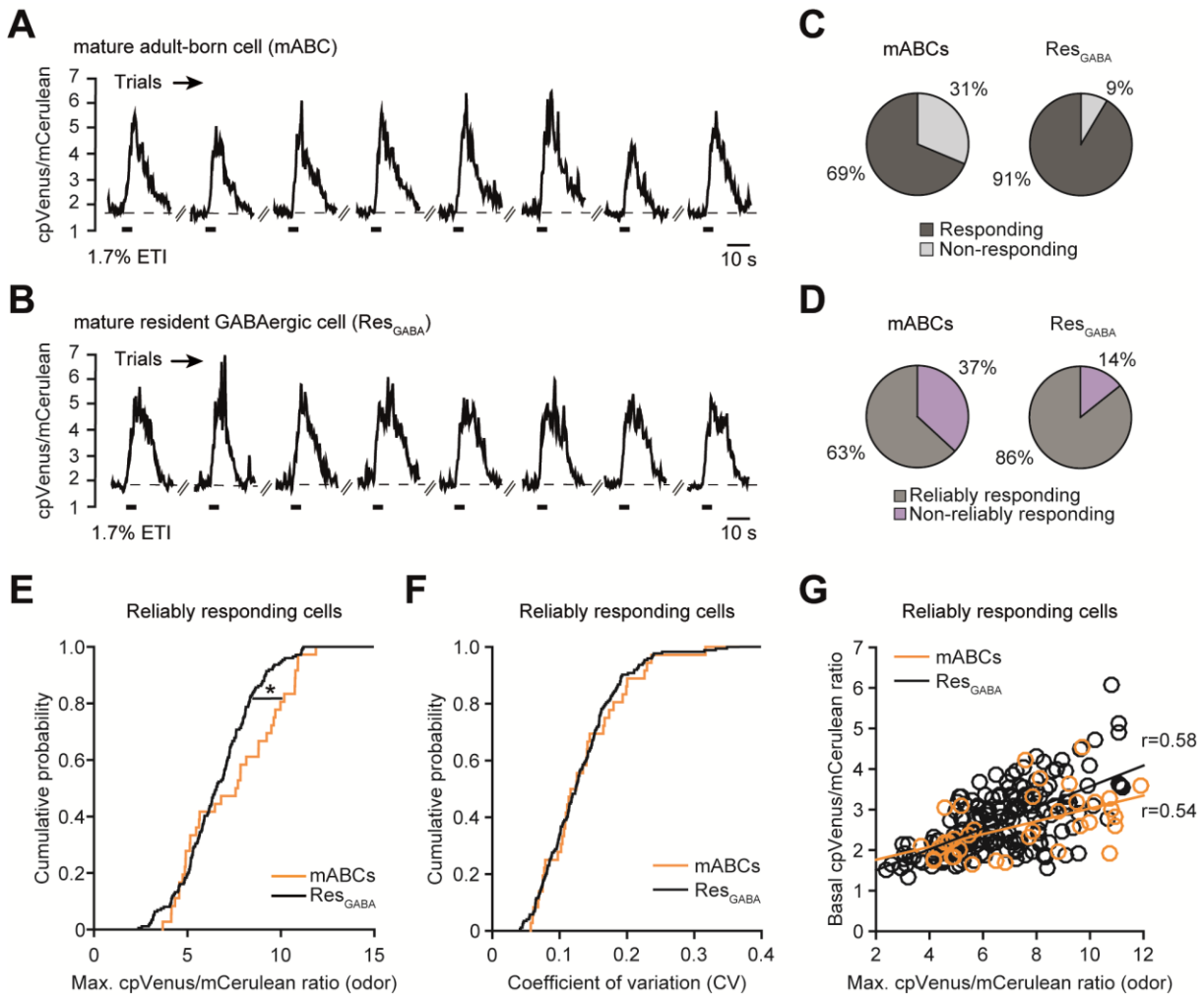
Figure 12. Odor-evoked responses of mABCs and Res$_{GABA}$ cells in awake mice.
Representative Ca^{2+} transients evoked by 8 repeated applications of the odorant ETI (1.7% saturated vapor) in a mABC **(A)** and a Res$_{GABA}$ cell **(B)**. **(C)** Pie charts displaying the fractions of responding and non-responding cells, which were significantly different between mABCs and Res$_{GABA}$ cells (p<0.0001; 83 mABCs versus 222 Res$_{GABA}$ cells; Chi-Square test). **(D)** Pie charts displaying the fractions of reliably and non-reliably responding cells, which were significantly different between mABCs and Res$_{GABA}$ cells (p<0.0003; 57 versus 203 cells; Chi-Square test). **(E)** Cumulative probability histograms display maximal ratios reached during odorant application for mABCs and Res$_{GABA}$ cells (p=0.038; 36 versus 174 cells; Kolmogorov-Smirnov test). **(F)** Cumulative probability histograms display the coefficient of variation (CV), measured between 8 trials in reliably responding cells (p=0.930; 36 versus 174 cells; Kolmogorov-Smirnov test). **(G)** Scatter plots show the basal ratios before odorant application plotted against the maximal ratios during odorant application (mABCs: r=0.54, p<0.0001; Res$_{GABA}$ cells: r=0.58, p<0.0001; Spearman's rank correlation).

In summary, in the awake state, odor-evoked responses of mABCs were sparser and less reliable compared to those of Res$_{GABA}$ cells. The maximal ratios during odorant application were higher in mABCs compared to Res$_{GABA}$ cells.

3.2 Ca^{2+} signaling of mABCs and Res$_{GABA}$ cells of anesthetized mice

Next, it was analyzed if mABCs are differently modulated by brain state compared to Res$_{GABA}$ cells. We used either 3CN, K/X or isoflurane anesthesia, to mimic changes in the brain state, and measured basal ratios of mABCs and Res$_{GABA}$ cells.

3.2.1 Anesthesia reduces basal Ca^{2+} levels of mABCs

The 3CN anesthesia strongly reduced basal ratios in mABCs as indicated by a left-shift in the cumulative probability histogram (Figure 13A). In addition, the fraction of spiking cells was significantly reduced, and the fraction of non-spiking cells increased accordingly (inset in Figure 13A; $p<0.001$, 90 cells from 8 mice; McNemar test for dependent proportions). Also K/X (Figure 13B) and isoflurane (Figure 13C) reduced the basal ratios significantly, leading to a higher fraction of non-spiking cells and a lower fraction of spiking cells (K/X: $p<0.001$, 79 cells from 8 mice; isoflurane: $p<0.001$, 106 cells from 8 mice; McNemar test for dependent proportions). To compare the effect of the 3 anesthetics, and to quantify the degree of reduction for each cell independently of its basal ratio in the awake state, we calculated the effect size (see 2.6.3). Cells with a ratio level of 2.5 or cells with a higher ratio level of 5.5 may all reach a ratio of, for example, 1.25 under anesthesia, but the absolute reduction for each cell is different; cells at lower ratios will show a smaller reduction than cells with higher ratios. Thus, the change of the ratio (from awake to anesthesia) was related to the maximal possible change. Because the ratio can only be reduced in a spiking cell, the effect size was calculated only for spiking cells. No significant difference was observed between the effects of the 3 anesthetics, when the median effect size per mouse was compared (Figure 13D; $p>0.05$; Kruskal-Wallis test). Although all 3 anesthetics reduced the ratios on a population level, single cells could be affected differently by different anesthetic drugs: the heatmap in Figure 13E displays the normalized ratio of the same cells under 3 different anesthetics. The ratio measured under the anesthetic was normalized to the respective control ratio in the awake state. For example, cell 16 decreased its ratio moderately under 3CN but stronger under K/X and isoflurane. Additionally, some cells (around 3.5%) increased their ratio under anesthesia (Figure 13E).

Figure 13. Effect of the anesthesia on basal ratios of mABCs.
Cumulative probability histograms showing basal ratios that shift towards lower levels under 3-component narcosis (3CN) **(A)**, ketamine/xylazine (K/X) **(B)** and isoflurane **(C)**. The vertical broken lines in all 3 panels indicate borders between spiking and non-spiking populations. Insets in all 3 panels display pie charts, showing a significant increase in the fraction of non-spiking cells and a significant decrease in the fraction of spiking cells (3CN: p<0.001, 90 cells from 8 mice; K/X: p<0.001, 79 cells from 8 mice; isoflurane: p<0.001, 106 cells from 8 mice; McNemar test for dependent proportions). **(D)** Box plots showing the median effect size per mouse under 3 different anesthetics. The median effect size was not significantly different between the 3 anesthetics (p>0.05; Kruskal-Wallis test). **(E)** Heatmap displays basal ratios of the same cells under 3 different anesthetics. The basal ratio measured under the respective anesthetic condition was normalized to the control basal ratios measured in the awake state (28 cells from 3 mice).

3.2.2   Anesthesia reduces basal Ca^{2+} levels of Res$_{GABA}$ cells

Next, we examined the effect of anesthetics on Res$_{GABA}$ cells. Also here, 3CN (Figure 14A), K/X (Figure 14B) and isoflurane (Figure 14C) reduced basal ratios. The population shifted significantly from spiking to non-spiking state (3CN: $p<0.001$, 215 cells from 8 mice; K/X: $p<0.001$, 221 cells from 8 mice; isoflurane: $p<0.001$, 231 cells from 8 mice; McNemar test for dependent proportions). The median effect size per mouse was significantly different between the three anesthetics (Figure 14D; $p<0.05$; Kruskal-Wallis test) and a Mann-Whitney post-hoc test revealed that isoflurane and K/X differed significantly in their effect size ($p=0.015$), but this was not the case for K/X and 3CN ($p=1.158$) or 3CN and isoflurane ($p=0.095$). Like mABCs, individual cells were differently affected dependent on the anesthetic drug used and some Res$_{GABA}$ cells (7%) showed ratio increases under anesthesia (Figure 14E).
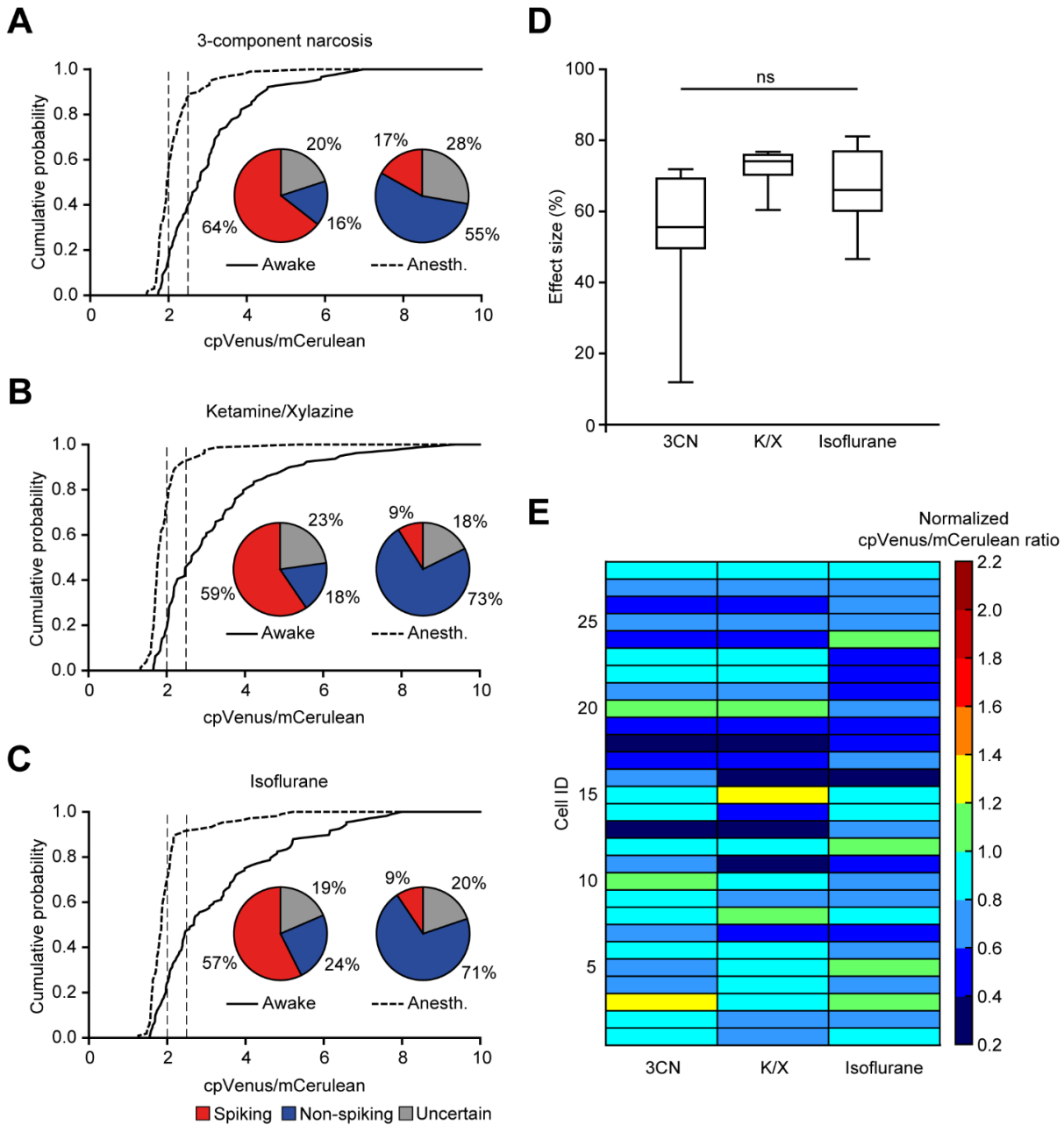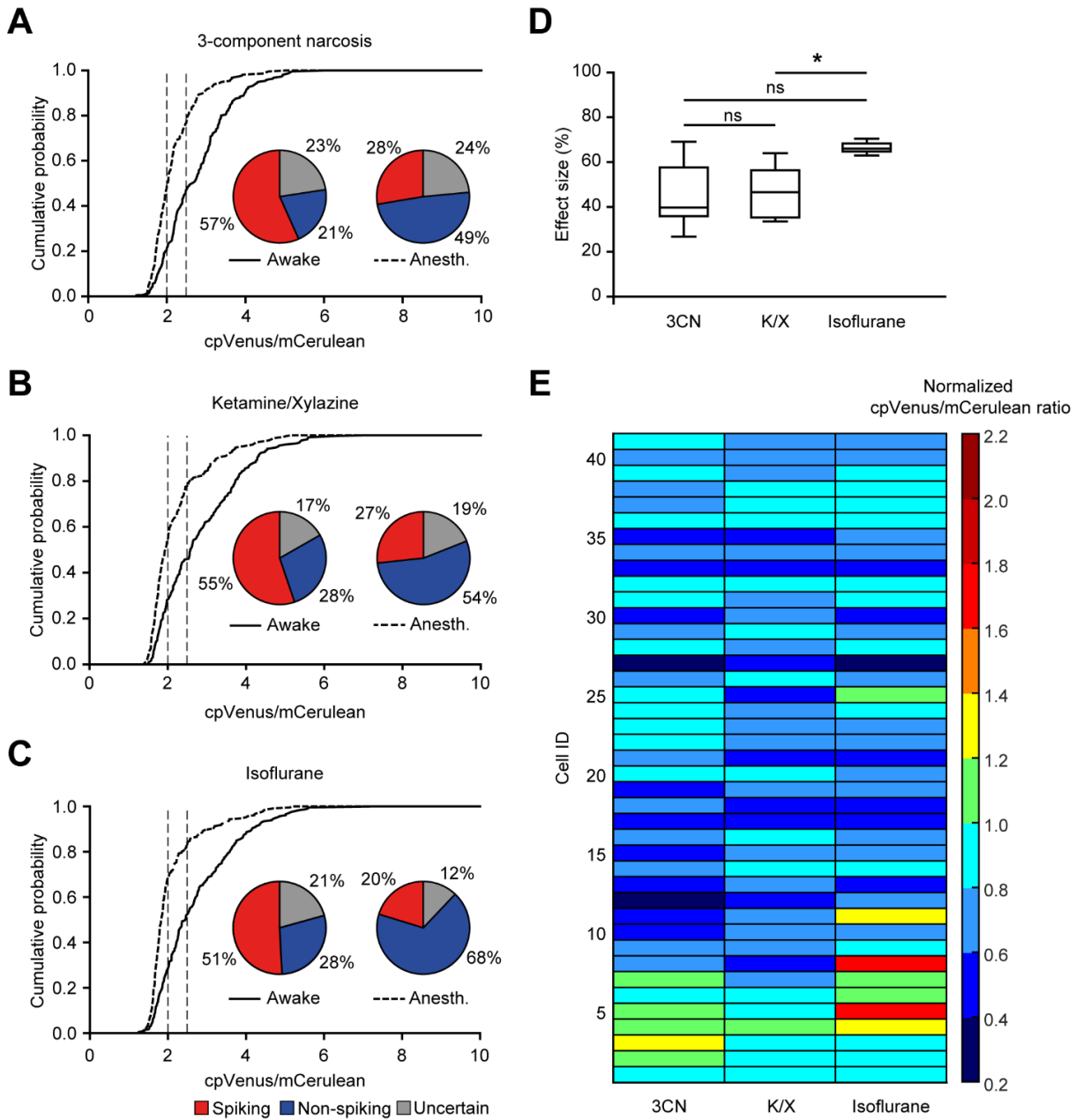
Figure 14. Effect of the anesthesia on basal ratios of Res_GABA cells.
Cumulative probability histograms showing basal ratios that shift towards lower levels under 3-component narcosis (3CN) **(A)**, ketamine/xylazine (K/X) **(B)** and isoflurane **(C)**. The vertical broken lines in all 3 panels indicate borders between spiking and non-spiking populations. Insets in all 3 panels display pie charts, showing a significant increase in the fraction of non-spiking cells and a significant decrease in the fraction of spiking cells (3CN: $p<0.001$, 215 cells from 8 mice; K/X: $p<0.001$, 221 cells from 8 mice; isoflurane: $p<0.001$, 231 cells from 8 mice; McNemar test for dependent proportions). **(D)** Box plots showing the median effect size per mouse under 3 different anesthetic conditions. The median effect size was significantly different between the 3 anesthetics ($p<0.05$; Kruskal-Wallis test). A Mann-Whitney post-hoc test revealed that basal ratios under K/X and isoflurane differed significantly from each other ($p=0.015$). **(E)** Heatmap displays basal ratios under the respective anesthetic condition normalized to the control basal ratios measured in the awake state (41 cells from one example mouse).

3.2.3 K/X has a stronger effect on mABCs than on Res$_{GABA}$ cells

Under 3CN anesthesia, the distribution of basal ratios was similar between mABCs and Res$_{GABA}$ cells (Figure 15A; p=0.240; 101 mABCs, 217 Res$_{GABA}$ cells; Kolmogorov-Smirnov test). Additionally, the fractions of spiking, non-spiking and uncertain cells between the two populations were similar under 3CN anesthesia (inset in Figure 15A; p=0.117; Chi-Square test). In contrast, K/X reduced basal ratios of mABCs stronger than those of Res$_{GABA}$ cells (Figure 15B; p=0.001; 79 mABCs, 220 Res$_{GABA}$ cells; Kolmogorov-Smirnov test). The fraction of spiking cells was lower, whereas the fraction of non-spiking cells was higher in mABCs compared to Res$_{GABA}$ cells under K/X (inset in Figure 15B; p=0.003; Chi-Square test). Isoflurane reduced the basal ratios in both cell groups to a similar extent as shown by the ratio distributions in Figure 15C (p=0.999; 106 mABCs, 232 Res$_{GABA}$ cells; Kolmogorov-Smirnov test). However, under isoflurane, the fractions of spiking, non-spiking and uncertain cells were significantly different between the two groups (inset in Figure 15C; p=0.016; Chi-Square test). Comparing the median effect size per mouse of each anesthetic revealed that all anesthetics reduced the basal ratios stronger in mABCs than in resident cells, but the level of significance was only reached for the effect of K/X anesthesia (Figure 15D; p<0.01; 2-way-ANOVA with a Bonferroni post-hoc test for multiple comparisons).

In summary, anesthesia reduced basal ratios in mABCs and Res$_{GABA}$ cells to levels below 2, thus reducing spiking activity. While there was no difference between the tested anesthetic drugs in the mABC population, in the Res$_{GABA}$ cell population isoflurane reduced basal ratios stronger compared to K/X anesthesia. From the three anesthetics used, K/X had a significantly stronger effect on mABCs compared to Res$_{GABA}$ cells.
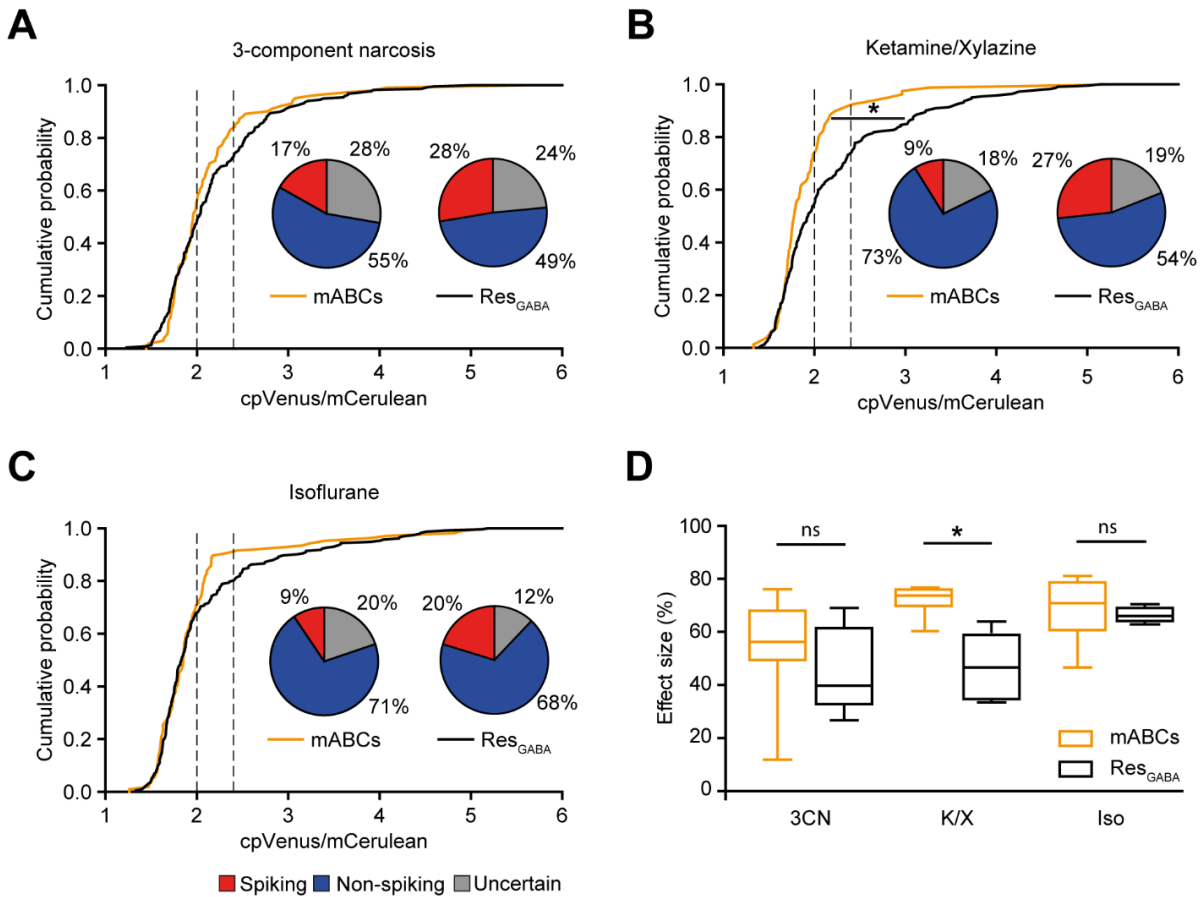
Figure 15. Basal ratios of mABCs compared to Res_GABA cells in anesthetized mice.
Cumulative probability histograms and pie charts taking from Figure 13 and Figure 14. **(A)** Cumulative probability histograms displaying basal ratios of mABCs and Res_GABA cells under 3CN, which were not significantly different between both cell types (p=0.240; 101 versus 217 cells; Kolmogorov-Smirnov test). Here and in the other panels, vertical broken lines indicate borders between non-spiking and spiking cells. Pie charts (inset) show the fraction of spiking, non-spiking and uncertain cells, which were not significantly different between mABCs and Res_GABA cells (p=0.117; Chi-Square test). **(B)** Cumulative probability histograms displaying basal ratios of mABCs and Res_GABA cells under K/X anesthesia, which were significantly different between both cell types (p=0.001; 79 versus 220 cells; Kolmogorov-Smirnov test). Pie charts (inset) show the fraction of spiking, non-spiking and uncertain cells, which were significantly different between mABCs and Res_GABA cells (p=0.003; Chi-Square test). **(C)** Cumulative probability histograms displaying basal ratios of mABCs and Res_GABA cells under isoflurane anesthesia, which were not significantly different between both cell types (p=0.999; 106 versus 232 cells; Kolmogorov-Smirnov test). Pie charts (inset) show the fraction of spiking, non-spiking and uncertain cells, which were significantly different between mABCs and Res_GABA cells (p=0.016; 106 versus 232 cells; Chi-Square test). **(D)** Box plots displaying the median effect size per mouse for mABCs and Res_GABA cells under 3 anesthetic conditions. All anesthetics had a stronger effect onto mABCs but only the effect of K/X reached the level of significance (p<0.01; 2-way-ANOVA with a Bonferroni post-hoc test for multiple comparisons).

3.2.4 Odor-response properties are different between mABCs and Res_GABA cells under anesthesia

After measuring odor-evoked responses in awake state, mice were anesthetized with 3CN and the odor-evoked responses of the same cells were re-analyzed. As shown in Figure 16A and Figure 16B, under anesthesia, both mABCs and Res_GABA cells

showed clear and reliable Ca^{2+} transients. The fraction of responding cells was again significantly lower for mABCs compared to Res$_{GABA}$ cells (Figure 16C; p<0.0001; 83 mABCs from 7 mice, 222 Res$_{GABA}$ cells from 5 mice; Chi-Square test), similar to what was seen in awake state. Yet, the fraction of reliably responding mABCs increased under anesthesia and became comparable to the fraction of reliably responding Res$_{GABA}$ cells (Figure 16D; p=0.088; 54 mABCs, 200 Res$_{GABA}$ cells; Chi-Square test). The maximal odor-evoked ratios were higher in mABCs compared to Res$_{GABA}$ cells (Figure 16E; p<0.0001; 44 mABCs, 159 Res$_{GABA}$ cells; Kolmogorov-Smirnov test). The distribution of CVs was not significantly different between mABCs and Res$_{GABA}$ cells (Figure 16F; p=0.308; 44 mABCs, 159 Res$_{GABA}$ cells; Kolmogorov-Smirnov test). Further, we analyzed the correlation between the basal ratios and corresponding maximal odor-evoked ratios in individual cells. Interestingly, while Res$_{GABA}$ cells maintained a linear relationship between basal and corresponding maximal ratios (Figure 16G; r=0.41, p<0.0001; Spearman's rank correlation), mABCs lost this relationship under anesthesia (Figure 16G; r=0.29, p=0.519; Spearman's rank correlation).
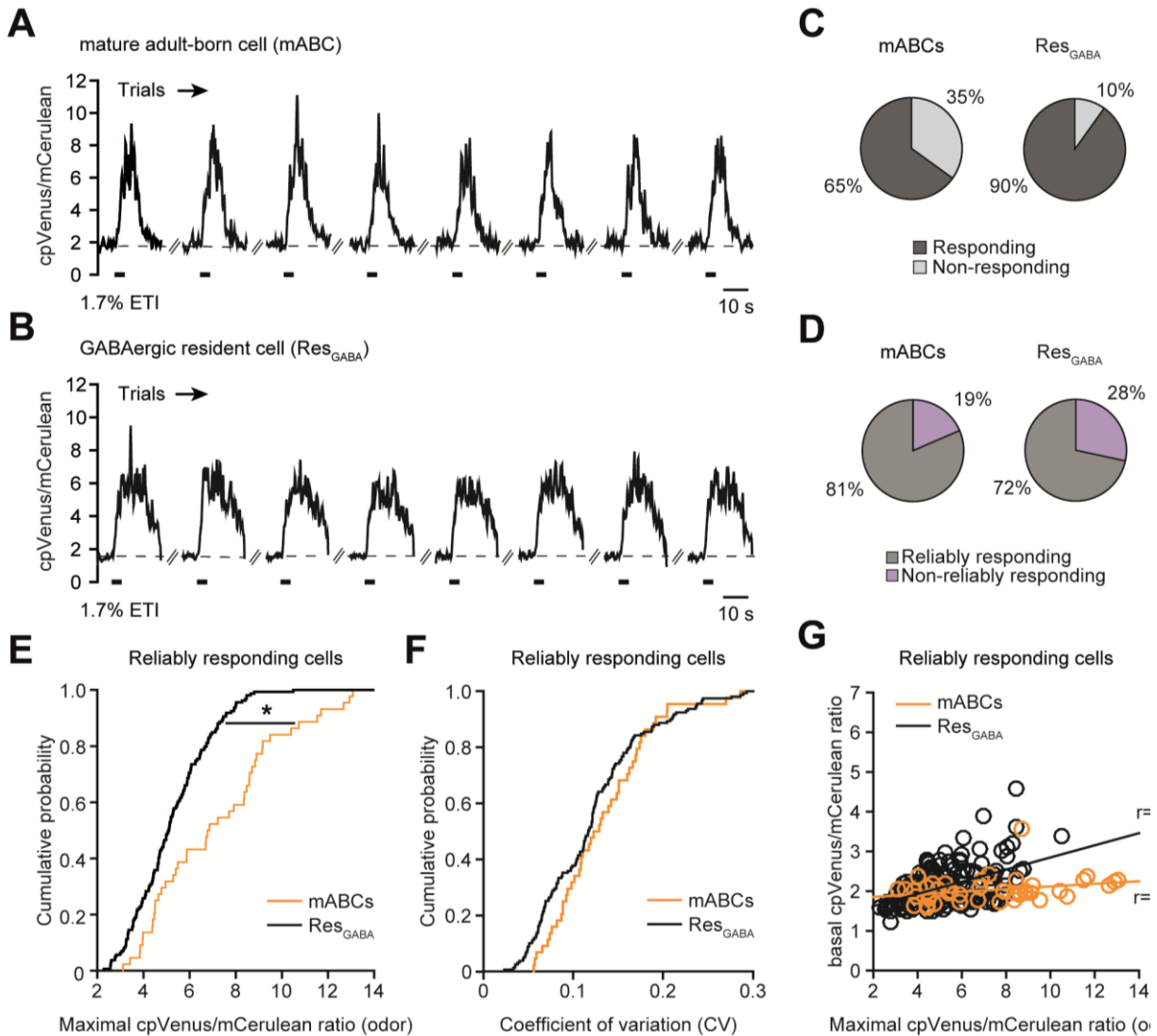
Figure 16. Odor-evoked responses of mABCs and Res$_{GABA}$ cells under anesthesia.
Representative Ca^{2+} transients evoked by 8 repeated applications of the odorant ETI (1.7% saturated vapor) in a mABC **(A)** and a Res$_{GABA}$ cell **(B)**. **(C)** Pie charts displaying the fractions of responding and non-responding cells, which were significantly different between mABCs and Res$_{GABA}$ cells (p<0.0001; 83 versus 222 cells; Chi-Square test). **(D)** Pie charts displaying the fractions of reliably and non-reliably responding cells, which were not significantly different between mABCs and Res$_{GABA}$ cells (p=0.088; 54 versus 200 cells; Chi-Square test). **(E)** Cumulative probability histograms display maximal ratios reached during odorant application for mABCs and Res$_{GABA}$ cells (p<0.0001; 44 versus 159 cells; Kolmogorov-Smirnov test). **(F)** Cumulative probability histograms display the CV, measured between 8 trials in reliably responding cells (p=0.308; 44 versus 159 cells; Kolmogorov-Smirnov test). **(G)** Scatter plot shows the basal ratios before odorant application plotted against the maximal ratios during odorant application (mABCs: r=0.29, p=0.519; Res$_{GABA}$ cells: r=0.41, p<0.0001; Spearman's rank correlation).

In summary, mABCs responded still less often to odorant application under anesthesia, but became as reliable as Res$_{GABA}$ cells. In addition, odor-evoked maximal ratios were still higher in mABCs compared to Res$_{GABA}$ cells.

3.3 Differential role of the neuromodulators of the ARAS system

Because high basal ratios, and thus spiking, of both mABCs and Res$_{GABA}$ cells were reduced under anesthesia, we tested whether centrifugal inputs arising from ARAS centers contribute to the high basal ratios (spiking activity) observed in the awake state. In addition, we tested if these centrifugal projections target mABCs differently compared to Res$_{GABA}$ cells. Hence, basal ratios of mABCs and Res$_{GABA}$ cells were measured before and after application of antagonists of noradrenergic, serotonergic, or cholinergic receptors to the OB of awake mice.

To do so we first implanted a slit-containing chronic cranial window (see chapter 2.3.2) and intended to apply blocker solutions four weeks after surgery, which is the usual recovery time before imaging. However, it turned out that during this time the dura mater in the slit became impermeable, so drugs did not diffuse into the OB. Blocker injection with glass pipettes was also not successful, as the dura mater was not penetrated but bending thus damaging the underlying brain tissue (data not shown). Therefore, experiments involving application of blocker solutions were performed 12-24 hours after cranial window implantation, with each imaging session ending at least 24 hours after surgery (see 2.5.5 for more details). All antagonists were diluted in the vehicle HEPES-buffered ringer solution and so the effect of HEPES-buffered ringer solution on basal ratios was tested first. For this, the basal ratios were measured in presence of the silicon elastomers Kwik-Cast/Sil (control) and again after removal of the plug and application of the HEPES-buffered ringer solution. Basal ratios after application were normalized to the respective control basal ratios measured beforehand. The box plot in Figure 17 displays the median normalized basal ratios per mouse, indicating that the ratios did not change significantly under HEPES-buffered ringer solution (p=0.437; 5 mice; Wilcoxon Signed-Rank test). Yet, for further analysis, we included only those cells that had a normalized basal ratio between 0.7 and 1.3 and classified them as 'stable' (81.2% of all cells).
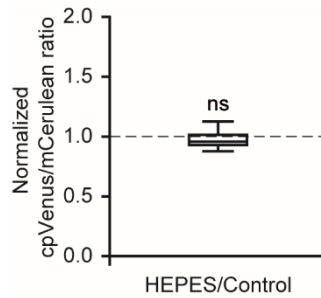
Figure 17. Effect of HEPES-buffered ringer solution on basal ratios.
Box plot displaying medians of normalized ratios per mouse (p=0.437; 5 mice; Wilcoxon Signed-Rank test).

3.3.1 Cholinergic and serotonergic receptor blocker reduce basal Ca^{2+} levels of mABCs

In the mABC population, application of the noradrenergic receptor blocker prazosin did not change basal ratios (Figure 18A, pie charts in inset: p=1.090, 35 cells from 5 mice; McNemar test for dependent proportions), whereas the serotonergic receptor blocker methysergide significantly reduced the basal ratios, resulting in a lower fraction of spiking and accordingly a higher fraction of non-spiking cells (Figure 18B, pie charts in inset: p=0.007, 35 cells from 5 mice; McNemar test for dependent proportions). Furthermore, the application of two cholinergic receptor blockers, mecamylamine and scopolamine, significantly reduced the basal ratios, and thus the fraction of spiking cells (Figure 18C, pie charts in inset: p=0.005, 35 cells from 5 mice; McNemar test for dependent proportions). The effect sizes of methysergide and mecamylamine/scopolamine were not significantly different from each other (Figure 18D; 5 mice; p=0.812, Wilcoxon Signed-Rank test), indicating a similar degree of inhibition. As it was the case under anesthesia, the overall ratio was reduced on a population level, but some individual cells showed an increase in ratio. In addition, individual cells responded differently to either methysergide or mecamylamine/scopolamine (Figure 18E).

Figure 18. Effect of receptor blockers on basal ratios of mABCs in awake mice.
Cumulative probability histograms showing basal ratios in the vehicle condition and during topical application of prazosin **(A)**, methysergide **(B)**, and mecamylamine/scopolamine **(C)**. Vertical broken lines indicate borders between spiking and non-spiking populations. Pie charts in inset showing the fractions of spiking, non-spiking and uncertain cells, which were not significantly different between vehicle and prazosin (p=1.090; 35 cells from 5 mice; McNemar test for dependent proportions), but between vehicle and methysergide (p=0.007; 35 cells from 5 mice; McNemar test for dependent proportions) and between vehicle and mecamylamine/scopolamine (p=0.005; 35 cells from 5 mice; McNemar test for dependent proportions). **(D)** Box plots showing the median effect size per mouse under 3 different receptor blockers. The median effect size was not significantly different between the serotonergic and the cholinergic receptor blocker (p=0.812, Wilcoxon Signed-Rank test). **(E)** Heatmap displaying basal ratios measured during blocker application normalized to the basal ratios measured in the vehicle condition (35 cells from 5 mice).

3.3.2 Cholinergic receptor blocker reduce basal Ca^{2+} levels of Res$_{GABA}$ cells

In Res$_{GABA}$ cells, prazosin and methysergide did not reduce basal ratios, as shown by similar cumulative probability histograms before and during the application of blockers (Figure 19A for prazosin and Figure 19B for methysergide). Likewise, the fractions of spiking and non-spiking cells did not change (prazosin: $p=0.863$; methysergide: $p=0.353$; the same 176 cells from 5 mice; McNemar test for dependent proportions). However, blockade of cholinergic receptors did reduce the basal ratios significantly (Figure 19C); the distribution of basal ratios shifted to the left and the fraction of spiking cells was reduced while the fraction of non-spiking cells was increased accordingly (inset; $p<0.0001$; McNemar test for dependent proportions). Again, despite the reduction of ratios at the population level, some individual cells increased their ratio in the presence of cholinergic receptor blockers. In addition, individual cells responded to prazosin and methysergide with either ratio decrease or increase (Figure 19D).
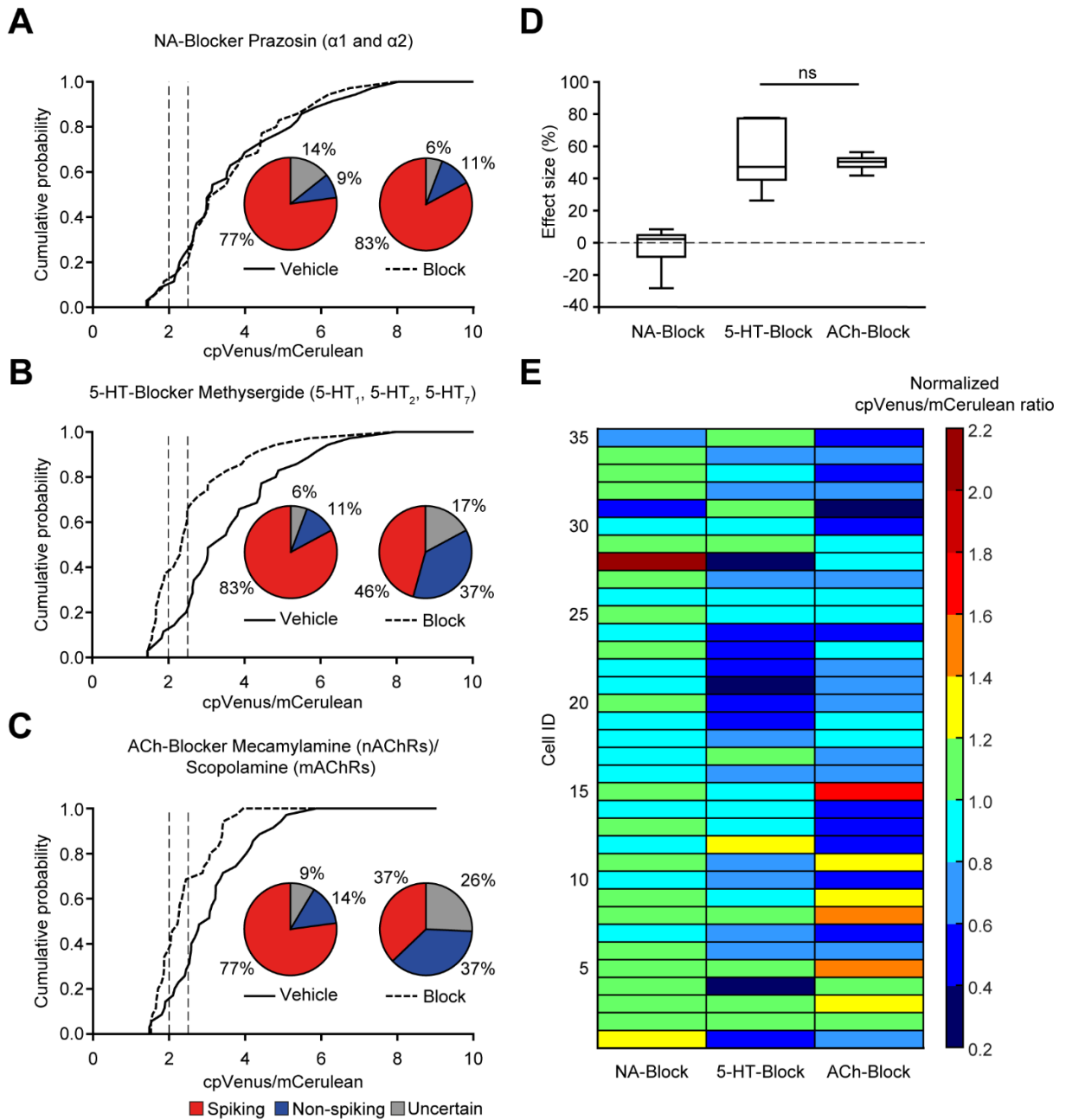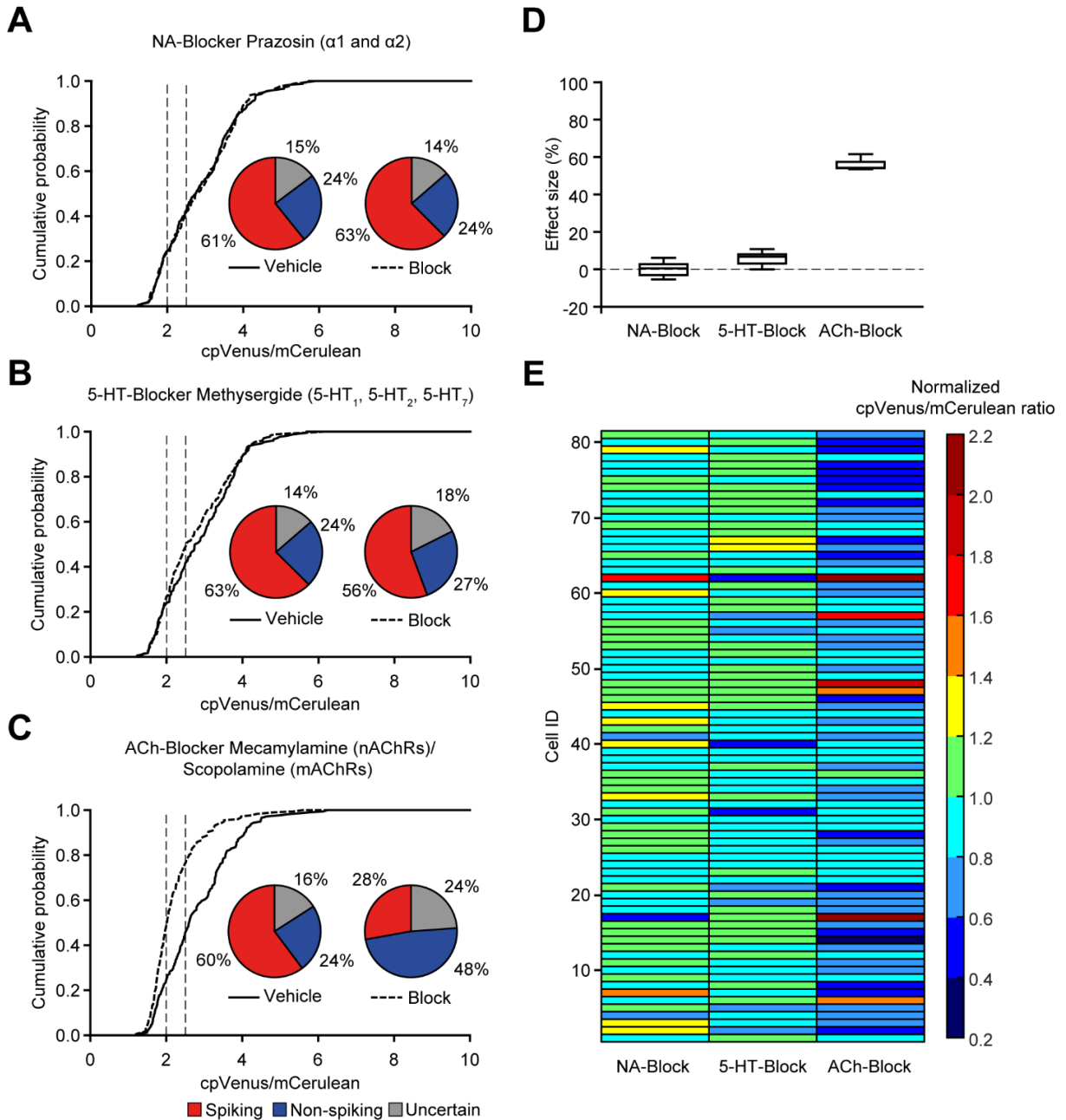
Figure 19. Effect of receptor blockers on basal ratios of Res$_{GABA}$ cells in awake mice. Cumulative probability histograms showing basal ratios in the vehicle condition and during topical application of prazosin **(A)**, methysergide **(B)**, and mecamylamine/scopolamine **(C)**. Vertical broken lines indicate borders between spiking and non-spiking populations. Pie charts in inset showing the fractions of spiking, non-spiking and uncertain cells, which were not significantly different between vehicle and prazosin (p=0.863; 176 cells from 5 mice; McNemar test for dependent proportions), or between vehicle and methysergide (p=0.353; 176 cells from 5 mice; McNemar test for dependent proportions), but between vehicle and mecamylamine/scopolamine (p<0.0001; 176 cells from 5 mice; McNemar test for dependent proportions). **(D)** Box plots showing the median effect size per mouse under 3 different receptor blockers. **(E)** Heatmap displaying basal ratios measured during blocker application normalized to the basal ratios measured in the vehicle condition (35 cells from 5 mice).

Comparing the effect sizes of receptor blockers between mABCs and Res$_{GABA}$ cells revealed that the serotonergic receptor blocker methysergide affected mABCs cells

significantly stronger than Res$_{GABA}$ cells (Figure 20; $p < 0.05$; 2-way-ANOVA with a Bonferroni post-hoc test for multiple comparisons), whereas the effect size of cholinergic receptor blockers on the two cell populations was similar.
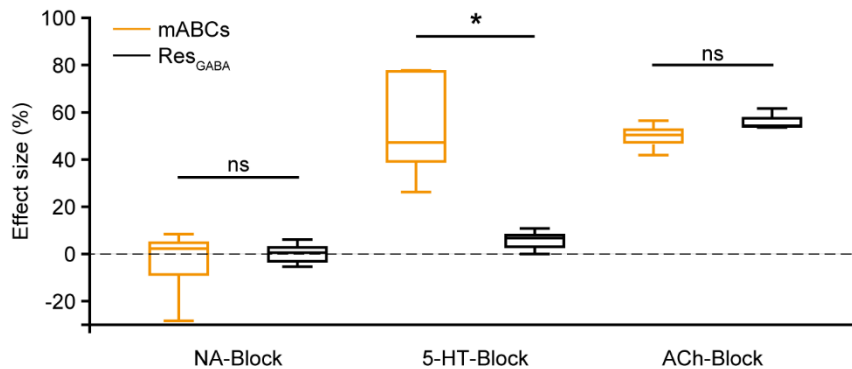
Figure 20. Effect of receptor blockers compared between mABCs and Res$_{GABA}$ cells.
Box plots show the median effect sizes per mouse for all 3 receptor blockers. The serotonergic receptor blocker methysergide reduced ratios of mABCs but not Res$_{GABA}$ cells, as seen by the significantly higher effect size ($p < 0.05$; 2-way-ANOVA with a Bonferroni post-hoc test for multiple comparisons).

In summary, the high basal ratios (spiking activity) of mABCs observed in the awake state might be caused by active serotonergic and cholinergic inputs, whereas the high basal ratios of Res$_{GABA}$ cells are likely to be caused by cholinergic inputs only. This indicates a distinct serotonergic innervation of mABCs or a responsiveness to activation of serotonin receptors, distinguishing them from Res$_{GABA}$ cells.

4 Discussion

Using two-photon Ca^{2+} imaging with the genetically encoded Ca^{2+} indicator Twitch-2B in awake head-restrained mice, we found that mature adult-born juxtaglomerular cells in the OB retain unique features compared to resident juxtaglomerular cells. For the first time, mature adult-born juxtaglomerular cells were analyzed in awake mice and were compared to resident GABAergic cells. This comparison revealed that in the awake state, basal ratios, indicative of intracellular basal Ca^{2+} levels, did not differ between mABCs and Res$_{GABA}$ cells. However, odor-response properties differed. The responses of mABCs were sparser, less reliable, but larger compared to those of Res$_{GABA}$ cells. Under anesthesia, mABCs responded to odorant application more reliably than in awake state, but still less often and with larger responses. From three anesthetics used, K/X anesthesia reduced high basal ratios of mABCs stronger than those of Res$_{GABA}$ cells. To decipher what role the centrifugal inputs of the ARAS system play for the high basal ratios of mABCs and Res$_{GABA}$ cells, we applied antagonists of noradrenergic, cholinergic, and serotonergic receptors. Application of the cholinergic receptor antagonists resulted in reduced basal ratios of both, mABCs and Res$_{GABA}$ cells, while application of the serotonergic receptor antagonist reduced basal ratios only in mABCs, but not Res$_{GABA}$ cells.

In summary, our data reveal that upon maturation, adult-born juxtaglomerular cells do not become identical to resident GABAergic cells, but retain distinct odor-response properties as well as a possible different receptor composition and innervation pattern (discussed below), likely endowing them with unique physiological functions.

4.1 Basal and odor-evoked Ca^{2+} signals

In the awake state, more than 50% of mABCs and Res$_{GABA}$ cells had high basal ratios above 2.4, indicating spiking activity, as TTX led to a reduction of basal ratios below 2.0 (Figure 9C). Although the spiking activity was not significantly different between mABCs and Res$_{GABA}$ cells (Figure 11D), odor-response properties were different (Figure 12E). First of all, a lower fraction of mABCs responded to odorant application. A possible explanation for this observation could be that mABCs receive more specific synaptic inputs so that responses are more selective (i.e. cells respond to a few out of many odorants). Previous studies described that ABCs become more se-

lective and respond to fewer odorants after maturation (Livneh *et al.* 2014; Wallace *et al.* 2017). Livneh *et al.* applied 7 different odorants and observed that around 50% of young ABCs respond to 3 odorants while 50% of mature ABCs and resident cells respond to only one odorant. Wallace *et al.* applied 8 different odorants and observed that around 50% of young adult-born GC dendrites respond to 3 odorants while 50% of mature GC dendrites did not respond to any odorant. However, in both studies mABCs' responses to multiple odorants were tested, while we tested responses to one particular odorant (ETI). Therefore, we cannot certainly say if the lower responsiveness observed here indicates that mABCs are more selective in the same sense. It might have also other reasons, as for instance, mABCs may also receive a stronger inhibition from neighboring cells in the network, and so respond less often than Res$_{GABA}$ cells.

Furthermore, mABCs showed higher maximal ratios during odorant application compared to Res$_{GABA}$ cells. As the higher ratio is indicative of higher spiking activity, this implies that more GABA is released from mABCs, leading to stronger hyperpolarization of postsynaptic cells (M/Ts and juxtaglomerular cells), or of OSN terminals. This overall inhibition could lead to sparser, more selective olfactory inputs which are forwarded by M/Ts to the olfactory cortex. On the other hand, higher ratios reflect higher intracellular Ca^{2+} levels, and these might induce more intracellular signaling cascades in mABCs that favor the suggested function of mABCs in learning and memory (1.2), such as Ca^{2+}-dependent short-term and long-term plasticity (Eccles 1983; Zucker and Regehr 2002; Cavazzini *et al.* 2005). For instance, during early long-term potentiation, Ca^{2+} activates kinases that phosphorylate AMPA receptor channels, which then are incorporated into the cell membrane and lead to strengthening of synaptic transmission. Also, Ca^{2+}-activated kinases phosphorylate transcription factors such as cAMP-response element-binding protein, leading to the synthesis of new proteins of which some are ion channels or receptors. Structural plasticity (dendrite and spine dynamics) was described for PGCs as well as GCs (1.2), while functional plasticity, such as short-term depression or long-term potentiation was so far predominantly described in GCs (Dietz and Murthy 2005; Nissant *et al.* 2009).

The underlying mechanism of higher maximal ratios during odorant application in mABCs might be due to a different composition of receptors or ion channels permeable for Ca^{2+} in the postsynaptic membrane. For instance, more NMDA receptors or

voltage-gated Ca^{2+} channels could be present, or they may exist in different isoforms or subunit compositions (Simms and Zamponi 2014; Hansen *et al.* 2017). Interestingly, we found that K/X anesthesia reduced basal ratios stronger in mABCs than Res_{GABA} cells. As ketamine is known to antagonize NMDA receptors, this could indicate that mABCs possess a different absolute number of NMDA receptors or subunit composition. Furthermore, as NMDA channels are also known to play a key role in long-term potentiation (Bliss and Lomo 1973), these differences in number or subunit composition might favor activity-dependent plasticity in mABCs. The anesthetic agent xylazine, which was applied together with ketamine, is unlikely to be responsible for the reduction of basal ratio levels, as xylazine targets α2 adrenergic receptors similar to medetomidine in the 3CN anesthesia, and 3CN did not reduce basal ratios as strong as K/X. Furthermore, it has been described that ABCs express more NMDA receptors when they are immature compared to when they are mature (Grubb *et al.* 2008). In addition, NMDA receptors in immature ABCs contain more NR2B subunits than NMDA receptors in mature ABCs (Grubb *et al.* 2008). However, this would contradict the assumption that mature ABCs in our study might have different NMDA receptors than Res_{GABA} cells. Further experiments would be required to test whether the number or subunit composition of functional NMDA receptors differs between mABCs and Res_{GABA} cells. For this purpose, one could topically apply NMDA receptor blockers (such as (2R)-amino-5-phosphonovaleric acid) and measure basal and odor-evoked ratios in mABCs and Res_{GABA} cells. Furthermore, electrophysiological recordings performed *in vivo* or in OB slices could be used to determine the electrical properties of NMDA receptors. In addition, expression level or subunit composition of NMDA receptors could be analyzed using immunohistochemical labeling (Telezhkin *et al.* 2016) or more quantitative protein-based techniques (Antonelli *et al.* 2016).

A previous study found differences between the spontaneous activities of immature (2-week-old) ABCs and resident cells under ketamine anesthesia (in combination with medetomidine) (Livneh *et al.* 2014). However, the spontaneous activity of mABCs was similar to that of resident cells. This is in contrast with our finding that also mABCs can have lower spontaneous activity (i.e. basal ratios) under K/X anesthesia. However, the difference in recording technique (electrophysiological recordings of single APs in Livneh's study versus Ca^{2+} imaging in our study) could be the reason for this discrepancy. Furthermore, in our study, differences in basal ratios between

mABCs and Res$_{GABA}$ cells were observed neither under the 3CN anesthesia nor under the isoflurane anesthesia or in the awake state. This indicates that effects observed by us under K/X anesthesia and by Livneh *et al.* under K/M anesthesia could be due to the presence of ketamine.

Furthermore, Livneh *et al.* observed under K/M anesthesia higher odor-evoked AP firing rates in immature (4-week-old) ABCs compared to resident cells (Livneh *et al.* 2014). But this difference did not remain in mature ABCs. This contrasts with the current finding that mABCs can have higher odor-evoked maximal ratios compared to Res$_{GABA}$ cells. However, the difference in recording techniques (see above) and in brain state (awake state versus K/M anesthesia) between our study and Livneh's study might explain this contradictory result.

As the immunostaining of DCX and Twitch-2B revealed that ca. 18% of Twitch-2B-expressing mABCs are younger than 21 days, this subpopulation could show different properties than mABCs. However, the collected data did not indicate that the group of Twitch-2B-expressing mABCs consisted of two clearly distinguishable populations showing distinct basal or odor-evoked maximal ratios. In addition, although the immunostaining showed that 18% of cells are younger than 21 days, how many cells have an age between 21 and 56 DPI is unknown. Thus, mABCs have a continuum of individual ages, which is unavoidable when using lentiviruses to label ABCs; an established method used by many studies before. So far, no marker has been described that specifically labels mature adult-born PGCs/SACs for subsequent analyses of their physiological properties *in vivo*, as was recently described for mature adult-born GCs in the OB (Quast *et al.* 2017). Under the current experimental paradigm, the exact age of individual adult-born PGCs/SACs could be determined by observing Twitch-2B-expressing cells daily from their arrival in the OB until they mature, i.e. over about 7 weeks. However, daily measurements over this extended time span in awake mice would likely be stressful to the animals, which might in turn affect ABC maturation and integration. Measurements under anesthesia would also be possible, however, it has been described that anesthesia disturbs synaptogenesis of newborn cells during development and could under some circumstances even lead to their death (Jevtovic-Todorovic 2012; Reddy 2012). In addition, it has been shown that in adult mice anesthesia impairs maturation and integration of adult-born hippocampal neurons (Krzisch *et al.* 2013). Therefore, repeated measurements under anesthesia

might as well affect ABCs' maturation and integration. Likewise, repeated imaging may induce cell damage due to excessive illumination.

4.2 Modulation by anesthesia and centrifugal inputs

Previous studies showed that anesthesia reduces spontaneous activity of GABAergic cells in the OB (Kato *et al.* 2012; Wachowiak *et al.* 2013; Cazakoff *et al.* 2014). We confirm and extend these findings for adult-born and resident GABAergic cells by showing that their basal ratios were reduced under anesthesia (Figure 13, Figure 14). In addition, here, three different anesthetics were used: K/X, isoflurane, and in this context previously not used mixture of medetomidine, midazolam and fentanyl, summarized as '3CN'. In Res$_{GABA}$ cells, isoflurane reduced basal ratios significantly stronger than K/X did (see Figure 14D). In contrast, in mABCs, all three anesthetics reduced basal ratios similarly strong although a trend for a stronger reduction under K/X anesthesia was observed (see Figure 13D). We wanted to test if centrifugal projections from ARAS nuclei contribute to the high basal ratios in the awake state. Therefore, for the first time, receptor blockers for acetylcholine, serotonin, or noradrenaline were applied onto the OB of awake mice and basal ratios of mABCs and Res$_{GABA}$ cells were measured. A major advantage of this approach in the awake mouse is that it avoids potentially confounding interference with anesthetic agents. However, some technical limitations should be considered. The concentration of blockers in our study was high compared to previous *in vivo* experiments in the OB of anesthetized mice, where a large area of the OB surface was perfused (Petzold *et al.* 2009; Rothermel *et al.* 2014). Therefore, it is unknown if the highly concentrated drugs led to unspecific effects. For example, they could bind to other than the targeted receptors, reach other areas of the brain, or cross the blood brain barrier, thereby inducing systemic effects. However, the high concentrations were chosen to guarantee that blockers diffusing through the small slit would reach sufficient concentrations in the olfactory bulb. For improvement, dose-response-curves could be recorded in further studies in order to find the lowest concentration that is blocking the specified receptors and reduces the basal ratios. This would diminish the possibility that drugs reach concentrations that could lead to unspecific effects. Another option is the use of optogenetic or chemogenetic approaches, which allows more specific blocking and better temporal control of the blockade. The chemogenetic blockade could be

achieved by expressing 'Designer Receptors Exclusively Activated by Designer Drugs' (DREAADs) (Urban and Roth 2015) in target cells (for instance, serotonergic cells), whereby the optogenetic blockade could be achieved by expressing light-sensitive ion channels or ion pumps leading to hyperpolarization in target cells (Zhang *et al.* 2010).

Upon blockade of noradrenergic receptors, changes in basal ratios of mABCs and Res$_{GABA}$ cells were not observed. This implies that noradrenergic inputs do not contribute to the high basal ratios observed in the awake state. This is in line with the observation that adrenergic fibers primarily target the external plexiform-, GC- and MC- layer (McLean *et al.* 1989; McLean and Shipley 1991) and that adrenergic receptors are primarily expressed on GCs and MCs, but very low on juxtaglomerular cells (McCune *et al.* 1993; Day *et al.* 1997; Hayar *et al.* 2001; Nai *et al.* 2010; Luhrs *et al.* 2016). When we applied the cholinergic receptor blockers, basal ratios of mABCs and Res$_{GABA}$ cells were reduced. These results imply that mABCs and Res$_{GABA}$ cells are both innervated by cholinergic fibers. Acetylcholine has been shown to excite GABAergic juxtaglomerular cells via nicotinergic receptors (Ravel *et al.* 1990; Castillo *et al.* 1999). To test if the high basal ratios reflect an inflow of Ca^{2+} via nAChRs, only the nAChR-blocker mecamylamine could be applied. Application of the serotonergic receptor blocker led to a reduction of basal ratios in mABCs, but not in Res$_{GABA}$ cells. This implies that only mABCs, but not Res$_{GABA}$ cells are innervated by serotonergic fibers. To investigate this interesting observation, analysis of serotonin receptor expression, or of the extent of serotonergic fiber innervation would be necessary (see, e.g., Deshpande *et al.* (2013) for the investigation of fiber innervation). To test whether serotonin in the OB is released from serotonergic fibers arising from the dorsal raphe nucleus, activity of serotonergic neurons in the dorsal raphe nucleus or of their terminals in the OB could be blocked directly via chemogenetic or optogenetic methods.

Our finding that mABCs were selectively blocked by the serotonergic receptor blocker suggests a specific role for serotonin in mABCs. Previous studies have described that serotonin increases neurogenesis and improves ABC survival, but it was unknown if serotonergic innervation differs between ABCs and resident cells. Furthermore, so far, many studies focused on the role of noradrenaline and acetylcholine in olfactory learning and memory, but less is known about the function of serotonin for olfaction.

In the following, I will discuss one described function of serotonin in the context of brain-state-dependent sensory processing. Serotonin was suggested to mediate pre-synaptic feedback inhibition onto OSNs via activation of GABAergic juxtaglomerular cells (Hardy *et al.* 2005; Petzold *et al.* 2009) and this presynaptic feedback inhibition was suggested to control the sensory gain (McGann 2013). Activity of serotonergic neurons is known to be brain-state-dependent with high activity levels during awake, resting states, predominantly during grooming and rhythmic movements, but not during attentive states of sensory acquisition (Jacobs and Azmitia 1992; Jones 2005). Therefore, one function of serotonin was suggested to be suppression of sensory perception (Jacobs and Fornal 1993; Jacobs and Fornal 1999; Hurley et al. 2004). In resting states, e.g., during grooming or eating, acquisition of new odorants might be not vital, and so perception is dampened. However, when the animal is actively searching for food or mates, or when it pays attention to predators, the gain of olfactory inputs might be raised to ensure unambiguous and fast odor perception. Gain adjustment or 'gating' is an important mechanism to filter out irrelevant information, which prevents an overload of sensory information (Freedman *et al.* 1987; Freedman *et al.* 1996; Schwartz and Simoncelli 2001). Serotonin has been demonstrated to modulate the sensory gain in various other species and brain areas (Hurley *et al.* 2004). For instance, in the olfactory system (Dacks *et al.* 2009; Petzold *et al.* 2009), the visual system (Waterhouse *et al.* 1990; Seillier *et al.* 2017), the inferior colliculus (Hurley *et al.* 2002), and the somatosensory system (Dugue *et al.* 2014).

As described in the introduction (1.2), it was suggested that ABCs enable plasticity to adapt to environmental changes. Since ABCs receive centrifugal inputs, whose activity is brain-state-dependent, Lazarini and Lledo in 2011 hypothesized that ABCs are coincidence detectors between the behavioral state (arousal, attention, expectation) of the animal and sensory inputs arising from the environment (Lazarini and Lledo 2011). Because the activity of serotonergic neurons is brain-state-dependent, our finding that mABCs receive selective serotonergic inputs favors the hypothesis that ABCs are mediators of brain state-dependent changes in sensory processing. This adds another aspect to the understanding of ABC function, specifically the function of adult-born PGCs/SACs, as they, in contrast to adult-born GCs, reside in the glomerular layer, which displays an intersection point between sensory inputs arriving from the environment and centrifugal inputs arriving from the brain. Since it is known that

ABCs start migrating into the OB during embryogenesis (Wichterle *et al.* 2001) and continue postnatally in the young and adult animal (Luskin 1993; Lois and Alvarez-Buylla 1994; De Marchis *et al.* 2007), it is very likely that ABCs can shape sensory processing according to the state of the animal, starting with its birth.

Because ketamine and the serotonergic receptor antagonist methysergide reduced basal ratios stronger in mABCs compared to Res$_{GABA}$ cells, it is tempting to speculate about a functional interaction between ketamine and serotonin. Ketamine is known to act on the serotonergic system (introduction chapter 1.3.3); specifically (1) by modulating the descending serotonergic pathways in the spinal cord (Larson 1984; Koizuka *et al.* 2005; Bee and Dickenson 2009), (2) by modulating serotonin synthesis and reuptake (Martin *et al.* 1982; Martin and Smith 1982; Yamamoto *et al.* 2013), and (3) by reducing firing of serotonergic neurons in the DRN (McCardle and Gartside 2012). In mouse hippocampus, it was described that ketamine increases 5-HT$_{2C}$ cluster microRNA levels, which may inhibit translation of 5-HT$_{2C}$ receptor mRNA (Grieco *et al.* 2017). Given that serotonin activates PGCs via 5-HT$_{2C}$ receptors, this observation is interesting. In regard of all these effects, it can be speculated that ketamine may affect mABC basal ratios in part by modulating serotonergic pathways. However, to prove this, further investigations would be required.

Anesthesia modulates ARAS centers (introduction chapter 1.3.3) and induces an EEG pattern similar to that seen in NREM sleep. Besides this, anesthesia and sleep are believed to share many additional features (Vanini *et al.* 2011). It is widely accepted that sleep is needed for memory consolidation (Alger *et al.* 2015; Chen and Wilson 2017). Moreover, olfactory ABCs were described to play a role in the acquisition of memory as well as in their consolidation (Kermen *et al.* 2010; Yokoyama *et al.* 2011). Kermen *et al.* described that the efficiency of learning positively correlated with ABC survival and with the duration of resting phase after the learning task, indicating that a resting phase is needed to consolidate previously learned behaviors. Yokoyama *et al.* described that ABCs were eliminated in the resting phase, more specifically in the postprandial sleep following food intake (a typical behavior dependent on olfaction), and that this ABC elimination during sleep was needed for consolidation of previously learned odor-driven behaviors. According to a hypothesis of Yamaguchi (Yamaguchi *et al.* 2013; Yamaguchi 2017), those ABCs that were active during the memory acquisition will survive while those that were not active will die during sleep.

Yamaguchi suggests that centrifugal inputs during sleep target ABCs and play a role of detectors that can initiate apoptosis when ABCs have been inactive during the acquisition. In conclusion, ABCs were shown to be important for memory consolidation in sleep, and it is hypothesized that those ABCs that were inactive during the acquisition period will be eliminated. Since our study showed that basal activity levels (basal ratios) of mABCs are reduced under anesthesia and under receptor blockade for centrifugal inputs arising from ARAS centers, we hypothesize that activity levels are also reduced during natural sleep. Measuring basal ratios of ABCs and Res$_{GABA}$ cells during sleep after the animal performed learning tasks might help us to understand which role ABCs play in memory consolidation. So far, the performance in learning tasks was correlated with the degree of neurogenesis or survival of ABCs. We suggest measuring activity of the same ABCs immediately during the memory acquisition period in the awake state and afterwards during consolidation in sleep states. Furthermore, comparing activity levels of mABCs and Res$_{GABA}$ cells during acquisition and consolidation could reveal the underlying physiology of mABCs important for their suggested function in learning. Successful two-photon imaging experiments in sleeping mice have been already performed (Maret *et al.* 2011; Cox *et al.* 2016; Niethard *et al.* 2016) and could act as guidelines for the planning of the above mentioned experiments.

In the awake state, mABCs responded less reliably to odorant application, but became as reliable as Res$_{GABA}$ cells under anesthesia (Figure 12D, Figure 16D). As we saw that mABCs receive excitatory inputs in the awake state (cholinergic and serotonergic projections), the basal activity level might arise from these projections. This would lead to more noise in the cell and a smaller signal-to-noise ratio, where 'signal' represents the odor-evoked activity and 'noise' represents the basal activity. As excitatory inputs reduce their activity under anesthesia, the reduction of 'noise' would increase the signal-to-noise ratio and enable mABCs to respond more reliably to odorant stimulation. This theory can be supported by modeling studies reviewed in D'Souza and Vijayaraghavan (2014), which describe the modulation of odor-evoked responses as a function of the basal activity induced by cholinergic inputs.

4.1 Future directions

Previous studies investigated ABC function mainly via relating ABC generation or survival to function/behavior. For instance, blocking neurogenesis led to impairment of odor discrimination or learning (1.2). Therefore, it has been proposed that ABCs have specific physiological properties that govern these functions. Physiological properties, such as basal or odor-evoked activities, were investigated, however, predominantly in slices or in anesthetized mice (1.2.1). As we showed, basal activity (basal ratios) of mABCs are altered under anesthesia, and so measurements in awake mice are a better reflection of ABC physiology. Measuring physiological properties of ABCs in awake mice paves the way to combine those measurements with behavior of the animal. In one study, adult-born GCs were activated via an optogenetic approach in awake mice and the animal's performance in an odor discrimination task was shown to improve (Alonso *et al.* 2012). However, studies measuring the basal activity of ABCs during a behavioral task have not been reported yet. This would give a clearer picture of how their physiological properties correlate with the olfactory behavior/function.

In the present study, we saw a reduction of basal ratios by blocking cholinergic and serotonergic receptors, and so a question arose how this blockade and the reduction of basal ratios would affect olfactory function/behavior. Interestingly, we observed increased motion of nose and whiskers in the animal after application of cholinergic receptor blockers (data not shown), indicating that the animal's perception might have changed. As acetylcholine was suggested to improve sensory perception in the OB (Linster *et al.* 2001; Mandairon *et al.* 2006), we hypothesize that the performance in a task like odor discrimination would be impaired during cholinergic receptor blockade. Moreover, since cholinergic fibers increase the basal activity in cells, it could be that the reduction of basal activity during cholinergic receptor blockade might be one responsible factor for the inability to discriminate odorants.

As serotonin was suggested to influence sensory gain, we hypothesize that the performance in a task like odor detection would be impaired during serotonergic receptor blockade. The threshold to detect odorants is an indicator for the sensory gain, as the threshold should be low when the sensory gain is high (indicating a high sensitivity). When serotonergic receptors on PGCs are blocked, PGCs will be excited less and

therefore inhibit OSNs less, resulting in stronger incoming olfactory input (sensory gain is increased). To combine physiology and function, basal ratios of mABCs and Res$_{GABA}$ cells could be measured during an odor detection task. Furthermore, the activity of OSN terminals in the OB could be analyzed in parallel. The activity of OSN terminals can be measured, e.g. using synaptopHluorin, which is a pH-sensitive fluorescent protein that was previously used to visualize presynaptic transmitter release from OSN terminals (Petzold *et al.* 2009). To determine if mABCs inhibit OSN presynapses differently than Res$_{GABA}$ cells do, mABCs or Res$_{GABA}$ cells could be optogenetically stimulated while transmitter release of OSNs is measured with synaptopHluorin.

In summary, combining physiological measurements with olfactory behavior provides a new way to study how ABCs process olfactory signals differently to resident cells and how this processing constitutes the suggested specific olfactory behavior.

4.2 Conclusion

In conclusion, we showed that mABCs become similar to Res$_{GABA}$ cells, but retain some unique features. For instance, mABCs had similar basal ratios - indicative of intracellular Ca^{2+} levels and spiking activity - as Res$_{GABA}$ cells in the awake state and under 3CN and isoflurane anesthesia. However, odor-evoked maximal ratios were found to be higher in mABCs compared to Res$_{GABA}$ cells in the awake as well as the anesthetized state. Furthermore, mABCs had significantly lower basal ratios under K/X anesthesia. The higher maximal ratios during odorant application and the lower basal ratios under K/X anesthesia point towards a potential mechanism of altered Ca^{2+} signaling required for the suggested role of ABCs in learning and memory. It was also observed that mABCs, but not Res$_{GABA}$ cells, reduce their basal ratios under serotonergic receptor blockade. This implies a specific role of serotonin for mABCs, as for example sensory gain control according to the animal's brain state.

5 References

Ache, B. W. and J. M. Young (2005). "Olfaction: diverse species, conserved principles." Neuron **48**(3): 417-430.

Alger, S. E., A. M. Chambers, et al. (2015). "The role of sleep in human declarative memory consolidation." Curr Top Behav Neurosci **25**: 269-306.

Alonso, M., G. Lepousez, et al. (2012). "Activation of adult-born neurons facilitates learning and memory." Nat Neurosci **15**(6): 897-904.

Alonso, M., C. Viollet, et al. (2006). "Olfactory discrimination learning increases the survival of adult-born neurons in the olfactory bulb." J Neurosci **26**(41): 10508-10513.

Alvarez-Buylla, A. and J. M. Garcia-Verdugo (2002). "Neurogenesis in adult subventricular zone." J Neurosci **22**(3): 629-634.

Antonelli, R., R. De Filippo, et al. (2016). "Pin1 Modulates the Synaptic Content of NMDA Receptors via Prolyl-Isomerization of PSD-95." J Neurosci **36**(20): 5437-5447.

Aroniadou-Anderjaska, V., F. M. Zhou, et al. (2000). "Tonic and synaptically evoked presynaptic inhibition of sensory input to the rat olfactory bulb via GABA(B) heteroreceptors." J Neurophysiol **84**(3): 1194-1203.

Bathellier, B., S. Lagier, et al. (2006). "Circuit properties generating gamma oscillations in a network model of the olfactory bulb." J Neurophysiol **95**(4): 2678-2691.

Bauer, S., E. Moyse, et al. (2003). "Effects of the α2-adrenoreceptor antagonist dexefaroxan on neurogenesis in the olfactory bulb of the adult rat in vivo: selective protection against neuronal death." Neuroscience **117**(2): 281-291.

Bee, L. A. and A. H. Dickenson (2009). "The importance of the descending monoamine system for the pain experience and its treatment." F1000 Med Rep **1**.

Belluzzi, O., M. Benedusi, et al. (2003). "Electrophysiological differentiation of new neurons in the olfactory bulb." J Neurosci **23**(32): 10411-10418.

Belnoue, L., N. Grosjean, et al. (2011). "A critical time window for the recruitment of bulbar newborn neurons by olfactory discrimination learning." J Neurosci **31**(3): 1010-1016.

Bliss, T. V. and T. Lomo (1973). "Long-lasting potentiation of synaptic transmission in the dentate area of the anaesthetized rabbit following stimulation of the perforant path." J Physiol **232**(2): 331-356.

Bonzano, S., S. Bovetti, et al. (2014). "Odour enrichment increases adult-born dopaminergic neurons in the mouse olfactory bulb." Eur J Neurosci **40**(10): 3450-3457.

Bovetti, S., A. Veyrac, et al. (2009). "Olfactory enrichment influences adult neurogenesis modulating GAD67 and plasticity-related molecules expression in newborn cells of the olfactory bulb." PLoS One **4**(7): e6359.

Boyd, A. M., H. K. Kato, et al. (2015). "Broadcasting of cortical activity to the olfactory bulb." Cell Rep **10**(7): 1032-1039.

Boyd, A. M., J. F. Sturgill, et al. (2012). "Cortical feedback control of olfactory bulb circuits." Neuron **76**(6): 1161-1174.

Brennan, P., H. Kaba, et al. (1990). "Olfactory recognition: a simple memory system." Science **250**(4985): 1223-1226.

Breton-Provencher, V., K. Bakhshetyan, et al. (2016). "Principal cell activity induces spine relocation of adult-born interneurons in the olfactory bulb." Nat Commun **7**: 12659.

Breton-Provencher, V., M. Lemasson, et al. (2009). "Interneurons produced in adulthood are required for the normal functioning of the olfactory bulb network and for the execution of selected olfactory behaviors." J Neurosci **29**(48): 15245-15257.

Breton-Provencher, V. and A. Saghatelyan (2012). "Newborn neurons in the adult olfactory bulb: unique properties for specific odor behavior." Behav Brain Res **227**(2): 480-489.

Brezun, J. M. and A. Daszuta (1999). "Depletion in serotonin decreases neurogenesis in the dentate gyrus and the subventricular zone of adult rats." Neuroscience **89**(4): 999-1002.

Brill, M. S., J. Ninkovic, et al. (2009). "Adult generation of glutamatergic olfactory bulb interneurons." Nat Neurosci **12**(12): 1524-1533.

Brinon, J. G., C. Crespo, et al. (2001). "Bilateral olfactory deprivation reveals a selective noradrenergic regulatory input to the olfactory bulb." Neuroscience **102**(1): 1-10.

Brown, E. N., R. Lydic, et al. (2010). "General anesthesia, sleep, and coma." N Engl J Med **363**(27): 2638-2650.

Brown, J. P., S. Couillard-Despres, et al. (2003). "Transient expression of doublecortin during adult neurogenesis." J Comp Neurol **467**(1): 1-10.

Brown, R. E., R. Basheer, et al. (2012). "Control of sleep and wakefulness." Physiol Rev **92**(3): 1087-1187.

Brunert, D., Y. Tsuno, et al. (2016). "Cell-Type-Specific Modulation of Sensory Responses in Olfactory Bulb Circuits by Serotonergic Projections from the Raphe Nuclei." J Neurosci **36**(25): 6820-6835.

Castillo, P. E., A. Carleton, et al. (1999). "Multiple and opposing roles of cholinergic transmission in the main olfactory bulb." J Neurosci **19**(21): 9180-9191.

Cavazzini, M., T. Bliss, et al. (2005). "Ca2+ and synaptic plasticity." Cell Calcium **38**(3-4): 355-367.

Cazakoff, B. N., B. Y. Lau, et al. (2014). "Broadly tuned and respiration-independent inhibition in the olfactory bulb of awake mice." Nat Neurosci **17**(4): 569-576.

Chao, H. T., H. Chen, et al. (2010). "Dysfunction in GABA signalling mediates autism-like stereotypies and Rett syndrome phenotypes." Nature **468**(7321): 263-269.

Chen, Z. and M. A. Wilson (2017). "Deciphering Neural Codes of Memory during Sleep." Trends Neurosci **40**(5): 260-275.

Christen-Zaech, S., R. Kraftsik, et al. (2003). "Early olfactory involvement in Alzheimer's disease." Can J Neurol Sci **30**(1): 20-25.

Cleland, T. A. and C. Linster (2005). "Computation in the olfactory system." Chem Senses **30**(9): 801-813.

Cleland, T. A. and P. Sethupathy (2006). "Non-topographical contrast enhancement in the olfactory bulb." BMC Neurosci **7**: 7.

Cooper-Kuhn, C. M., J. Winkler, et al. (2004). "Decreased neurogenesis after cholinergic forebrain lesion in the adult rat." J Neurosci Res **77**(2): 155-165.

Correa-Sales, C., B. C. Rabin, et al. (1992). "A hypnotic response to dexmedetomidine, an alpha 2 agonist, is mediated in the locus coeruleus in rats." Anesthesiology **76**(6): 948-952.

Cox, J., L. Pinto, et al. (2016). "Calcium imaging of sleep-wake related neuronal activity in the dorsal pons." Nat Commun **7**: 10763.

Coyle, J. T., D. L. Price, et al. (1983). "Alzheimer's disease: a disorder of cortical cholinergic innervation." Science **219**(4589): 1184-1190.

Cummings, D. M., J. S. Snyder, et al. (2014). "Adult neurogenesis is necessary to refine and maintain circuit specificity." J Neurosci **34**(41): 13801-13810.

D'Souza, R. D., P. V. Parsa, et al. (2013). "Nicotinic receptors modulate olfactory bulb external tufted cells via an excitation-dependent inhibitory mechanism." J Neurophysiol **110**(7): 1544-1553.

D'Souza, R. D. and S. Vijayaraghavan (2012). "Nicotinic receptor-mediated filtering of mitral cell responses to olfactory nerve inputs involves the alpha3beta4 subtype." J Neurosci **32**(9): 3261-3266.

D'Souza, R. D. and S. Vijayaraghavan (2014). "Paying attention to smell: cholinergic signaling in the olfactory bulb." Front Synaptic Neurosci **6**: 21.

Dacks, A. M., D. S. Green, et al. (2009). "Serotonin modulates olfactory processing in the antennal lobe of Drosophila." J Neurogenet **23**(4): 366-377.

Danielson, N. B., P. Kaifosh, et al. (2016). "Distinct Contribution of Adult-Born Hippocampal Granule Cells to Context Encoding." Neuron **90**(1): 101-112.

Day, H. E., S. Campeau, et al. (1997). "Distribution of alpha 1a-, alpha 1b- and alpha 1d-adrenergic receptor mRNA in the rat brain and spinal cord." J Chem Neuroanat **13**(2): 115-139.

de Almeida, L., M. Idiart, et al. (2013). "A model of cholinergic modulation in olfactory bulb and piriform cortex." J Neurophysiol **109**(5): 1360-1377.

References

De Marchis, S., S. Bovetti, et al. (2007). "Generation of distinct types of periglomerular olfactory bulb interneurons during development and in adult mice: implication for intrinsic properties of the subventricular zone progenitor population." J Neurosci **27**(3): 657-664.

Deshpande, A., M. Bergami, et al. (2013). "Retrograde monosynaptic tracing reveals the temporal evolution of inputs onto new neurons in the adult dentate gyrus and olfactory bulb." Proc Natl Acad Sci U S A **110**(12): E1152-1161.

Detari, L., D. D. Rasmusson, et al. (1999). "The role of basal forebrain neurons in tonic and phasic activation of the cerebral cortex." Prog Neurobiol **58**(3): 249-277.

Devanand, D. P., S. Lee, et al. (2015). "Olfactory deficits predict cognitive decline and Alzheimer dementia in an urban community." Neurology **84**(2): 182-189.

Devore, S. and C. Linster (2012). "Noradrenergic and cholinergic modulation of olfactory bulb sensory processing." Front Behav Neurosci **6**: 52.

Dietz, S. B. and V. N. Murthy (2005). "Contrasting short-term plasticity at two sides of the mitral-granule reciprocal synapse in the mammalian olfactory bulb." J Physiol **569**(Pt 2): 475-488.

Doetsch, F., I. Caille, et al. (1999). "Subventricular zone astrocytes are neural stem cells in the adult mammalian brain." Cell **97**(6): 703-716.

Doty, R. L. (2005). "Clinical studies of olfaction." Chem Senses **30 Suppl 1**: i207-209.

Doty, R. L. (2017). "Olfactory dysfunction in neurodegenerative diseases: is there a common pathological substrate?" Lancet Neurol **16**(6): 478-488.

Doty, R. L. and V. Kamath (2014). "The influences of age on olfaction: a review." Front Psychol **5**: 20.

Doucette, W., J. Milder, et al. (2007). "Adrenergic modulation of olfactory bulb circuitry affects odor discrimination." Learn Mem **14**(8): 539-547.

Dringenberg, H. C. and C. H. Vanderwolf (1998). "Involvement of direct and indirect pathways in electrocorticographic activation." Neurosci Biobehav Rev **22**(2): 243-257.

Dugue, G. P., M. L. Lorincz, et al. (2014). "Optogenetic recruitment of dorsal raphe serotonergic neurons acutely decreases mechanosensory responsivity in behaving mice." PLoS One **9**(8): e105941.

Durand, M., V. Coronas, et al. (1998). "Developmental and aging aspects of the cholinergic innervation of the olfactory bulb." Int J Dev Neurosci **16**(7-8): 777-785.

Eccles, J. C. (1983). "Calcium in long-term potentiation as a model for memory." Neuroscience **10**(4): 1071-1081.

Eger, E. I., 2nd (1981). "Isoflurane: a review." Anesthesiology **55**(5): 559-576.

Enwere, E., T. Shingo, et al. (2004). "Aging results in reduced epidermal growth factor receptor signaling, diminished olfactory neurogenesis, and deficits in fine olfactory discrimination." J Neurosci **24**(38): 8354-8365.

Feierstein, C. E., F. Lazarini, et al. (2010). "Disruption of Adult Neurogenesis in the Olfactory Bulb Affects Social Interaction but not Maternal Behavior." Front Behav Neurosci **4**: 176.

Ferrero, D. M. and S. D. Liberles (2010). "The secret codes of mammalian scents." Wiley Interdiscip Rev Syst Biol Med **2**(1): 23-33.

Fletcher, M. L. and D. A. Wilson (2002). "Experience modifies olfactory acuity: acetylcholine-dependent learning decreases behavioral generalization between similar odorants." J Neurosci **22**(2): RC201.

Förster, T. (1948). "Zwischenmolekulare Energiewanderung und Fluoreszenz." Annalen der Physik **437**(1-2): 55-75.

Freedman, R., L. E. Adler, et al. (1987). "Neurobiological studies of sensory gating in schizophrenia." Schizophr Bull **13**(4): 669-678.

Freedman, R., L. E. Adler, et al. (1996). "Inhibitory gating of an evoked response to repeated auditory stimuli in schizophrenic and normal subjects. Human recordings, computer simulation, and an animal model." Arch Gen Psychiatry **53**(12): 1114-1121.

Gage, F. H. (2004). "Structural plasticity of the adult brain." Dialogues Clin Neurosci **6**(2): 135-141.

Gheusi, G., H. Cremer, et al. (2000). "Importance of newly generated neurons in the adult olfactory bulb for odor discrimination." Proc Natl Acad Sci U S A **97**(4): 1823-1828.

Gheusi, G. and P. M. Lledo (2014). "Adult neurogenesis in the olfactory system shapes odor memory and perception." Prog Brain Res **208**: 157-175.

Gire, D. H. and N. E. Schoppa (2009). "Control of on/off glomerular signaling by a local GABAergic microcircuit in the olfactory bulb." J Neurosci **29**(43): 13454-13464.

Godoy, M. D., R. L. Voegels, et al. (2015). "Olfaction in neurologic and neurodegenerative diseases: a literature review." Int Arch Otorhinolaryngol **19**(2): 176-179.

Gomez, C., J. G. Brinon, et al. (2005). "Heterogeneous targeting of centrifugal inputs to the glomerular layer of the main olfactory bulb." J Chem Neuroanat **29**(4): 238-254.

Gomez, C., J. G. Brinon, et al. (2007). "Changes in the serotonergic system in the main olfactory bulb of rats unilaterally deprived from birth to adulthood." J Neurochem **100**(4): 924-938.

Grieco, S. F., D. Velmeshev, et al. (2017). "Ketamine up-regulates a cluster of intronic miRNAs within the serotonin receptor 2C gene by inhibiting glycogen synthase kinase-3." World J Biol Psychiatry **18**(6): 445-456.

Grubb, M. S., A. Nissant, et al. (2008). "Functional maturation of the first synapse in olfaction: development and adult neurogenesis." J Neurosci **28**(11): 2919-2932.

Hansen, K. B., F. Yi, et al. (2017). "NMDA Receptors in the Central Nervous System." Methods Mol Biol **1677**: 1-80.

Hardy, A., B. Palouzier-Paulignan, et al. (2005). "5-Hydroxytryptamine action in the rat olfactory bulb: in vitro electrophysiological patch-clamp recordings of juxtaglomerular and mitral cells." Neuroscience **131**(3): 717-731.

Hasselmo, M. E. and L. M. Giocomo (2006). "Cholinergic modulation of cortical function." J Mol Neurosci **30**(1-2): 133-135.

Hayar, A., P. M. Heyward, et al. (2001). "Direct excitation of mitral cells via activation of alpha1-noradrenergic receptors in rat olfactory bulb slices." J Neurophysiol **86**(5): 2173-2182.

Himmelheber, A. M., M. Sarter, et al. (2000). "Increases in cortical acetylcholine release during sustained attention performance in rats." Brain Res Cogn Brain Res **9**(3): 313-325.

Holtmaat, A., T. Bonhoeffer, et al. (2009). "Long-term, high-resolution imaging in the mouse neocortex through a chronic cranial window." Nat Protoc **4**(8): 1128-1144.

Holtmaat, A. and K. Svoboda (2009). "Experience-dependent structural synaptic plasticity in the mammalian brain." Nat Rev Neurosci **10**(9): 647-658.

Huang, L., K. Ung, et al. (2016). "Task Learning Promotes Plasticity of Interneuron Connectivity Maps in the Olfactory Bulb." J Neurosci **36**(34): 8856-8871.

Hunter, A. J. and T. K. Murray (1989). "Cholinergic mechanisms in a simple test of olfactory learning in the rat." Psychopharmacology (Berl) **99**(2): 270-275.

Hurley, L. M., D. M. Devilbiss, et al. (2004). "A matter of focus: monoaminergic modulation of stimulus coding in mammalian sensory networks." Curr Opin Neurobiol **14**(4): 488-495.

Hurley, L. M., A. M. Thompson, et al. (2002). "Serotonin in the inferior colliculus." Hear Res **168**(1-2): 1-11.

Huupponen, E., A. Maksimow, et al. (2008). "Electroencephalogram spindle activity during dexmedetomidine sedation and physiological sleep." Acta Anaesthesiol Scand **52**(2): 289-294.

Imai, T. (2014). "Construction of functional neuronal circuitry in the olfactory bulb." Semin Cell Dev Biol **35**: 180-188.

Jacobs, B. L. and E. C. Azmitia (1992). "Structure and function of the brain serotonin system." Physiol Rev **72**(1): 165-229.

Jacobs, B. L. and C. A. Fornal (1993). "5-HT and motor control: a hypothesis." Trends Neurosci **16**(9): 346-352.

Jacobs, B. L. and C. A. Fornal (1999). "Activity of serotonergic neurons in behaving animals." Neuropsychopharmacology **21**(2 Suppl): 9S-15S.

References

Jevtovic-Todorovic, V. (2012). "Developmental synaptogenesis and general anesthesia: a kiss of death?" Curr Pharm Des **18**(38): 6225-6231.

Jones, B. E. (2003). "Arousal systems." Front Biosci **8**: s438-451.

Jones, B. E. (2005). "From waking to sleeping: neuronal and chemical substrates." Trends Pharmacol Sci **26**(11): 578-586.

Jones, B. E. and T. Z. Yang (1985). "The efferent projections from the reticular formation and the locus coeruleus studied by anterograde and retrograde axonal transport in the rat." J Comp Neurol **242**(1): 56-92.

Kadohisa, M. (2013). "Effects of odor on emotion, with implications." Front Syst Neurosci **7**: 66.

Kaneko, N., H. Okano, et al. (2006). "Role of the cholinergic system in regulating survival of newborn neurons in the adult mouse dentate gyrus and olfactory bulb." Genes Cells **11**(10): 1145-1159.

Kapoor, V., A. C. Provost, et al. (2016). "Activation of raphe nuclei triggers rapid and distinct effects on parallel olfactory bulb output channels." Nat Neurosci **19**(2): 271-282.

Kasa, P. (1986). "The cholinergic systems in brain and spinal cord." Prog Neurobiol **26**(3): 211-272.

Kaslin, J., J. Ganz, et al. (2008). "Proliferation, neurogenesis and regeneration in the non-mammalian vertebrate brain." Philos Trans R Soc Lond B Biol Sci **363**(1489): 101-122.

Kato, H. K., M. W. Chu, et al. (2012). "Dynamic sensory representations in the olfactory bulb: modulation by wakefulness and experience." Neuron **76**(5): 962-975.

Kermen, F., S. Sultan, et al. (2010). "Consolidation of an olfactory memory trace in the olfactory bulb is required for learning-induced survival of adult-born neurons and long-term memory." PLoS One **5**(8): e12118.

Kevetter, G. A. and S. S. Winans (1981). "Connections of the corticomedial amygdala in the golden hamster. II. Efferents of the "olfactory amygdala"." J Comp Neurol **197**(1): 99-111.

Kiyokage, E., Y. Z. Pan, et al. (2010). "Molecular identity of periglomerular and short axon cells." J Neurosci **30**(3): 1185-1196.

Koizuka, S., H. Obata, et al. (2005). "Systemic ketamine inhibits hypersensitivity after surgery via descending inhibitory pathways in rats." Can J Anaesth **52**(5): 498-505.

Komiyama, T., T. R. Sato, et al. (2010). "Learning-related fine-scale specificity imaged in motor cortex circuits of behaving mice." Nature **464**(7292): 1182-1186.

Kovalchuk, Y., R. Homma, et al. (2015). "In vivo odourant response properties of migrating adult-born neurons in the mouse olfactory bulb." Nat Commun **6**: 6349.

Krzisch, M., S. Sultan, et al. (2013). "Propofol anesthesia impairs the maturation and survival of adult-born hippocampal neurons." Anesthesiology **118**(3): 602-610.

Kunze, W. A., A. D. Shafton, et al. (1992). "Intracellular responses of olfactory bulb granule cells to stimulating the horizontal diagonal band nucleus." Neuroscience **48**(2): 363-369.

Lagier, S., P. Panzanelli, et al. (2007). "GABAergic inhibition at dendrodendritic synapses tunes gamma oscillations in the olfactory bulb." Proc Natl Acad Sci U S A **104**(17): 7259-7264.

Larsen, C. M., I. C. Kokay, et al. (2008). "Male pheromones initiate prolactin-induced neurogenesis and advance maternal behavior in female mice." Horm Behav **53**(4): 509-517.

Larson, A. A. (1984). "Interactions between ketamine and phencyclidine and dorsal root potentials (DRPs), evoked from the raphe nuclei." Neuropharmacology **23**(7A): 785-791.

Lazarini, F. and P. M. Lledo (2011). "Is adult neurogenesis essential for olfaction?" Trends Neurosci **34**(1): 20-30.

Lazarini, F., M. A. Mouthon, et al. (2009). "Cellular and behavioral effects of cranial irradiation of the subventricular zone in adult mice." PLoS One **4**(9): e7017.

Le Jeune, H., I. Aubert, et al. (1996). "Developmental profiles of various cholinergic markers in the rat main olfactory bulb using quantitative autoradiography." J Comp Neurol **373**(3): 433-450.

Lee, M. G., O. K. Hassani, et al. (2005). "Cholinergic basal forebrain neurons burst with theta during waking and paradoxical sleep." J Neurosci **25**(17): 4365-4369.

Lee, S. H. and Y. Dan (2012). "Neuromodulation of brain states." Neuron **76**(1): 209-222.

Lepousez, G., A. Nissant, et al. (2014). "Olfactory learning promotes input-specific synaptic plasticity in adult-born neurons." Proc Natl Acad Sci U S A **111**(38): 13984-13989.

Lepousez, G., M. T. Valley, et al. (2013). "The impact of adult neurogenesis on olfactory bulb circuits and computations." Annu Rev Physiol **75**: 339-363.

Li, G. and T. A. Cleland (2013). "A two-layer biophysical model of cholinergic neuromodulation in olfactory bulb." J Neurosci **33**(7): 3037-3058.

Linster, C., P. A. Garcia, et al. (2001). "Selective loss of cholinergic neurons projecting to the olfactory system increases perceptual generalization between similar, but not dissimilar, odorants." Behav Neurosci **115**(4): 826-833.

Livneh, Y., Y. Adam, et al. (2014). "Odor processing by adult-born neurons." Neuron **81**(5): 1097-1110.

Livneh, Y., N. Feinstein, et al. (2009). "Sensory input enhances synaptogenesis of adult-born neurons." J Neurosci **29**(1): 86-97.

Livneh, Y. and A. Mizrahi (2011). "Experience-dependent plasticity of mature adult-born neurons." Nat Neurosci **15**(1): 26-28.

Livneh, Y. and A. Mizrahi (2011). "Long-term changes in the morphology and synaptic distributions of adult-born neurons." J Comp Neurol **519**(11): 2212-2224.

Lledo, P. M., M. Alonso, et al. (2006). "Adult neurogenesis and functional plasticity in neuronal circuits." Nat Rev Neurosci **7**(3): 179-193.

Lledo, P. M. and A. Saghatelyan (2005). "Integrating new neurons into the adult olfactory bulb: joining the network, life-death decisions, and the effects of sensory experience." Trends Neurosci **28**(5): 248-254.

Lois, C. and A. Alvarez-Buylla (1994). "Long-distance neuronal migration in the adult mammalian brain." Science **264**(5162): 1145-1148.

Lorincz, M. L. and A. R. Adamantidis (2017). "Monoaminergic control of brain states and sensory processing: Existing knowledge and recent insights obtained with optogenetics." Prog Neurobiol **151**: 237-253.

Luhrs, L., C. Manlapaz, et al. (2016). "Function of brain alpha2B-adrenergic receptor characterized with subtype-selective alpha2B antagonist and KO mice." Neuroscience **339**: 608-621.

Luskin, M. B. (1993). "Restricted proliferation and migration of postnatally generated neurons derived from the forebrain subventricular zone." Neuron **11**(1): 173-189.

Ma, M. and M. Luo (2012). "Optogenetic activation of basal forebrain cholinergic neurons modulates neuronal excitability and sensory responses in the main olfactory bulb." J Neurosci **32**(30): 10105-10116.

Macrides, F., B. J. Davis, et al. (1981). "Cholinergic and catecholaminergic afferents to the olfactory bulb in the hamster: a neuroanatomical, biochemical, and histochemical investigation." J Comp Neurol **203**(3): 495-514.

Magavi, S. S., B. D. Mitchell, et al. (2005). "Adult-born and preexisting olfactory granule neurons undergo distinct experience-dependent modifications of their olfactory responses in vivo." J Neurosci **25**(46): 10729-10739.

Mak, G. K., E. K. Enwere, et al. (2007). "Male pheromone-stimulated neurogenesis in the adult female brain: possible role in mating behavior." Nat Neurosci **10**(8): 1003-1011.

Mak, G. K. and S. Weiss (2010). "Paternal recognition of adult offspring mediated by newly generated CNS neurons." Nat Neurosci **13**(6): 753-758.

Mandairon, N., C. J. Ferretti, et al. (2006). "Cholinergic modulation in the olfactory bulb influences spontaneous olfactory discrimination in adult rats." Eur J Neurosci **24**(11): 3234-3244.

References

Mandairon, N., S. Peace, et al. (2008). "Noradrenergic modulation in the olfactory bulb influences spontaneous and reward-motivated discrimination, but not the formation of habituation memory." Eur J Neurosci **27**(5): 1210-1219.

Mandairon, N., J. Sacquet, et al. (2006). "Long-term fate and distribution of newborn cells in the adult mouse olfactory bulb: Influences of olfactory deprivation." Neuroscience **141**(1): 443-451.

Mandairon, N., S. Sultan, et al. (2011). "Involvement of newborn neurons in olfactory associative learning? The operant or non-operant component of the task makes all the difference." J Neurosci **31**(35): 12455-12460.

Maret, S., U. Faraguna, et al. (2011). "Sleep and waking modulate spine turnover in the adolescent mouse cortex." Nat Neurosci **14**(11): 1418-1420.

Martin, L. L., R. L. Bouchal, et al. (1982). "Ketamine inhibits serotonin uptake in vivo." Neuropharmacology **21**(2): 113-118.

Martin, L. L. and D. J. Smith (1982). "Ketamine inhibits serotonin synthesis and metabolism in vivo." Neuropharmacology **21**(2): 119-125.

McCardle, C. E. and S. E. Gartside (2012). "Effects of general anaesthetics on 5-HT neuronal activity in the dorsal raphe nucleus." Neuropharmacology **62**(4): 1787-1796.

McCune, S. K., M. M. Voigt, et al. (1993). "Expression of multiple alpha adrenergic receptor subtype messenger RNAs in the adult rat brain." Neuroscience **57**(1): 143-151.

McGann, J. P. (2013). "Presynaptic inhibition of olfactory sensory neurons: new mechanisms and potential functions." Chem Senses **38**(6): 459-474.

McGann, J. P., N. Pirez, et al. (2005). "Odorant representations are modulated by intra- but not interglomerular presynaptic inhibition of olfactory sensory neurons." Neuron **48**(6): 1039-1053.

McLean, J. H., A. Darby-King, et al. (1993). "Serotonergic influence on olfactory learning in the neonate rat." Behav Neural Biol **60**(2): 152-162.

McLean, J. H. and M. T. Shipley (1987). "Serotonergic afferents to the rat olfactory bulb: I. Origins and laminar specificity of serotonergic inputs in the adult rat." J Neurosci **7**(10): 3016-3028.

McLean, J. H. and M. T. Shipley (1991). "Postnatal development of the noradrenergic projection from locus coeruleus to the olfactory bulb in the rat." J Comp Neurol **304**(3): 467-477.

McLean, J. H., M. T. Shipley, et al. (1989). "Chemoanatomical organization of the noradrenergic input from locus coeruleus to the olfactory bulb of the adult rat." J Comp Neurol **285**(3): 339-349.

Mechawar, N., A. Saghatelyan, et al. (2004). "Nicotinic receptors regulate the survival of newborn neurons in the adult olfactory bulb." Proc Natl Acad Sci U S A **101**(26): 9822-9826.

Ming, G. L. and H. Song (2011). "Adult neurogenesis in the mammalian brain: significant answers and significant questions." Neuron **70**(4): 687-702.

Mion, G. and T. Villevieille (2013). "Ketamine pharmacology: an update (pharmacodynamics and molecular aspects, recent findings)." CNS Neurosci Ther **19**(6): 370-380.

Mizrahi, A. (2007). "Dendritic development and plasticity of adult-born neurons in the mouse olfactory bulb." Nat Neurosci **10**(4): 444-452.

Mizrahi, A., J. Lu, et al. (2006). "In vivo imaging of juxtaglomerular neuron turnover in the mouse olfactory bulb." Proc Natl Acad Sci U S A **103**(6): 1912-1917.

Mombaerts, P., F. Wang, et al. (1996). "Visualizing an olfactory sensory map." Cell **87**(4): 675-686.

Moreno, M. M., K. Bath, et al. (2012). "Action of the noradrenergic system on adult-born cells is required for olfactory learning in mice." J Neurosci **32**(11): 3748-3758.

Moreno, M. M., C. Linster, et al. (2009). "Olfactory perceptual learning requires adult neurogenesis." Proc Natl Acad Sci U S A **106**(42): 17980-17985.

Moriizumi, T., T. Tsukatani, et al. (1994). "Olfactory disturbance induced by deafferentation of serotonergic fibers in the olfactory bulb." Neuroscience **61**(4): 733-738.

Mouret, A., G. Gheusi, et al. (2008). "Learning and survival of newly generated neurons: when time matters." J Neurosci **28**(45): 11511-11516.

Mouret, A., K. Murray, et al. (2009). "Centrifugal drive onto local inhibitory interneurons of the olfactory bulb." Ann N Y Acad Sci **1170**: 239-254.

Murphy, G. J., D. P. Darcy, et al. (2005). "Intraglomerular inhibition: signaling mechanisms of an olfactory microcircuit." Nat Neurosci **8**(3): 354-364.

Nagayama, S., R. Homma, et al. (2014). "Neuronal organization of olfactory bulb circuits." Front Neural Circuits **8**: 98.

Nai, Q., H. W. Dong, et al. (2010). "Activation of alpha1 and alpha2 noradrenergic receptors exert opposing effects on excitality of main olfactory bulb granule cells." Neuroscience **169**(2): 882-892.

Nelson, L. E., T. Z. Guo, et al. (2002). "The sedative component of anesthesia is mediated by GABA(A) receptors in an endogenous sleep pathway." Nat Neurosci **5**(10): 979-984.

Nelson, L. E., J. Lu, et al. (2003). "The alpha2-adrenoceptor agonist dexmedetomidine converges on an endogenous sleep-promoting pathway to exert its sedative effects." Anesthesiology **98**(2): 428-436.

Niethard, N., M. Hasegawa, et al. (2016). "Sleep-Stage-Specific Regulation of Cortical Excitation and Inhibition." Curr Biol **26**(20): 2739-2749.

Ninkovic, J., T. Mori, et al. (2007). "Distinct modes of neuron addition in adult mouse neurogenesis." J Neurosci **27**(40): 10906-10911.

Nissant, A., C. Bardy, et al. (2009). "Adult neurogenesis promotes synaptic plasticity in the olfactory bulb." Nat Neurosci **12**(6): 728-730.

Otazu, G. H., H. Chae, et al. (2015). "Cortical Feedback Decorrelates Olfactory Bulb Output in Awake Mice." Neuron **86**(6): 1461-1477.

Pan, W. H., S. Y. Yang, et al. (2004). "Neurochemical interaction between dopaminergic and noradrenergic neurons in the medial prefrontal cortex." Synapse **53**(1): 44-52.

Pan, Y. W., G. C. Chan, et al. (2012). "Inhibition of adult neurogenesis by inducible and targeted deletion of ERK5 mitogen-activated protein kinase specifically in adult neurogenic regions impairs contextual fear extinction and remote fear memory." J Neurosci **32**(19): 6444-6455.

Pan, Y. W., C. T. Kuo, et al. (2012). "Inducible and targeted deletion of the ERK5 MAP kinase in adult neurogenic regions impairs adult neurogenesis in the olfactory bulb and several forms of olfactory behavior." PLoS One **7**(11): e49622.

Pandipati, S., D. H. Gire, et al. (2010). "Adrenergic receptor-mediated disinhibition of mitral cells triggers long-term enhancement of synchronized oscillations in the olfactory bulb." J Neurophysiol **104**(2): 665-674.

Park, K., J. You, et al. (2015). "Cranial window implantation on mouse cortex to study microvascular change induced by cocaine." Quant Imaging Med Surg **5**(1): 97-107.

Parrish-Aungst, S., M. T. Shipley, et al. (2007). "Quantitative analysis of neuronal diversity in the mouse olfactory bulb." J Comp Neurol **501**(6): 825-836.

Pepeu, G. and M. Grazia Giovannini (2017). "The fate of the brain cholinergic neurons in neurodegenerative diseases." Brain Res **1670**: 173-184.

Petzold, G. C., A. Hagiwara, et al. (2009). "Serotonergic modulation of odor input to the mammalian olfactory bulb." Nat Neurosci **12**(6): 784-791.

Pinto, J. M. (2011). "Olfaction." Proc Am Thorac Soc **8**(1): 46-52.

Piochon, C., M. Kano, et al. (2016). "LTD-like molecular pathways in developmental synaptic pruning." Nat Neurosci **19**(10): 1299-1310.

Pirez, N. and M. Wachowiak (2008). "In vivo modulation of sensory input to the olfactory bulb by tonic and activity-dependent presynaptic inhibition of receptor neurons." J Neurosci **28**(25): 6360-6371.

Porteros, A., C. Gomez, et al. (2007). "Chemical organization of the macaque monkey olfactory bulb: III. Distribution of cholinergic markers." J Comp Neurol **501**(6): 854-865.

Pressler, R. T., T. Inoue, et al. (2007). "Muscarinic receptor activation modulates granule cell excitability and potentiates inhibition onto mitral cells in the rat olfactory bulb." J Neurosci **27**(41): 10969-10981.

Quast, K. B., K. Ung, et al. (2017). "Developmental broadening of inhibitory sensory maps." Nat Neurosci **20**(2): 189-199.

Ramirez-Amaya, V., D. F. Marrone, et al. (2006). "Integration of new neurons into functional neural networks." J Neurosci **26**(47): 12237-12241.

Ravel, N., H. Akaoka, et al. (1990). "The effect of acetylcholine on rat olfactory bulb unit activity." Brain Res Bull **24**(2): 151-155.

Ravel, N., A. Elaagouby, et al. (1994). "Scopolamine injection into the olfactory bulb impairs short-term olfactory memory in rats." Behav Neurosci **108**(2): 317-324.

Reddy, S. V. (2012). "Effect of general anesthetics on the developing brain." J Anaesthesiol Clin Pharmacol **28**(1): 6-10.

Rochefort, C., G. Gheusi, et al. (2002). "Enriched odor exposure increases the number of newborn neurons in the adult olfactory bulb and improves odor memory." J Neurosci **22**(7): 2679-2689.

Roman, F. S., I. Simonetto, et al. (1993). "Learning and memory of odor-reward association: selective impairment following horizontal diagonal band lesions." Behav Neurosci **107**(1): 72-81.

Roome, C. J. and B. Kuhn (2014). "Chronic cranial window with access port for repeated cellular manipulations, drug application, and electrophysiology." Front Cell Neurosci **8**: 379.

Ross, G. W., H. Petrovitch, et al. (2008). "Association of olfactory dysfunction with risk for future Parkinson's disease." Ann Neurol **63**(2): 167-173.

Rosser, A. E. and E. B. Keverne (1985). "The importance of central noradrenergic neurones in the formation of an olfactory memory in the prevention of pregnancy block." Neuroscience **15**(4): 1141-1147.

Rothermel, M., R. M. Carey, et al. (2014). "Cholinergic inputs from Basal forebrain add an excitatory bias to odor coding in the olfactory bulb." J Neurosci **34**(13): 4654-4664.

Sailor, K. A., M. T. Valley, et al. (2016). "Persistent Structural Plasticity Optimizes Sensory Information Processing in the Olfactory Bulb." Neuron **91**(2): 384-396.

Sakamoto, M., N. Ieki, et al. (2014). "Continuous postnatal neurogenesis contributes to formation of the olfactory bulb neural circuits and flexible olfactory associative learning." J Neurosci **34**(17): 5788-5799.

Sakamoto, M., I. Imayoshi, et al. (2011). "Continuous neurogenesis in the adult forebrain is required for innate olfactory responses." Proc Natl Acad Sci U S A **108**(20): 8479-8484.

Salcedo, E., T. Tran, et al. (2011). "Activity-dependent changes in cholinergic innervation of the mouse olfactory bulb." PLoS One **6**(10): e25441.

Sara, S. J., A. Vankov, et al. (1994). "Locus coeruleus-evoked responses in behaving rats: a clue to the role of noradrenaline in memory." Brain Res Bull **35**(5-6): 457-465.

Sarter, M. and J. P. Bruno (1997). "Cognitive functions of cortical acetylcholine: toward a unifying hypothesis." Brain Res Brain Res Rev **23**(1-2): 28-46.

Sawada, M., N. Kaneko, et al. (2011). "Sensory input regulates spatial and subtype-specific patterns of neuronal turnover in the adult olfactory bulb." J Neurosci **31**(32): 11587-11596.

Schwartz, O. and E. P. Simoncelli (2001). "Natural signal statistics and sensory gain control." Nat Neurosci **4**(8): 819-825.

Seillier, L., C. Lorenz, et al. (2017). "Serotonin decreases the gain of visual responses in awake macaque V1." J Neurosci.

Semba, K. (2000). "Multiple output pathways of the basal forebrain: organization, chemical heterogeneity, and roles in vigilance." Behav Brain Res **115**(2): 117-141.

Shakhawat, A. M., C. W. Harley, et al. (2012). "Olfactory bulb alpha2-adrenoceptor activation promotes rat pup odor-preference learning via a cAMP-independent mechanism." Learn Mem **19**(11): 499-502.

Shea, S. D., L. C. Katz, et al. (2008). "Noradrenergic induction of odor-specific neural habituation and olfactory memories." J Neurosci **28**(42): 10711-10719.

Shepherd, G. M. (2004). The synaptic organization of the brain. Oxford ; New York, Oxford University Press.

Shepherd, G. M., W. R. Chen, et al. (2007). "The olfactory granule cell: from classical enigma to central role in olfactory processing." Brain Res Rev **55**(2): 373-382.

Shingo, T., C. Gregg, et al. (2003). "Pregnancy-stimulated neurogenesis in the adult female forebrain mediated by prolactin." Science **299**(5603): 117-120.

Shipley, M. T. and G. D. Adamek (1984). "The connections of the mouse olfactory bulb: a study using orthograde and retrograde transport of wheat germ agglutinin conjugated to horseradish peroxidase." Brain Res Bull **12**(6): 669-688.

Simms, B. A. and G. W. Zamponi (2014). "Neuronal voltage-gated calcium channels: structure, function, and dysfunction." Neuron **82**(1): 24-45.

Siopi, E., M. Denizet, et al. (2016). "Anxiety- and Depression-Like States Lead to Pronounced Olfactory Deficits and Impaired Adult Neurogenesis in Mice." J Neurosci **36**(2): 518-531.

Soucy, E. R., D. F. Albeanu, et al. (2009). "Precision and diversity in an odor map on the olfactory bulb." Nat Neurosci **12**(2): 210-220.

Soumier, A., M. Banasr, et al. (2010). "Region- and phase-dependent effects of 5-HT(1A) and 5-HT(2C) receptor activation on adult neurogenesis." Eur Neuropsychopharmacol **20**(5): 336-345.

Sultan, S., N. Mandairon, et al. (2010). "Learning-dependent neurogenesis in the olfactory bulb determines long-term olfactory memory." FASEB J **24**(7): 2355-2363.

Telezhkin, V., C. Schnell, et al. (2016). "Forced cell cycle exit and modulation of GABAA, CREB, and GSK3beta signaling promote functional maturation of induced pluripotent stem cell-derived neurons." Am J Physiol Cell Physiol **310**(7): C520-541.

Thestrup, T., J. Litzlbauer, et al. (2014). "Optimized ratiometric calcium sensors for functional in vivo imaging of neurons and T lymphocytes." Nat Methods **11**(2): 175-182.

Urban, D. J. and B. L. Roth (2015). "DREADDs (designer receptors exclusively activated by designer drugs): chemogenetic tools with therapeutic utility." Annu Rev Pharmacol Toxicol **55**: 399-417.

Valley, M. T., T. R. Mullen, et al. (2009). "Ablation of mouse adult neurogenesis alters olfactory bulb structure and olfactory fear conditioning." Front Neurosci **3**: 51.

Vanini, G., P. Torterolo, et al. (2011). Neuroscientific Foundations of Anesthesiology. The Shared Circuits of Sleep and Anesthesia.

Vassar, R., S. K. Chao, et al. (1994). "Topographic organization of sensory projections to the olfactory bulb." Cell **79**(6): 981-991.

Vucinic, D., L. B. Cohen, et al. (2006). "Interglomerular center-surround inhibition shapes odorant-evoked input to the mouse olfactory bulb in vivo." J Neurophysiol **95**(3): 1881-1887.

Wachowiak, M., M. N. Economo, et al. (2013). "Optical dissection of odor information processing in vivo using GCaMPs expressed in specified cell types of the olfactory bulb." J Neurosci **33**(12): 5285-5300.

Wachowiak, M., J. P. McGann, et al. (2005). "Inhibition [corrected] of olfactory receptor neuron input to olfactory bulb glomeruli mediated by suppression of presynaptic calcium influx." J Neurophysiol **94**(4): 2700-2712.

Wallace, J. L., M. Wienisch, et al. (2017). "Development and Refinement of Functional Properties of Adult-Born Neurons." Neuron.

Wang, W., S. Lu, et al. (2015). "Inducible activation of ERK5 MAP kinase enhances adult neurogenesis in the olfactory bulb and improves olfactory function." J Neurosci **35**(20): 7833-7849.

Waterhouse, B. D., S. A. Azizi, et al. (1990). "Modulation of rat cortical area 17 neuronal responses to moving visual stimuli during norepinephrine and serotonin microiontophoresis." Brain Res **514**(2): 276-292.

Whitman, M. C. and C. A. Greer (2007). "Synaptic integration of adult-generated olfactory bulb granule cells: basal axodendritic centrifugal input precedes apical dendrodendritic local circuits." J Neurosci **27**(37): 9951-9961.

Wichterle, H., D. H. Turnbull, et al. (2001). "In utero fate mapping reveals distinct migratory pathways and fates of neurons born in the mammalian basal forebrain." Development **128**(19): 3759-3771.

Wienisch, M., D. G. Blauvelt, et al. (2012). Two-Photon Imaging of Neural Activity in Awake, Head-Restrained Mice. Neuronal Network Analysis: Concepts and Experimental Approaches. T. Fellin and M. Halassa. Totowa, NJ, Humana Press**:** 45-60.

Willhite, D. C., K. T. Nguyen, et al. (2006). "Viral tracing identifies distributed columnar organization in the olfactory bulb." Proc Natl Acad Sci U S A **103**(33): 12592-12597.

Wilms, C. D. and M. Hausser (2014). "Twitching towards the ideal calcium sensor." Nat Methods **11**(2): 139-140.

Wilson, R. I. and Z. F. Mainen (2006). "Early events in olfactory processing." Annu Rev Neurosci **29**: 163-201.

Xu, H. T., F. Pan, et al. (2007). "Choice of cranial window type for in vivo imaging affects dendritic spine turnover in the cortex." Nat Neurosci **10**(5): 549-551.

Yamaguchi, M. (2017). "The role of sleep in the plasticity of the olfactory system." Neurosci Res **118**: 21-29.

Yamaguchi, M., H. Manabe, et al. (2013). "Reorganization of neuronal circuits of the central olfactory system during postprandial sleep." Front Neural Circuits **7**: 132.

Yamamoto, S., H. Ohba, et al. (2013). "Subanesthetic doses of ketamine transiently decrease serotonin transporter activity: a PET study in conscious monkeys." Neuropsychopharmacology **38**(13): 2666-2674.

Yang, Y. and Q. Zhou (2009). "Spine modifications associated with long-term potentiation." Neuroscientist **15**(5): 464-476.

Yokoyama, T. K., D. Mochimaru, et al. (2011). "Elimination of adult-born neurons in the olfactory bulb is promoted during the postprandial period." Neuron **71**(5): 883-897.

Zaborszky, L., J. Carlsen, et al. (1986). "Cholinergic and GABAergic afferents to the olfactory bulb in the rat with special emphasis on the projection neurons in the nucleus of the horizontal limb of the diagonal band." J Comp Neurol **243**(4): 488-509.

Zhang, F., V. Gradinaru, et al. (2010). "Optogenetic interrogation of neural circuits: technology for probing mammalian brain structures." Nat Protoc **5**(3): 439-456.

Zucker, R. S. and W. G. Regehr (2002). "Short-term synaptic plasticity." Annu Rev Physiol **64**: 355-405.

6 Statement of Contributions

According to § 9 (2):

For this dissertation, I designed the experiments together with Prof. Dr. O. Garaschuk, I performed the experiments, and I analyzed the data.

The master student A. Alsema has contributed to the analysis of the basal ratios of the resident GABAergic cell population during her laboratory rotation under my supervision. Her analysis is part of Figure 11 and Figure 14.

Natalie Fomin-Thunemann, MSc.

Eberhard Karls University Tuebingen
Institute for Physiology
Department of Neurophysiology
Keplerstr.15
72074 Tuebingen, Germany

Email: n.fomin87@gmail.com
natalie.fomin@uni-tuebingen.de
Phone: +49 176 31102683

PERSONAL INFORMATION

Day of birth: 01/12/1987
Birth place: Omsk, Russia
Nationality: German

EDUCATION AND TRAINING

since 2011	**Ph.D. thesis** in the Institute for Physiology, Department of Neurophysiology, University of Tuebingen, Tuebingen, about "*Physiological properties of mature adult-born neurons in the olfactory bulb of awake mice.*" Supervisor: Prof. Dr. Olga Garaschuk.
2010-2011	**Master thesis** in the Laboratory for Signal Transduction and Transgenic Models, Interfaculty Institute of Biochemistry, University of Tuebingen, Tuebingen, about *"Characterization of the cGMP pathway in cells of the brain."* Supervisor: Prof. Dr. Robert Feil.
2009-2011	**Master of Science** in Cellular and Molecular Neuroscience, Graduate School of Neuroscience, Tuebingen.
Jul-Aug 2009	**Bachelor thesis** in the Laboratory for Integrative Sensory Physiology, Institute for Animal Physiology, Justus Liebig University, Giessen, about *"Plasticity of the T-neuron in Tettigonia viridissima."* Supervisor: Prof. Dr. Lakes-Harlan.
2006-2009	**Bachelor of Science** in Biology at the Justus Liebig University, Giessen.

WORK EXPERIENCE

Aug-Nov 2010	**Lab rotation** with the project title: *'Looking at the propagation of slow waves in the rat cortex during sleep'* in the Laboratory for Physiology of Cortico-Hippocampal Interaction, Werner Reichardt Center for Integrative Neuroscience, Tuebingen. Supervisor: Dr. Anton Sirota.
Feb-Apr 2010	**Lab rotation** with the project title: *'Lingo-1 overexpression and its counteraction by Retinoic acid'* in the Laboratory for Neuroregeneration and Repair, Hertie-Institute for Clinical Brain Research, Tuebingen. Supervisor: Dr. Simone Di Giovanni.
Sep 2008	**Internship** in the Laboratory of Neurophysiology (PI: Prof. Dr. Wolf Singer), Max-Planck-Institute for Brain Research, Frankfurt.
Mar 2002	**Internship** in the Laboratory of Cellular Biophysics (PI: Dr. Thomas Gensch), Forschungszentrum Jülich.

PUBLICATIONS

Articles

(1) B. Brawek, Y. Liang, D. Savitska, K. Li, **N. Fomin-Thunemann**, Y. Kovalchuk, E. Zirdum, J. Jakobsson, O. Garaschuk. "A new approach for ratiometric in vivo calcium imaging of microglia". *Sci Rep.* 2017; Jul 20; 7(1):6030*.

(2) M. Thunemann, **N. Fomin**, C. Krawutschke, M. Russwurm, R. Feil. "Visualization of cGMP with cGi biosensors." *Methods Mol Biol.* 2013; 1020:89-120.

(3) R. Puttagunta, A. Schmandke, E. Floriddia, P. Gaub, **N. Fomin**, NB Ghyselinck, S. Di Giovanni. "RA-RAR-β counteracts myelin-dependent inhibition of neurite outgrowth via Lingo-1 repression." *J Cell Biol.* 2011; 193(7):1147-1156.

Meeting Abstracts

(1) S. Fink, **N. Fomin-Thunemann**, J. Sheppard, M. Schmidt, O. Garaschuk. *"Default glomerular activity maps in the olfactory bulb of awake mice."* 12th Göttingen Meeting of the German Neuroscience Society, Göttingen, Germany 2017.

(2) **N. Fomin**, S. Fink, Y. Kovalchuk, Y. Liang, O. Garaschuk. *"Distinct physiological properties of mature adult-born neurons in the olfactory bulb of awake mice."* 45th Meeting of the Society for Neuroscience, Chicago, USA 2015.

(3) S. Fink, Y. Kovalchuk, **N. Fomin**, M. Carr, M. Hermes, S. Dierenberger, O. Griesbeck, O. Garaschuk. *"Odor-evoked activity patterns of mitral cells in the mouse olfactory bulb in vivo."* 91st Meeting of the German Society for Physiology, Dresden, Germany 2012.

(4) M. Thunemann, **N. Fomin**, M. Hillenbrand, T. Ott, M. Russwurm, R. Feil. *"Visualization of cGMP in living cells and tissues of transgenic mice."* 78th Meeting of the DGPT, Dresden, Germany 2012.

(5) M. Thunemann, **N. Fomin**, M. Hillenbrand, S. Kroll, A. Wilhelm, P. Messer, T. Ott, M. Russwurm, R. Feil. *"Generation and characterization of transgenic mice carrying cGMP FRET sensors (cGi's)."* Poster session in the Interfaculty Institute of Biochemistry, Tuebingen, Germany 2011.

FURTHER TRAINING

Oct 2016 - Feb 2017	Course (15 x 2 hrs): *"Physiological and Physical Basis of Functional Brain Imaging"*.
Apr-Jul 2016	Course (14 x 2 hrs): *"Embodiment, Emotion and Experience"*.
Oct 2014 - Feb 2015	Course (15 x 2 hrs): *"Methods in Neuropsychology"*.
Jun 2013	Course (6 x 2 hrs): *"Advanced Matlab"*.
Apr 2013	Course (4 x 2 hrs): *"Introduction to Matlab"*.
Mar 2013	Course (2 x 8 hrs): *"Introduction to Programming"*.
Mai 2012	Course (2 x 5 hrs): *"Statistics with SPSS"*.

PERSONAL SKILLS AND COMPETENCES

Languages	Russian	▪ Good
	German	▪ Reading/Writing/Speaking (excellent)
	English	▪ Reading/Writing/Speaking (excellent)
Laboratory techniques	General	▪ Molecular Biology ▪ Cell Biology ▪ Biochemistry
	Cell culture	▪ Primary culture of neurons/astrocytes from mice
	Experimental animals	▪ Surgery on rodents (craniotomy for acute or chronic imaging, insertion of electrodes for intracranial recordings, stereotactic virus injection into the mouse brain)
	Microscopy	▪ Live cell/FRET imaging ▪ Confocal Imaging/2-Photon Calcium imaging
Computer skills	▪ Image analysis (e.g. with ImageJ) ▪ Graphical design (e.g. with Adobe Illustrator) ▪ Data analysis with MATLAB, IGOR and SPSS	